國立臺灣大學工學院土木工程學系

碩士論文

Graduate Institute of Civil Engineering

College of Engineering

National Taiwan University

Master Thesis

地中壁於黏土層中深開挖對系統勁度及壁體變位之影響

Effect of Cross Walls on System Stiffness and Wall Displacement for Excavations in Soft Clay

王姿勻

Zih-Yun Wang

指導教授：葛宇甯　博士　謝旭昇　博士

Advisor: Louis Ge, Ph.D., Hsii-Sheng Hsieh, Ph.D.

中華民國 108 年 7 月

July, 2019

doi:10.6342/NTU201900743

國立臺灣大學碩士學位論文
口試委員會審定書

地中壁於黏土層中深開挖對系統勁度及壁體變位之影響

Effect of Cross Walls on System Stiffness and Wall Displacement for Excavations in Soft Clay

本論文係　王姿勻君（R06521107）在國立臺灣大學土木工程學系碩士班完成之碩士學位論文，於民國 108 年 07 月 24 日承下列考試委員審查通過及口試及格，特此證明

口試委員：

葛宇甯　教授（指導教授）　葛宇甯

謝旭昇　教授（指導教授）　謝旭昇

楊國鑫　教授　楊國鑫

熊彬成　教授　熊彬成

系主任　謝　尚　賢　謝尚賢

（簽名）

doi:10.6342/NTU201900743

致謝

「現在努力一點，未來的你才會感謝現在的自己！」

這句話貫穿了碩士兩年，每當研究卡關、徬徨無助時，這句話總能給我滿滿的力量。

感謝我的指導老師　葛宇甯教授，一直以來在研究路上給予的資源，無論是提早進研究所、選擇研究方向、甚至是實習的機會、以及支持我參加國外研討會。這些都給予我充分的選擇及思考空間，也讓我在這之中學習到寶貴的經驗。心中除了無限的感激之外，更多的是無以言表的感謝！畢竟這些都是以前的自己不敢想像的經驗。同時也感謝　謝旭昇博士，除了開挖工地的實務內容外，也給予我許多案例專研；介紹我進入地工技術基金會，參與 T3-STONE 的案例測試；除此之外，也細心修改論文的英文文法，也點出寫作的盲點及改進之處。對於謝博士的用心及提拔，我不勝感激。

感謝同窗好友呂昕臻，在修課時一起討論作業、在閒暇時聊聊八卦、分享 KUSO 影片以及出門放鬆心情，讓枯燥乏味、了無生趣的研究生活增添多采多姿的回憶。感謝同窗好友游家奇，一起討論艱難的基設作業及考試。感謝葛門的學姊吳軒蘋在踏入數值分析之初細心教導；感謝同窗楊敏昀、王竣民在研究卡關時，討論數值分析所遇到的難題、提供後處理程式，讓我能廣泛地應用到研究中並縮短時間。

最感謝的是我的家人，在就學期間父母除了提供經濟上的支助外，也全力支持我的選擇；每當心情糟糕透頂時，總能給予我建議、耐心地鼓勵我。

doi:10.6342/NTU201900743

ABSTRACT

Cross walls are usually adopted to prevent excessive deformation of diaphragm wall and to minimize damage to the adjacent buildings. Three case histories were selected to demonstrate the presence of cross wall does have a significant effect on minimizing wall displacement. According to the validation of case histories, it is noted that the three-dimensional effect induced by cross wall is pronounced for the excavation in soft clay, which results in a pretty small field observation that is far below the results predicted by the design chart proposed by Clough et al.

In order to have a better prediction on the wall displacement, this study incorporates the effect of cross wall within Clough's chart by adjusting the system stiffness and factor of safety against basal heave. In addition, Clough's original design curves are extrapolated to cover the uncharted area of both high system stiffness and high factor of safety against basal heave.

The strengthening effect of cross wall leads to increase of system stiffness and factor of safety against basal heave that can be quantified by simplified approaches, which are incorporated within Clough's scheme. With the revised scheme, the wall displacement under the influence of cross walls can be reasonably estimated, if the condition of soil, retaining wall and layout of project site had all been known. Other case histories are also studied to validate the revised scheme.

Three-dimensional numerical analyses are also carried out to further calibrate the effect of cross walls. It is found that the spacing of cross walls is the most important factor that governs the magnitude of wall displacement. A typical spacing of 15 m between cross walls appears to be the optimal layout of cross walls if a low value of wall displacement is desired.

Keywords: deep excavation, system stiffness, cross wall, three-dimensional effect

doi:10.6342/NTU201900743

摘要

地中壁工法為常用於目前深開挖工程的輔助措施，以防止連續壁產生過多之側向變形量並減少對相鄰建築物的影響。Clough 等人於 1989 年提出設計曲線，其考慮了土壤及擋土措施的效應，可初估開挖所造成的牆體位移。然而，由地中壁引起之三向度效應對於連續壁的抑制非常明顯。所謂的三向度效應為考慮輔助措施的存在以及開挖基地的大小。首先，針對三個已完成的開挖案例進行 PLAXIS 3D 分析，以驗證地中壁的存在確實對於抑制連續壁的側向位移有顯著的影響，以及發現其現地結果遠小於 Clough 曲線的預測值。

由案例探討可知 Clough 曲線已經不敷使用，若不進一步優化 Clough 曲線，將使得設計過於保守。因此，為了更準確地預測連續壁的側向位移，本研究在原始 Clough 的架構下結合地中壁的影響，透過系統勁度和基地底面隆起安全係數的調整來量化其地中壁效應；優化曲線後並延伸以涵蓋高系統勁度和高基地底面隆起安全係數，可用於估算地中壁影響下之牆體位移；另外，也蒐集其他案例來檢討其準確性及合理性。另外，進行三維數值分析進一步了解地中壁的影響，經過數值模擬發現地中壁間距為決定壁體位移的重要因素。根據數值結果，可得出 15 米的地中壁間距似乎能發揮其最佳之效益。

根據參數研究的結果，歸納出以下結論：一、修正後的 Clough 曲線可合理預估開挖所引致之壁體位移，並滿足設計所需。二、若要發揮地中壁之最大效益，15 米的地中壁間距為最佳之設計值。

關鍵字：深開挖、系統勁度、地中壁、三向度效應

doi:10.6342/NTU201900743

CONTENTS

doi:10.6342/NTU201900743

doi:10.6342/NTU201900743

doi:10.6342/NTU201900743

LIST OF FIGURES

doi:10.6342/NTU201900743

doi:10.6342/NTU201900743

doi:10.6342/NTU201900743

LIST OF TABLES

doi:10.6342/NTU201900743

doi:10.6342/NTU201900743

doi:10.6342/NTU201900743

LIST OF SYMBOLS

ENGLISH

Symbols	Unit	Description
A	m^2	cross sectional area
B	m	width of excavation zone
C	-	coefficient depends on factor of safety against basal heave
c	kPa	cohesion of soil
c'	kPa	effective cohesion of soil
D	m	distance from the excavation depth to the stiff layer
d	m	distance from the selected section to the corner
d_c	m	spacing of cross walls
d_T	m	influence zone
E	kPa	Young's modulus of the wall
E_s	kPa	Young's modulus of the soil
E'	kPa	effective Young's modulus of soil
E_u	kPa	undrained Young's modulus of soil
$E_{u,inc}$	kPa/m	increment of undrained Young's modulus per meter
F_b	-	factor of safety against basal heave
F_{b_adj}	-	adjusted factor of safety against basal heave
F_s	-	side friction of the buttress wall in each soil layer
f_s	kPa	unit side friction of buttress wall
f_c'	MPa	compressive strength of concrete
H	m	total height of the diaphragm wall
H_e	m	excavation depth
h_{avg}	m	average vertical support spacing
I	m^4	moment of inertia per unit length of the wall
I_{CL}	-	magnification factor
k	-	factor depends on system stiffness
K_h	-	horizontal modulus of subgrade reaction
K_h*	-	equivalent horizontal modulus of subgrade reaction
K_P	kPa	coefficient of the passive earth pressure
L	m	(1) length of excavation zone (2) length of primary wall (3) length of buttress wall

doi:10.6342/NTU201900743

Symbols	Unit	Description
L_{CW}	m	length of cross wall
m	-	undrained shear strength ratio ($=s_u/\sigma_v'$)
N	-	blow count of Standard Penetration Test
N_{CW}	-	number of buttress wall
N_c	-	constant value of 5.7
N_{CW}	m	number of cross wall
P_P	kN	passive earth pressure
P_{PR}	kN	increased passive resistance induced by the buttress walls
P_{PE}	kN	equivalent passive earth pressure
PSR	-	Plane Strain Ratio
PSR_{Ou}	-	Plane Strain Ratio proposed by Ou
PSR_{Finno}	-	Plane Strain Ratio proposed by Finno
q	kPa	surcharge load of adjacent building
R	-	relative stiffness ratio
R_{int}	-	reduction of interface strength
S	-	system stiffness
S_c	-	combined system stiffness
S_H	m	average horizontal support spacing
S_V	m	average vertical support spacing
SI	-	inclinometer
s_u	kPa	undrained shear strength
s_u*	kPa	equivalent undrained shear strength
s_{ub}	kPa	undrained shear strength below excavation surface
s_{ub}*	kPa	undrained shear strength below excavation surface considering cross wall effect
s_{ub_adj}	kPa	average undrained shear strength having considered cross wall effect
s_{uu}	kPa	average undrained shear strength above excavation surface
$s_{u,inc}$	kPa/m	increment per meter in cohesion
t	m	thickness of structural element
x_{min}	m	minimal value of numerical analysis domain in x direction
x_{max}	m	maximal value of numerical analysis domain in x direction
y_{min}	m	minimal value of numerical analysis domain in y direction
y_{max}	m	maximal value of numerical analysis domain in y direction
z_{ref}	m	reference level

doi:10.6342/NTU201900743

GREEK

Symbols	Unit	Description
δ	°	friction angle between soil and wall
δ_{clough}	mm	maximum lateral wall displacement from Clough's chart
δ_{field}	mm	maximum lateral wall displacement by field observation
δ_{hm}	mm	maximum lateral wall deflection
$\delta_{hm,d}$	mm	maximum lateral wall deflection at the distance of d from the corner
$\delta_{hm,ps}$	mm	maximum lateral wall deflection under plane strain condition
δ_{rev}	mm	maximum lateral wall displacement from revised scheme
δ_{3D_with}	mm	maximum lateral wall displacement from PLAXIS 3D with cross wall
$\delta_{3D\_without}$	mm	maximum lateral wall displacement from PLAXIS 3D without cross wall
$\delta_{spacing}$	mm	maximum lateral wall displacement at various spacing of cross wall
σ_v	kPa	total overburden pressure
σ_v'	kPa	effective overburden pressure
α	-	empirical value (=1.0)
β	-	coefficient (=2.0)
μ	-	factor depending on the value of system stiffness
κ	-	number of friction side of the cross wall (1 or 2)
ϕ'	°	effective friction angle
ϕ_u	°	undrained friction angle
v'	-	effective Poisson ratio
v_u	-	undrained Poisson ratio
γ	kN/m^3	unit weight of the structural element
γ_s	kN/m^3	average unit weight of the soil

doi:10.6342/NTU201900743

Chapter 1 Introduction

1.1 Background and Motivation

To cope with the rapid growing demand of the underground space, it is necessary to construct multi-level basement for new buildings. The wall displacement induced by the excavation would increase with the excavation depth of multi-level basement. In urban area with soft clay deposit like Taipei city, it is often required that the diaphragm wall displacement of a deep excavation be limited to a low level to minimize the damage to the adjacent buildings.

As the auxiliary measures such as cross walls and buttress walls are installed in the excavation zone, not only the undrained shear strength of clay within the excavation zone would equivalently increase, but the three-dimensional effect would also be obvious. The so-called three dimensional effect accounts for the presence of buttress walls and cross walls in strengthening the stiffness of excavation support system, and the wall deflection can significantly be reduced if there is a pronounced three-dimensional effect in the excavation zone.

Clough et al. (1989) first presented a relationship among the wall displacement, system stiffness and factor of safety against basal heave for excavation in clay. By applying the relationship to the excavation in soft clay, the maximum lateral displacement of the diaphragm wall can be rapidly predicted. However, the requirement for the

doi:10.6342/NTU201900743

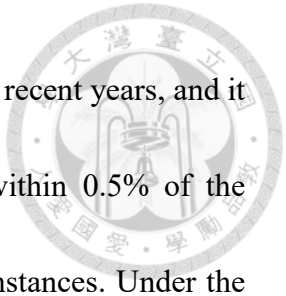

excavation projects to control wall displacement are more rigorous in recent years, and it is desirable that the maximum wall displacement be controlled within 0.5% of the excavation depth, or below 0.3% of the excavation depth in some instances. Under the circumstances, Clough's chart is no longer applicable to estimate the wall deformation at such low displacement level. It is obvious that there is a need to incorporate the effect of cross walls in Clough's original chart of system stiffness and to extend Clough's design curves toward the area of high system stiffness and high factor of safety against basal heave. Due to extensive use of the cross walls in modern excavations, the potential factor of cross walls that impacts the displacement of diaphragm wall should be further explored.

1.2 Research Objectives

Cross wall is an essential part for modern excavation to refrain wall deflection, to reduce the ground settlement induced by excavation and to increase the passive resistance. As the strengthening effect of cross walls is particularly evident in soft clay, the cross walls are widely installed in recent years. In this research, two parts are discussed in detail. First, the system stiffness and factor of safety against basal heave proposed in Clough's original chart will be modified to incorporate the effect of cross walls, which lacks in the present form of Clough's chart. Clough's original design curves will also be extended to meet modern requirements and keep its original advantage about rapidly estimating the maximum wall displacement. Second, parametric studies through three-dimensional

doi:10.6342/NTU201900743

numerical software will be conducted to identify the important factors that govern the effectiveness of cross walls.

By fulfilling these two parts, we can have a better understanding on the behavior of diaphragm wall for excavation with cross walls, and utilize the modified Clough's chart to reasonably estimate the wall displacement for excavations with cross walls. The objectives of this study are itemized as follows:

1. To modify the Clough's original curves to incorporate the effect of cross walls and extrapolate the original curves. In addition, the applicability of the regression equation is evaluated by other cases. Afterwards, an appropriate range of the regression equation is described.
2. To identify the important factors that control the diaphragm wall for the excavations with cross walls. The optimal spacing of cross walls is also examined.

1.3 Research Outline

The flow chart of this study is shown in Figure 1.1, and the outline is given as follows:

1. Chapter 2 reviews previous studies on system stiffness, Plane Strain Ratio as well as the effect of auxiliary measures on the retaining wall. In addition, various characteristics and effect of cross walls are presented.
2. Chapter 3 demonstrates the cross walls that play a significant role in reducing the deflection of diaphragm wall through three case histories. Comparisons between

doi:10.6342/NTU201900743

numerical results by PLAXIS 3D, field observation and predictions by Clough's chart are discussed.

3. Chapter 4 revises the original Clough's chart by extending the curves into the uncharted area. The pronounced effect of cross walls would lead to an increase of both system stiffness and factor of safety against basal heave. In addition, this outcome would be applied to the previous three cases.
4. Chapter 5 conducts three-dimensional numerical parametric analyses to explore the key factors that governs the strengthening behavior of cross walls.
5. Chapter 6 validates the effectiveness and applicability of the above two parametric studies, the revised Clough's chart and the key factor of cross walls, by reviewing four additional case histories.
6. Chapter 7 summarizes the studies, and provides recommendations for future work.

doi:10.6342/NTU201900743

Introduction (Chapter 1)

- Research motivation and objectives

Literature Review (Chapter 2)

- System stiffness (S)
- Plane Strain Ratio (PSR)
- Relative stiffness ratio (R)
- Diaphragm wall design with auxiliary measures
- Finite element program

Case Histories (Chapter 3)

- Model validation of three case histories with cross walls

Revision of Clough's chart (Chapter 4)

- Extrapolation of design curves
- Combined system stiffness
- Adjusted factor of safety against basal heave

Parametric Studies on the Effect of Cross Walls (Chapter 5)

- Numerical scheme
- Spacing of cross walls

Applications of Parametric Studies (Chapter 6)

- Application of the revised Clough's scheme on 4 additional cases
- Application of effect of cross walls spacing on 7 cases with alternating sand/clay layers

Conclusions and Recommendations (Chapter 7)

- Summary, conclusions and recommendations

Figure 1.1 Flow chart

doi:10.6342/NTU201900743

Chapter 2 Literature Review

Deep excavation is a soil-structure interaction problem, where its stability could be observed by monitoring of the wall displacement. Therefore, evaluating the lateral movement of the retaining wall is an important part of design that may involves a complicated numerical analysis. Clough et al. (1989) first presented a relationship among the wall displacement, system stiffness and factor of safety against basal heave as shown in Figure 2.1, which allows engineers to estimate the possible maximum wall displacement. A similar chart was proposed by Bryson et al. (2012), which uses relative stiffness ratio instead of system stiffness as an index to evaluate wall displacements is also described in next section.

For modern excavations in the populated urban area, the project site is narrower and deeper that the corner effect and three-dimensional effect are much pronounced than in the past, and cross walls are often adopted in the excavation zone to refrain the wall deflection to a low level. If the plane strain condition is adopted for design, the results tend to be conservative. Under the circumstances, it would be overly conservative if the plane strain condition is considered in excavation. The Plane Strain Ratio was first proposed by Ou et al. (1996) to quantify the three-dimensional effect. Afterwards, some scholars suggested other ways to present the Plane Strain Ratio. These approaches are described in the following sections.

doi:10.6342/NTU201900743

2.1 System Stiffness

Clough et al. (1989) first presented a relationship among wall displacement, system stiffness and factor of safety against basal heave (F_b) for excavations in clay as shown in Figure 2.1. By applying the relationship, the maximum wall displacement could be estimated rapidly. In Figure 2.1, the x-axis is the system stiffness (S) defined by Clough et al. (1989):

$$S = \frac{EI}{\gamma_w h_{avg}^4} \tag{2.1}$$

where E is Young's modulus of retaining wall, I is the moment of inertia per unit length of retaining wall and h_{avg} is the average vertical support spacing. The y-axis is the maximum wall movement (δ_{hm}) normalized by the excavation depth (H_e). A series of curves was proposed for different factor of safety against basal heave (F_b), which is determined based on the equations by Terzaghi (1943). Based on the relationship between the excavation width (B) and the distance from the excavation surface to the stiff soil layer (D), F_b can be written in the following forms. If D is larger or equal to $B/\sqrt{2}$, the equation for F_b is shown as follows.

$$F_b = \frac{N_c \times s_{ub} \times B/\sqrt{2}}{(\gamma H_e + q) \times B/\sqrt{2} - s_{uu} H_e} \tag{2.2}$$

If D is smaller than $B/\sqrt{2}$, the equation for F_b is in following form.

$$F_b = \frac{N_c \times s_{ub} \times D}{(\gamma H_e + q) \times D - s_{uu} H_e} \tag{2.3}$$

where N_c is constant value of 5.7, q represents the load of the adjacent building, and

doi:10.6342/NTU201900743

s_{uu} and s_{ub} represent the average undrained shear strength of clay above and below the excavation surface, respectively. The calculation of F_b is schematically shown in Figure 2.2.

Clough et al. also collected field data and numerical results as shown in Figure 2.3. In general, the field data reasonably followed the predicted trend curves, although there was indication that the curves might be on the conservative side for projects with slurry walls. In summary, Clough's chart can be used to give reasonable estimation of the wall movements.

doi:10.6342/NTU201900743

2.2 Plane Strain Ratio

Ou et al. (1996) conducted a great amount of finite element analyses to evaluate the relationship between the maximum wall displacement and distance from corners to various sections. According to the geometry of the site and the distance from the corner, the Plane Strain Ratio (PSR) can be estimated, which is the ratio of the maximum wall displacement under plane strain condition and the wall displacement under three-dimensional condition. PSR is expressed as:

$$PSR = \frac{\delta_{hm,d}}{\delta_{hm,ps}} \tag{2.4}$$

where $\delta_{hm,d}$ is the maximum wall displacement for a particular section at a distance (d) from the corner, $\delta_{hm,ps}$ is the maximum wall displacement under plane strain condition.

A chart presented by Ou et al. (1996), which defines the relationship between the PSR, the ratio of the geometry of the site (B/L) and the distance from the section to the corner (d) is shown in Figure 2.4. L is the length of the primary wall that the maximum wall displacement and plane strain condition were evaluated. B is the length of the complementary wall. The definition of L and B are schematically shown in Figure 2.5. The center section of a relatively long wall would be more or less at a plane strain state. As PSR value reaches 1, the section is in a plane strain condition. If PSR is close to 0.1, the section is thought to be pronouncedly affected by the corner.

The PSR defined by Finno et al. (2007) is similar to that of Ou et al. (1996). The

doi:10.6342/NTU201900743

maximum lateral movement from the results of a three-dimensional simulation divided by that from a plane strain simulation is termed as the Plane Strain Ratio. For parametric studies, a bottom-up construction with 4 levels of struts was adopted in analyses. The length of the primary wall and the complementary wall both varied from 20 to 160 m, and excavation depths varied from 9.8, 13.4 and 16.3 m were adopted for 3D numerical analyses. Parameters used for analyses are summarized in Table 2.1 and Table 2.2. In all, there were 50 cases and 3 different wall stiffness. Through a total of 150 finite element analyses, a PSR equation can be deduced:

$$PSR = \left(1 - e^{-kC(L/H_e)}\right) + 0.05\left(\frac{L}{B} - 1\right) \tag{2.5}$$

$$C = 1 - \{0.5(1.8 - F_b)\} \tag{2.6}$$

$$k = 1 - 0.0001(S) \tag{2.7}$$

where C depends on the factor of safety against basal heave (F_b), and k depends on system stiffness (S) which was proposed by Clough et al. (1989) shown in Equation (2.1).

Finno et al. (2007) indicated that the PSR is not only affected by the site geometry, but also contributed by other factors such as the ratio of the wall length to the excavation depth (L/H_e), the system stiffness (S) and the factor of safety against basal heave (F_b). Figure 2.6(a) and Figure 2.6(b) show the relationship between L/H_e and L/B with PSR, respectively. It is evident in Figure 2.6(a), that for the ratio of L/H_e greater than 6, the PSR value is approximately equals to 1. If the L/H_e ratio is less than 2, the wall

doi:10.6342/NTU201900743

displacement is more restrained by the sides of the excavation. Figure 2.6(b) shows the relationship between PSR and L/B. As L/B ratio is smaller than 0.5, the corner effect is more pronounced. Of these factors, the ratio of the length of the primary wall to the excavation depth (L/H_e) is the more dominant factor for the range of their parametric studies. A comparison between published data and the result of parametric study is shown in Figure 2.7. In summary, the magnitude of the corner effects depends on the excavation geometry, the stiffness of the lateral support system and the factor of safety against basal heave. In general, a greater corner effect is observed for a relatively deep excavation, as evidenced by the value of L/H_e smaller than 6 and the value of L/B less than 1. Conversely, as L/H_e is larger than 6 and L/B is larger than 1, the center section of the excavation would be under plane strain condition.

doi:10.6342/NTU201900743

2.3 Relative Stiffness Ratio

Bryson and Zapata (2012) proposed a new concept, relative stiffness ratio, based on the system stiffness defined by Clough et al. (1989). They constructed three-dimensional finite element models to mimic the real behavior of the excavation. For parametric studies, the artificial excavation is conducted in three homogenous but different materials, which are stiff clay, medium clay and soft clay, respectively. The differences between the various clay types were their undrained shear strength, as shown in Table 2.3. Sixteen different structural models were adopted for analyses as shown in Table 2.4. Model 1 was regarded as the reference model. It must be mentioned that only one parameter was varied in Models 2 and 3, which is the spacing of horizontal supports. The effect of varying the vertical support spacing was investigated in Models 4 to 7. In Models 8 to 16, the wall stiffness was the variable. Through 48 results, the relative stiffness ratio (R) is given as:

$$R = \frac{E_s}{E} \cdot \frac{S_H S_V H}{I} \cdot \frac{\gamma_s H_e}{s_u} \tag{2.8}$$

where E_s is the Young's modulus of soil; E is the Young's modulus of wall, and I is the moment of inertia per unit length of wall. S_H is the average horizontal spacing of the horizontal supports; S_V is the average vertical spacing of the vertical supports. H is the total height of the wall, H_e is the excavation depth, γ_s is the unit weight of the soil; s_u is the undrained shear strength of soil at the bottom of the excavation. The authors incorporated most of the influence factors to evaluate the overall stiffness which did not

doi:10.6342/NTU201900743

have a single variable such as the vertical support spacing $\left(h_{avg}^4 = S_V^4\right)$ proposed by Clough et al. (1989). It is obvious that the horizontal support spacing is also an important factor as shown in Figure 2.8.

Results of the parametric studies were compared with the Clough's chart as shown in Figure 2.9. For stiff clay, the results were coincided with the Clough's curve. It is also observed that numerical results deviate from Clough's curve at areas with low system stiffness. However, Bryson and Zapata's results fail to match the Clough's curves for soft clay. In addition, other researchers also provided insightful comments on the system stiffness. Long (2001) asserted the lateral wall deformation in stiff clay is largely independent of the system stiffness. Moormann (2004) also stated that in soft clay there is a wide scatter of the data, and there are lacks of dependency of lateral wall movement on system stiffness owing to the variation of other factors such as ground water level, geometrical irregularities, workmanship and pre-stress of strut. The chart of relative stiffness ratio was presented in Figure 2.10. The lateral displacement was normalized by the total height of the wall. The factor of safety is calculated using following equation.

$$FS = \frac{s_u N_c + \sqrt{2} s_u (H_e/B) + 2 s_u (D/B)}{\gamma_s H_e} \tag{2.9}$$

which was a modified version of the Terzaghi (1943) equation reported by Ukritchon et al. (2003), it considered the effects of the wall embedment below the excavation surface.

doi:10.6342/NTU201900743

2.4 Diaphragm Wall Design with Auxiliary Measures

Auxiliary measures such as buttress wall and cross wall are often adopted within the excavation zone to restrain the wall deformation and to improve the stability of the excavation. Usually, these auxiliary measures are constructed before the excavation and completed at the same time as the retaining wall. The auxiliary measures above the excavation surface are removed by step-by-step excavation. The auxiliary measures below the excavation surface remain intact, and should be regarded as a form of soil improvement, which is equivalent to an increase of the undrained shear strength for the soil mass within the excavation zone, resulting in the increment of the factor of safety against basal heave.

A simplified method to quantify the strengthening effect of buttress walls and cross walls was proposed by Hsieh and Lu (1999). In this method, it was postulated that the buttress wall is a form of ground improvement, which enhances the equivalent subgrade reaction coefficient (K_h^*) and soil strength parameters (K_P^*, s_u^*). The equivalent parameters are presented in detail in following section.

2.4.1 Equivalent soil parameters in cohesive soil

For the deriving of equivalent strength, some assumptions were made. For one, the side friction of buttress walls leads to an increase of the passive resistance as shown in Figure 2.11. The passive earth pressure is described in following form.

doi:10.6342/NTU201900743

$$P_P = K_P \sigma_v + \beta s_u \ \text{(kPa)} \tag{2.10}$$

where K_P is equal to 1, as the cohesive soil is fully saturated, and β is equal to 2 based on Rankine's earth pressure theory. The other one, the unit side friction of buttress wall (f_s) is expressed as follows.

$$f_s = \alpha s_u \ \text{(kPa)} \tag{2.11}$$

where α is an empirical value of 1.0, and s_u is the undrained shear strength. The side friction of a buttress wall in the soil layer can be shown as follows.

$$F_s = f_s \times L \times 2 \ \text{(kN)} \tag{2.12}$$

where F_s is the side friction of the buttress wall in each soil layer, L is the length of buttress wall, and the coefficient value of 2 represents dual sides of buttress wall. Since the total increment of passive resistance is proportional to the amount of the buttress walls, the increment in passive resistance is shown as follows.

$$P_{PR} = F_s \times N/B = \alpha s_u \times L \times 2 \times N/B \ \text{(kN)} \tag{2.13}$$

where N is the number of buttress walls, B is the length of diaphragm wall strengthened by the buttress walls, which is schematically shown in Figure 2.12. Combining Equation (2.10) and Equation (2.13), the equivalent passive earth pressure (P_{PE}) can be written as follows.

$$P_{PE} = P_P + P_{PR}$$

$$= (K_P \sigma_v + \beta s_u) + (\alpha s_u \times L \times 2 \times N/B)$$

doi:10.6342/NTU201900743

$$= \sigma_v + \left(1 + \alpha \times L \times 2 \times N/(B\beta)\right)\beta s_u \quad (2.14)$$

since the cohesive soil is saturated, K_P value is equal to 1. The magnification factor (I_{CL}) is expressed as follows.

$$I_{CL} = 1 + 2 \times \alpha \times L \times N/(B\beta) \quad (2.15)$$

In summary, the undrained shear strength (s_u) and modulus of subgrade reaction (K_h) are enlarged by the magnification factor (I_{CL}), the equivalent strength (s_u^*) and stiffness (K_h^*) can be expressed by multiplying the original strength and stiffness with the I_{CL}, respectively:

$$s_u^* = I_{CL} \times s_u \ \text{(kPa)} \quad (2.16)$$

$$K_h^* = I_{CL} \times K_h \ \text{(kN/m}^3\text{)} \quad (2.17)$$

2.4.2 Equivalent soil parameters in non-cohesive soil

To derive the equivalent strength parameters, some assumptions were made. For one, the side friction of buttress walls leads to an increase of the passive resistance. General form of the passive earth pressure is written as Equation (2.10). The unit side friction of buttress wall (f_s) is expressed as follows.

$$f_s = K_P \times \sigma_v' \times \tan\delta \ \text{(kPa)} \quad (2.18)$$

where K_P is the coefficient of passive earth pressure, δ is the friction angle between soil and buttress wall. The side friction of a buttress wall in the soil layer can be expressed as Equation (2.12). Since the increment of passive resistance (P_{PR}) is proportional to the

doi:10.6342/NTU201900743

amount of buttress walls, the equation for P_{PR} is written as follows.

$$P_{PR} = F_s \times N/B = K_P \times \sigma_v' \times \tan\delta \times L \times 2 \times N/B \quad \text{(kN)} \qquad (2.19)$$

Based upon Equation (2.10) and Equation (2.19), the equivalent passive earth pressure (P_{PE}) can be described as follows.

$$P_{PE} = P_P + P_{PR}$$

$$= K_P\sigma_v' + K_P \times \sigma_v' \times \tan\delta \times L \times 2 \times N/B$$

$$= \sigma_v'(K_P + K_P \times \tan\delta \times L \times 2 \times N/B) \qquad (2.20)$$

2.4.3 Characteristics of cross walls

Cross walls are commonly used in some Asia countries like Japan and Taiwan to limit the excavation-induced ground settlements. Wu et al. (2013) used 22 cases histories including 11 excavations with cross walls and 11 excavations without cross walls to quantify the effect of cross walls. It was found that the cross walls can effectively reduce the ground settlements by minimizing wall displacements, and the maximum wall displacements for cases with cross walls are within 0.1% H_e to 0.35% H_e, compared with the excavations without cross walls being within 0.3%H_e to 0.8%H_e. The details of the study are shown in Figure 2.13. It is evident that cross walls have major influence on limiting the wall displacement and the associated ground settlement.

doi:10.6342/NTU201900743

2.5 The Finite Element Program

In this section, the finite element program PLAXIS is briefly introduced. The constitutive law of soils used in this research is described in detail in chapter 3. The details on the construction of three-dimensional numerical models, the selection of parameters and the drained/undrained analysis option of soil are also discussed in chapter 3.

PLAXIS is a two- or three-dimensional finite element program for the analysis of deformation, stability and ground water flow in geotechnical engineering. The development of PLAXIS began in 1987 at Delft University of Technology as an initiative of the Dutch Ministry of Public Works and Water Management. The initial purpose was focused on the study for the soft soils of the lowlands of Holland. In subsequent years, PLAXIS was extended to cover most other areas of geotechnical engineering. PLAXIS was intended to provide a tool for practical analysis to be used by geotechnical engineers who are not necessarily numerical specialists. Currently, it is widely applied in various practices and researches of geotechnical engineering such as tunnel, deep excavation and slope. In this research, PLAXIS 3D is used to obtain the possible wall deflection induced by excavation.

doi:10.6342/NTU201900743

Table 2.1 Summary of 3D finite-element analyses for parametric study (Finno et al., 2007)

Stratigraphy	Height of cut, H_e/F_b	Primary length of cut, L (m)	Secondary length of cut, B (m)
A	9.8/1.7	20	20, 40, 80
	13.4/1.68	40	20, 40, 80
	16.3/1.8	80	20, 40, 80, 160*
		160	80*
B	9.8/1.7	20	20, 40
	13.4/1.68	40	20, 40, 80
	16.3/1.8	80	40, 80

Note: System stiffness of 32, 320, and 3,200 were considered for each of the 50 cases.
*Analyzed for H_e equal to 9.8 m only.

Table 2.2 Hardening soil parameters used in parametric study (Finno et al., 2007)

Parameter	Sand	Soft clay	Medium clay	Stiff clay
E_{50}^{ref} (kPa)	7,185	421	1,284	17,723
E_{50}^{ref} (kPa)	7,185	295	884	12,406
c^{ref} (kPa)	1	1	1	1
ϕ (°)	37	24	26	32
ψ (°)	5	0	0	0
M	0.5	0.8	0.85	0.85

doi:10.6342/NTU201900743

Table 2.3 Hardening soil parameters used for finite-element modeling (Bryson et al., 2012)

Hardening soil parameter		Chicago clay (soft clay; undrained)	Taipei silty clay (medium clay; undrained)	Gault clay (stiff clay; undrained)
Parameter	Unit			
γ_{unsat}	kN/m^3	18.1	18.1	20
γ_{sat}	kN/m^3	18.1	18.1	20
$k_x = k_z$	m/day	0.00015	0.00015	0.00015
k_y	m/day	0.00009	0.00009	0.00009
E_{50}^{ref}	kN/m^2	2,350	6,550	14,847
E_{oed}^{ref}	kN/m^2	1,600	2,380	4,267
E_{ur}^{ref}	kN/m^2	10,000	19,650	44,540
c_{ref}	kN/m^2	0.05	0.05	0.05
φ	°	24.1	29	33
Ψ	°	0	0	0
υ_{ur}	-	0.2	0.2	0.2
p^{ref}	kN/m^2	100	100	100
Power	-	1.0	1.0	1.0
K_0^{nc}	-	0.59	0.55	1.5
$c_{increment}$	kN/m^3	0	0	0
y_{ref}	m	0	0	0
C_k	-	1.00×10^{15}	1.00×10^{15}	1.00×10^{15}
R_f	-	0.7	0.95	0.96
$T_{strength}$	kN/m^2	0	0	0
R_{inter}	-	1	1	1
$\delta - \text{inter}$	m	0	0	0

doi:10.6342/NTU201900743

Table 2.4 Wall rigidity values used in finite-element models
(Bryson et al., 2012)

Model	α	$\alpha \times EI$ (kN·m^2/m)
1-7	1	540,675.00
8	0.05	27,033.75
9	0.1	54,067.50
10	0.25	135,168.75
11	0.5	270,337.50
12	5	2,703,375.00
13	10	5,406,750.00
14	25	13,516,875.00
15	100	54,067,500.00
16	250	135,168,750.00

doi:10.6342/NTU201900743

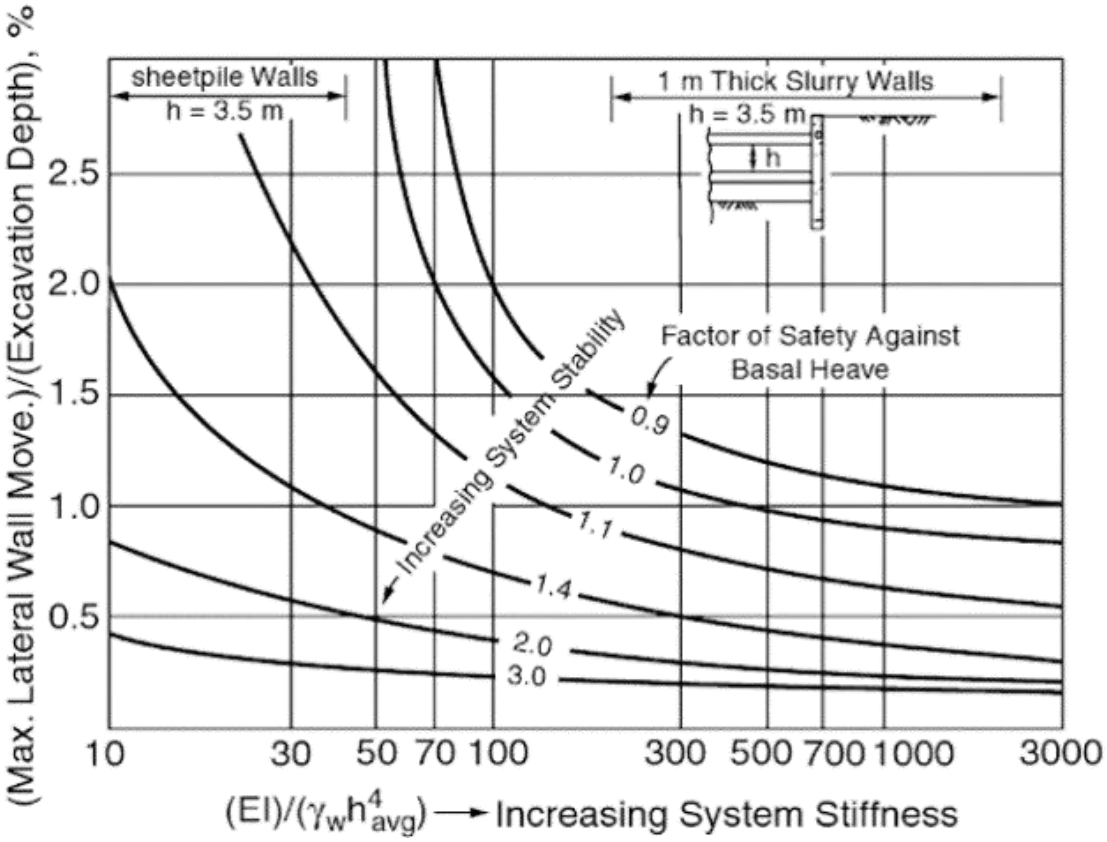

Figure 2.1 Relationship between maximum wall movement and system stiffness (Clough et al., 1989)

doi:10.6342/NTU201900743

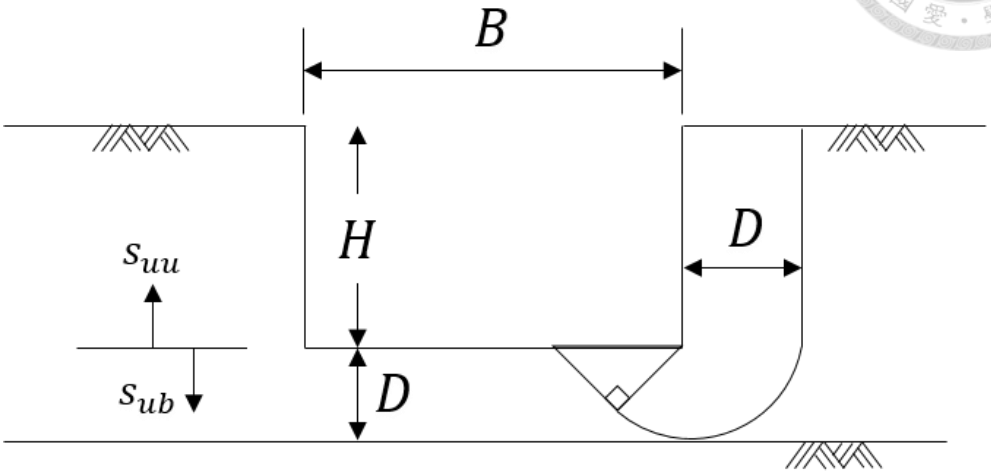

(a) D $< \left(\sqrt{2}/2\right)B$

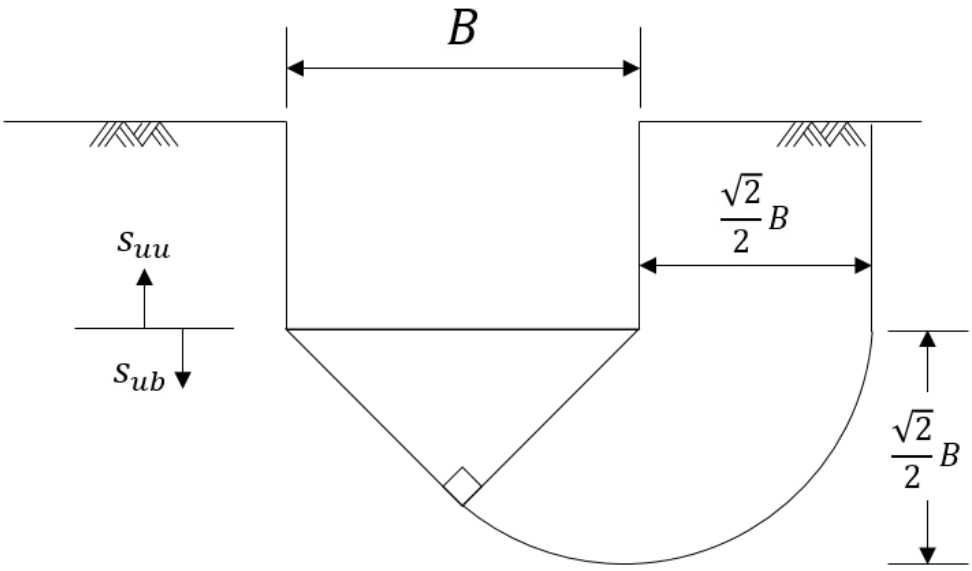

(b) D $> \left(\sqrt{2}/2\right)B$

Figure 2.2 Factor of safety against basal heave (Terzaghi 1943)

doi:10.6342/NTU201900743

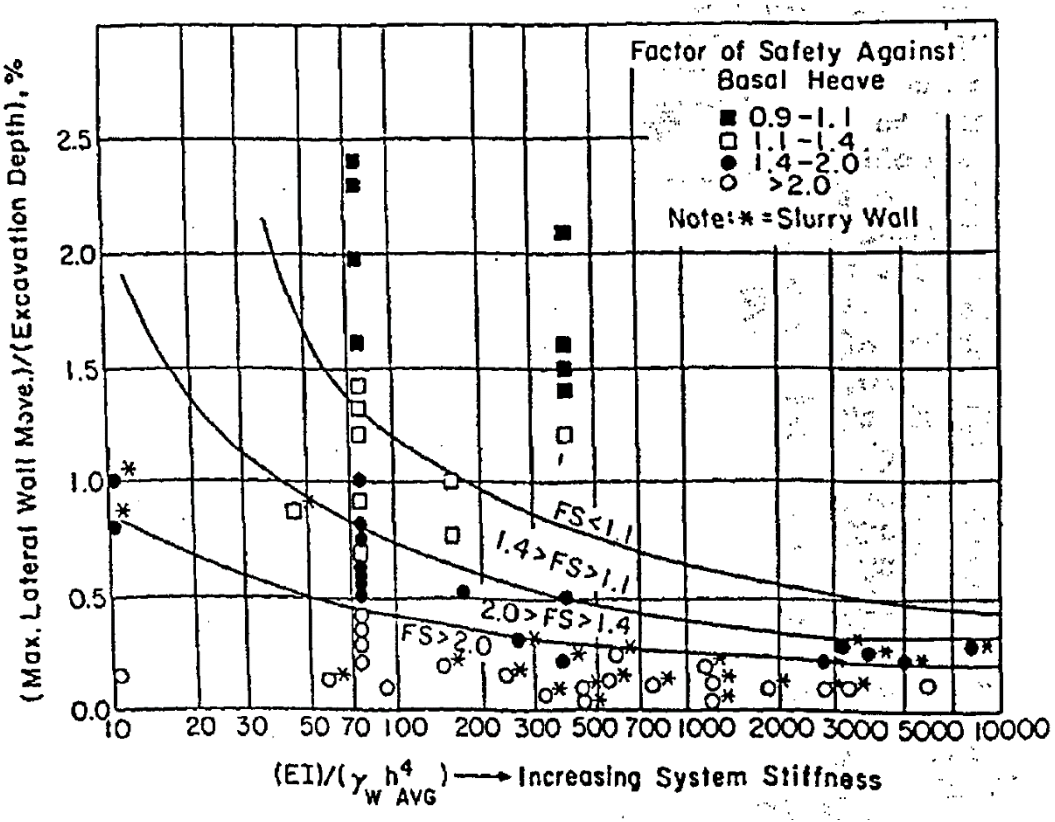

Figure 2.3 Comparison of chart solution for support system movements in clays and case history data
(Clough et al., 1989)

doi:10.6342/NTU201900743

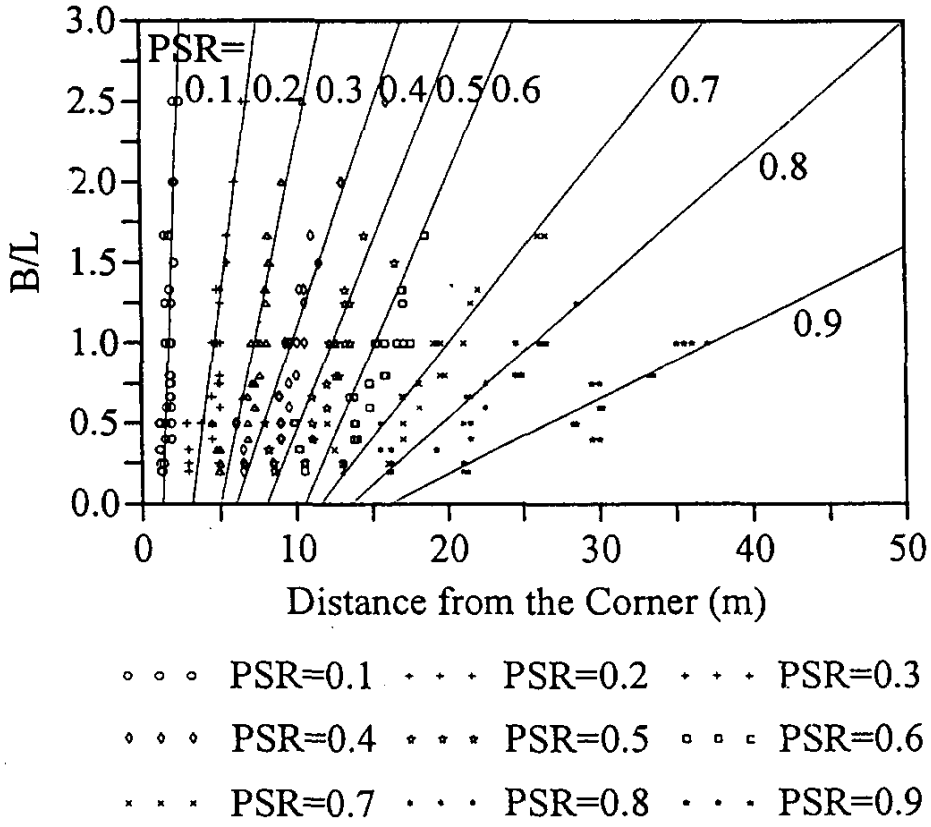

Figure 2.4 Relationship between ratio of the excavation geometry and distance from corner for various PSR
(Ou et al., 1996)

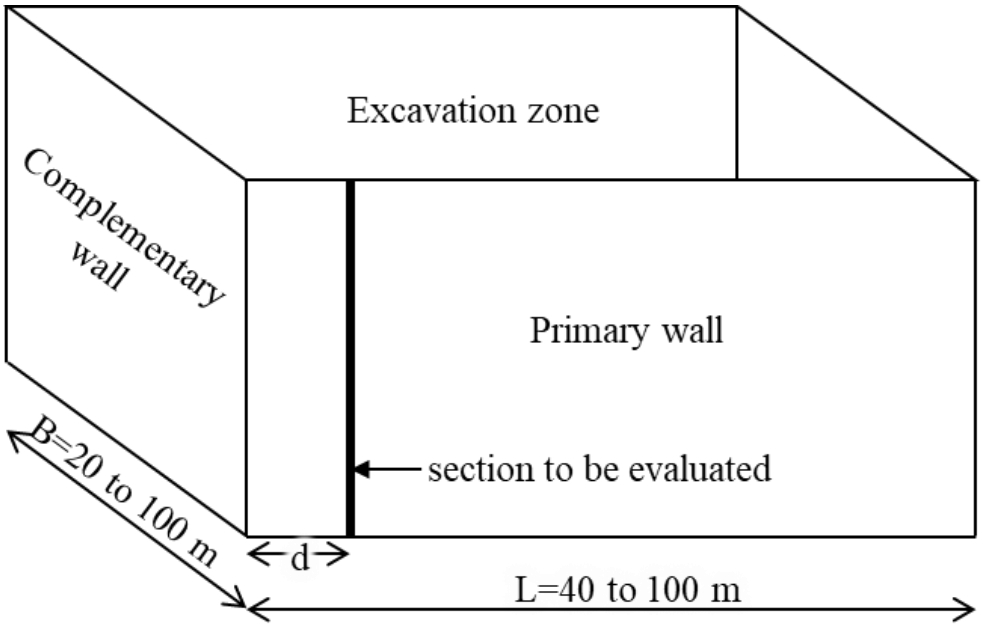

Figure 2.5 Definition of the excavation length L, the excavation width B and distance from the evaluated section to corner
(Ou et al.,1996)

doi:10.6342/NTU201900743

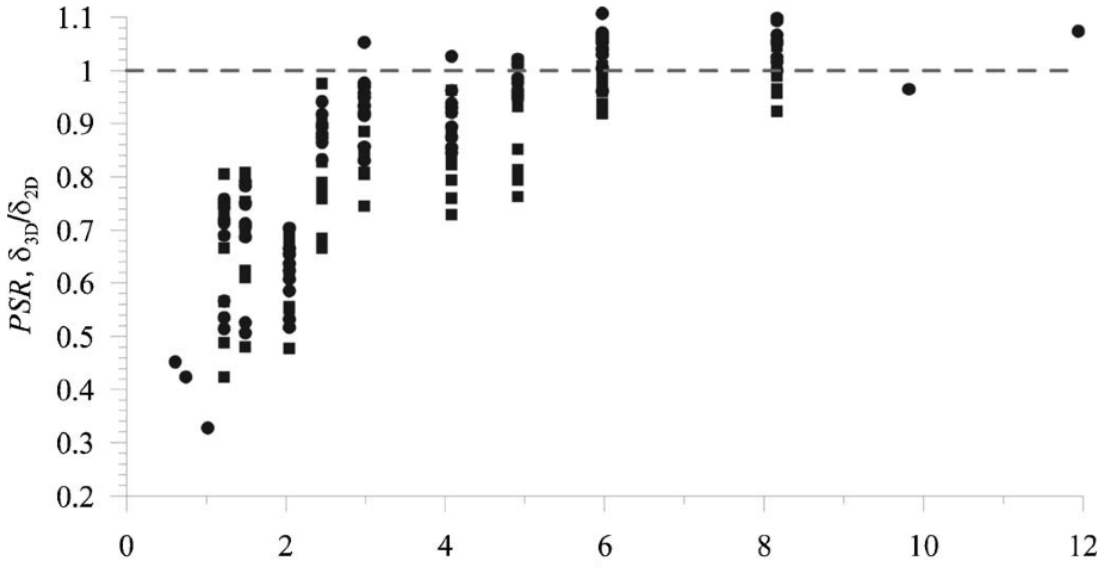

(a) L/H_e

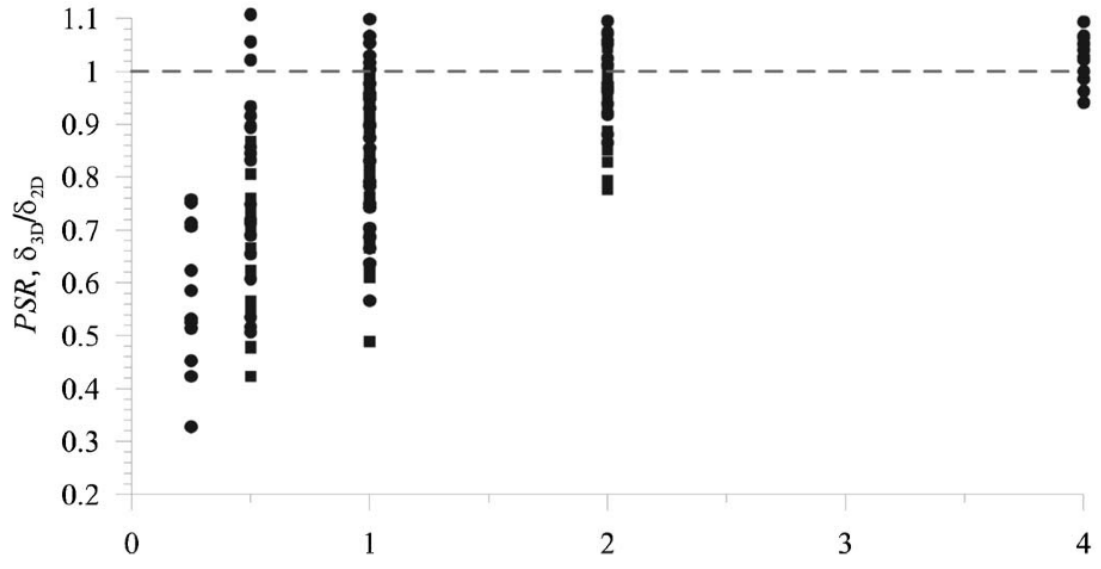

(b) L/B

Figure 2.6 Effect of plan dimensions and excavation depth on PSR (Finno et al., 2007)

doi:10.6342/NTU201900743

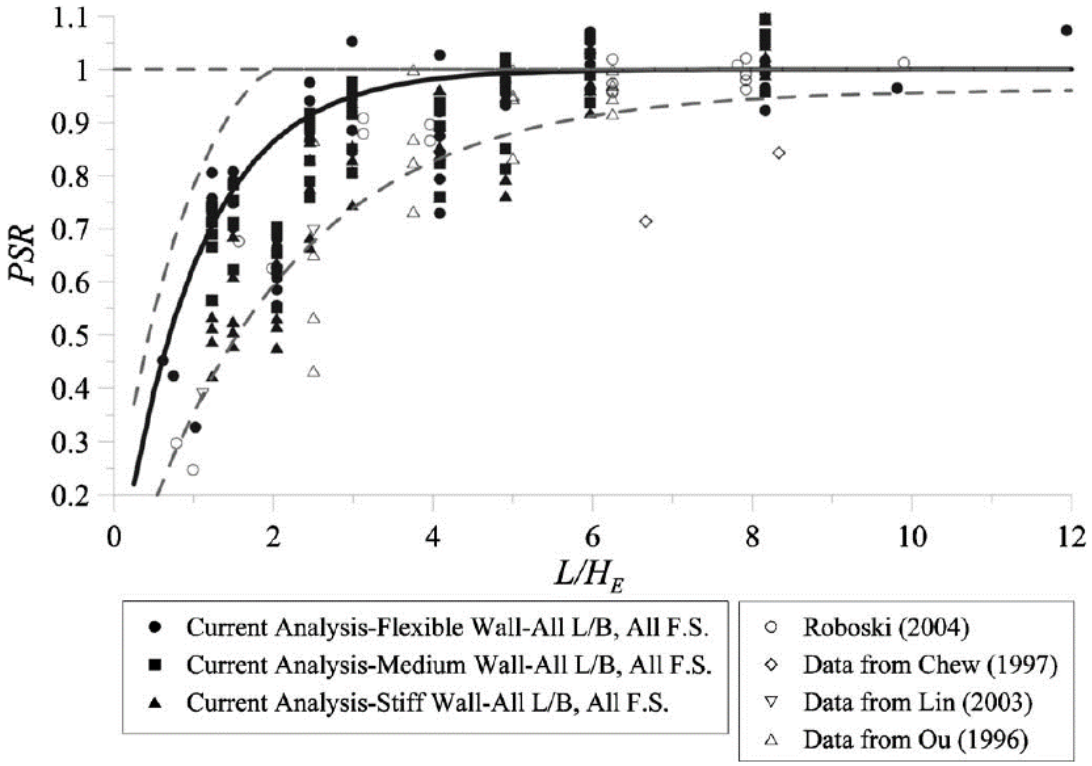

Figure 2.7 Comparison between published data and results of parametric study (Finno et al., 2007)

doi:10.6342/NTU201900743

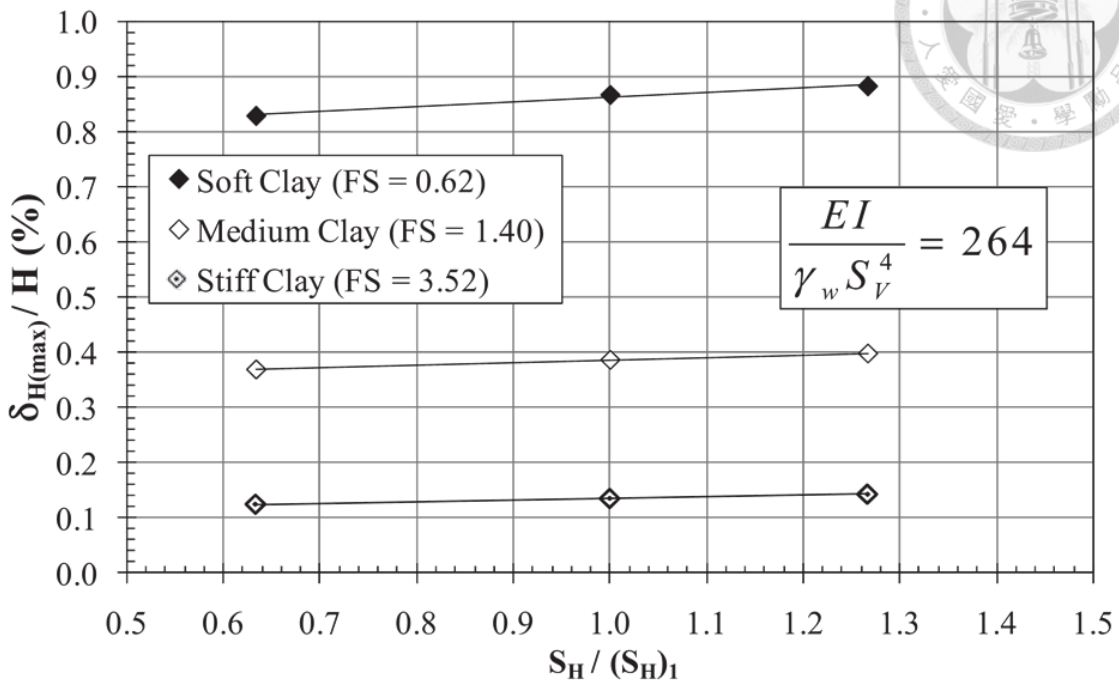

(a) Variation of the horizontal spacing

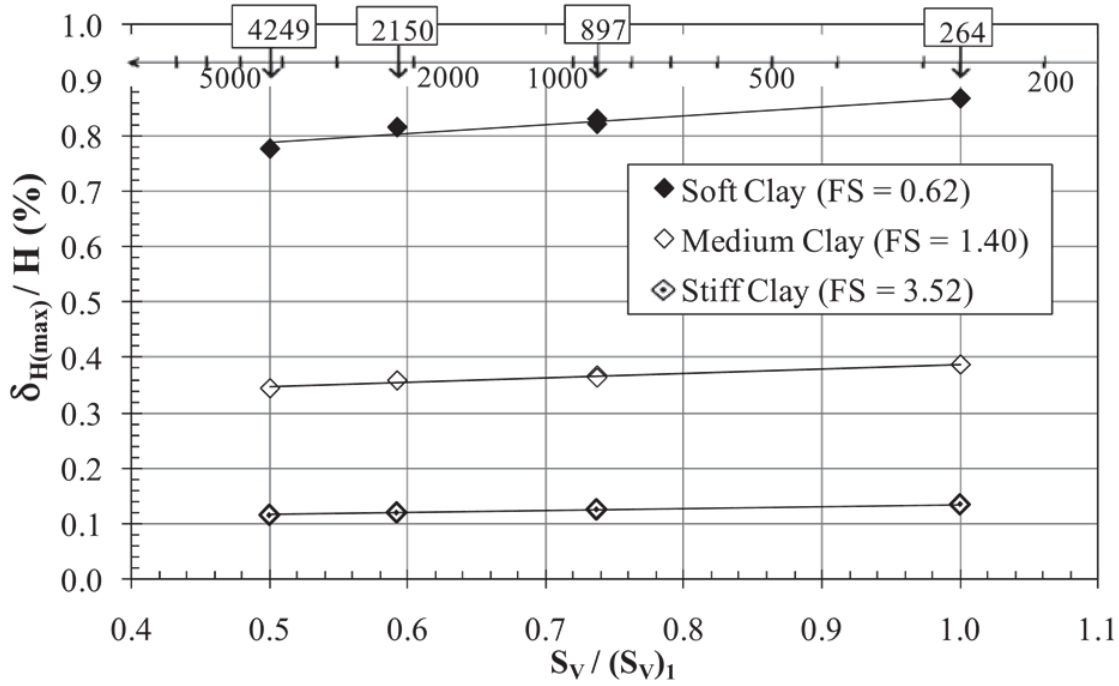

(b) Variation of the vertical spacing

Figure 2.8 Influence of support spacing on lateral deformations (Bryson et al., 2012)

doi:10.6342/NTU201900743

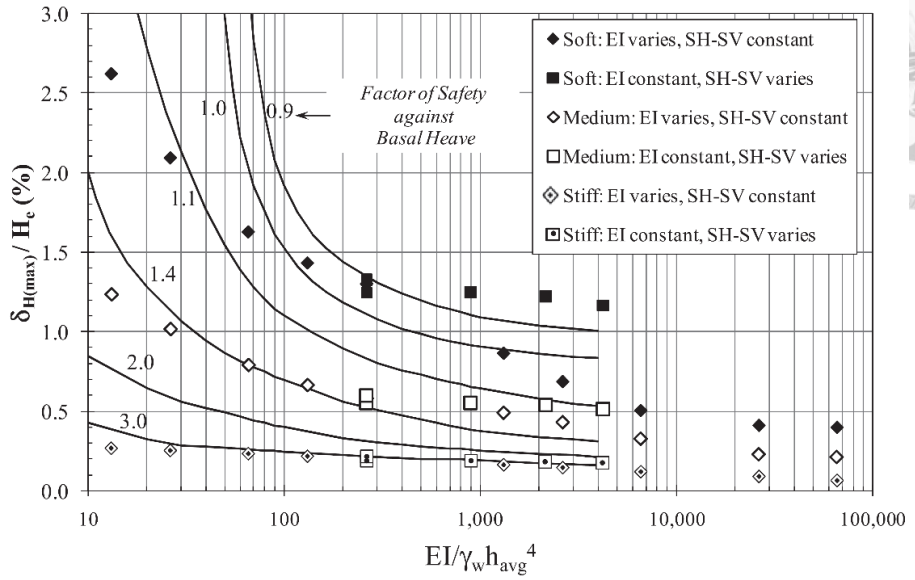

Figure 2.9 Comparison of the parametric studies with the Clough's design chart (Bryson et al., 2012)

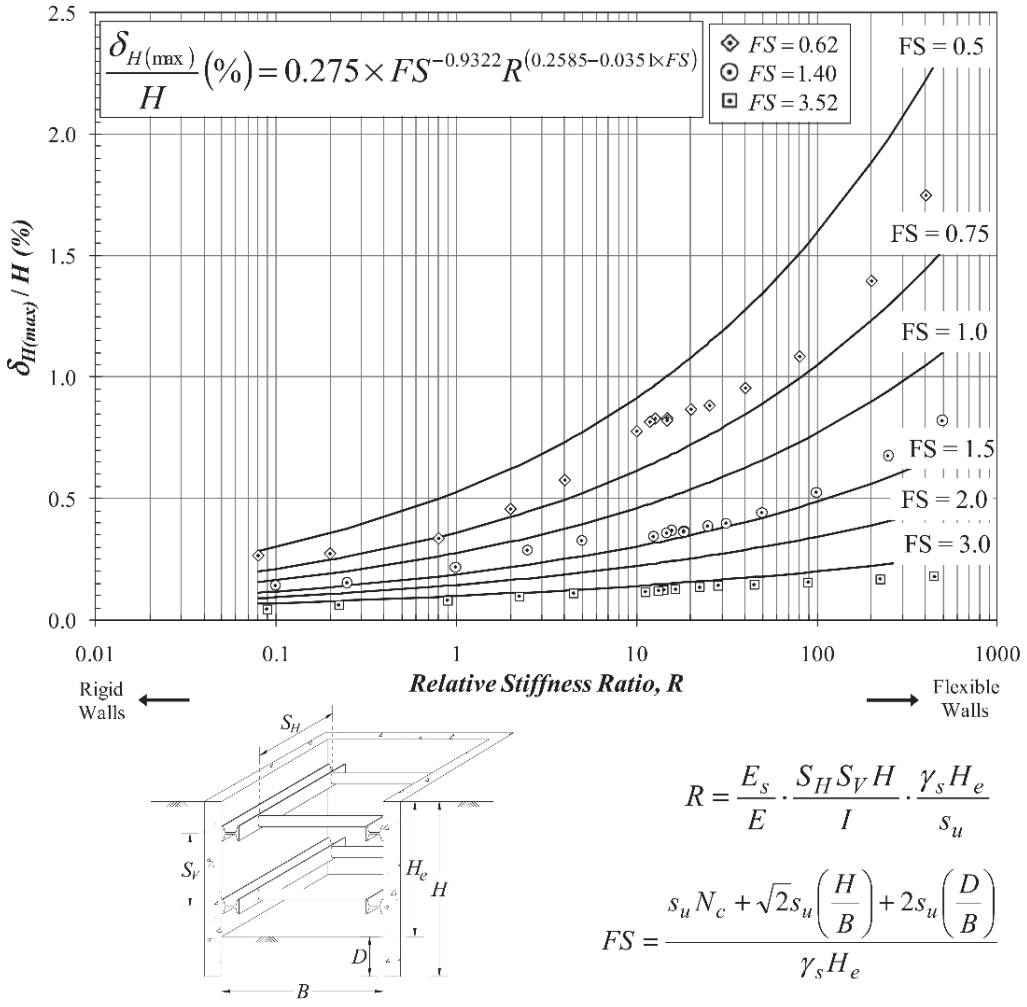

Figure 2.10 Relative stiffness ratio design chart (Bryson et al., 2012)

doi:10.6342/NTU201900743

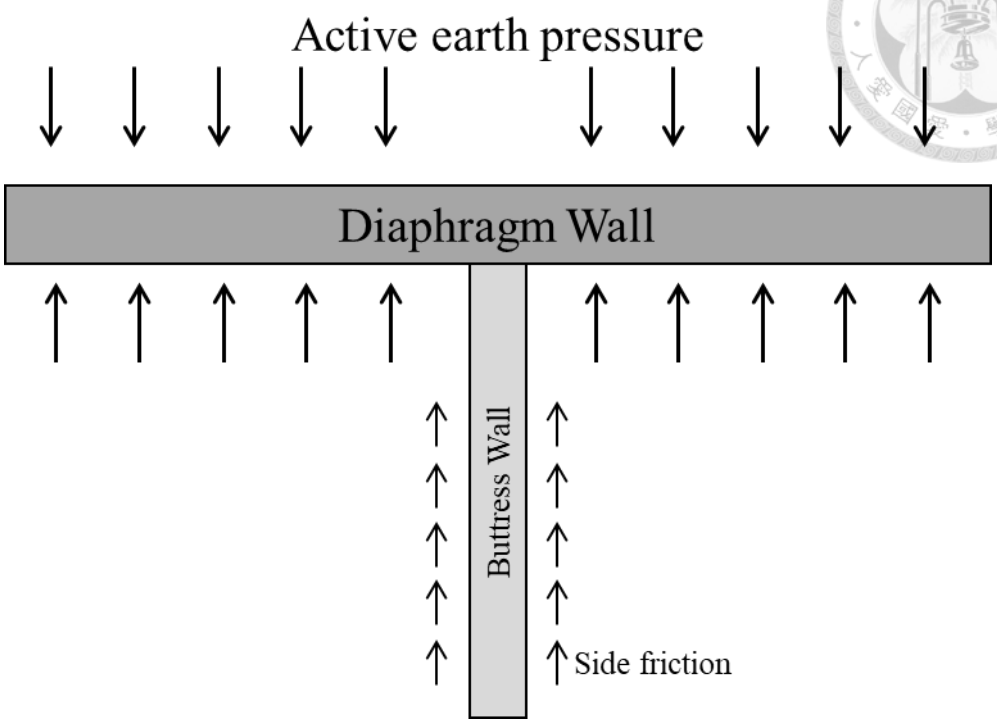

Figure 2.11 Basic configuration of buttress wall

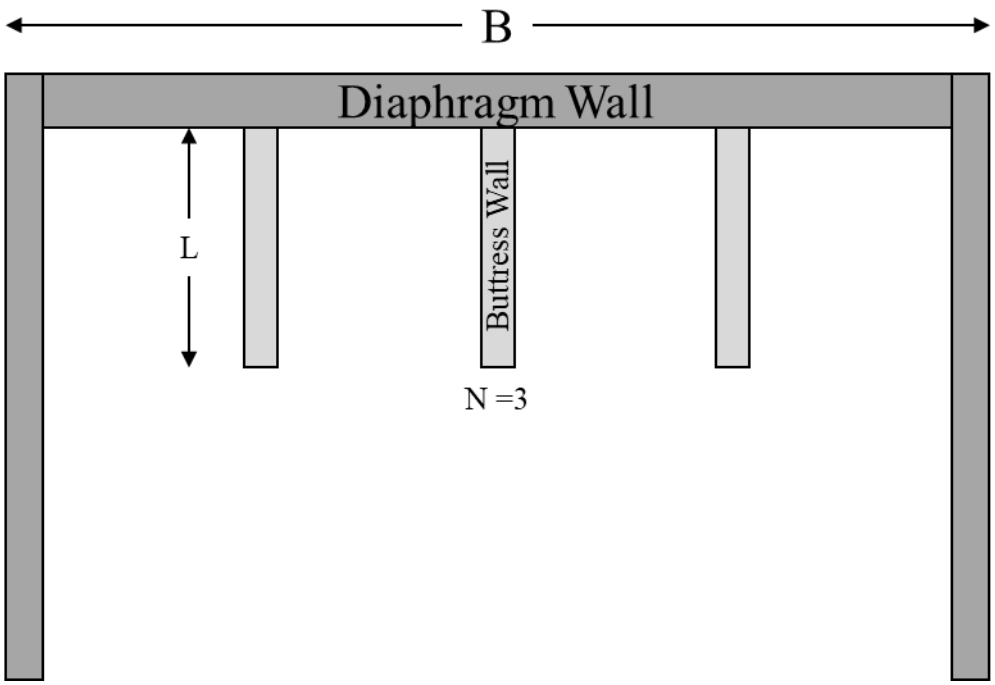

Figure 2.12 Input parameters for simplified approach

doi:10.6342/NTU201900743

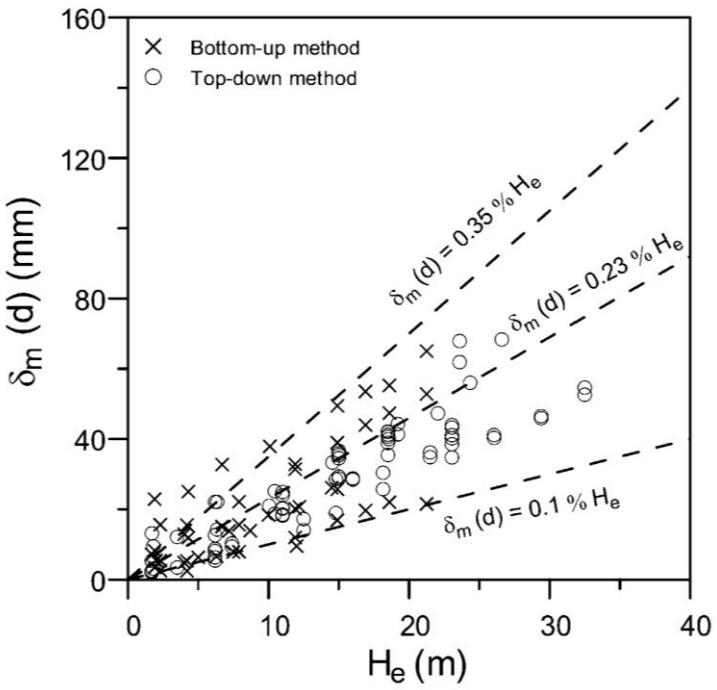

(a) With cross wall cases

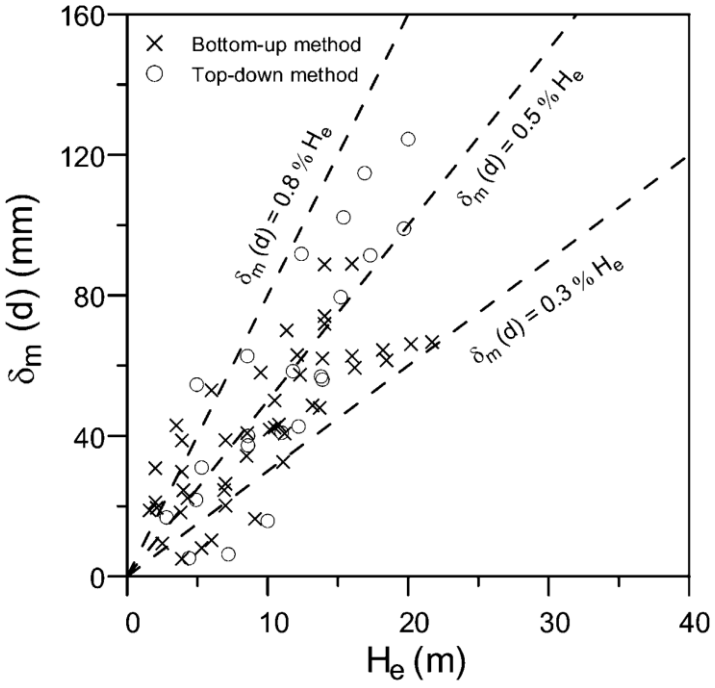

(b) Without cross wall cases

Figure 2.13 H_e versus $\delta_m(d)$ for excavations (Wu et al. 2013)

doi:10.6342/NTU201900743

Chapter 3 Case Histories

In chapter 3, it is to be demonstrated by three case histories that the presence of cross walls has significant influence on the deflection of retaining wall. These three case histories had all been completed, and the wall deformations had been back calculated by the three-dimensional numerical finite element program PLAXIS 3D. Two kinds of numerical analyses were performed, one with the effect of cross walls, while the other ignoring the effect of cross walls. These numerical results are compared with the field observation and the estimated values obtained from Clough's chart shown in Figure 2.1.

Essentially, the numerical results ignoring the effect of cross walls should be similar with the values estimated by Clough's chart, as Clough's original scheme lacks the effect of cross wall. On the other hand, the numerical results considering the effect of cross walls should be comparable to the field observation, because the three-dimensional numerical model is thought to closely simulate the in-situ condition. The details of each case history is described in following sections, including the excavation sequence, plan layout of project site, the selection of parameters for numerical analyses and the construction of numerical model, etc.

doi:10.6342/NTU201900743

3.1 Case A

3.1.1 Project overview

Case A locates at Da-an District of Taipei City, and details of project can be found in Hsieh et al. (2017). Case A project is a 17-story office building with 4 levels of basement. The excavation zone is a polygon with a maximum length and width of 40 m and 38 m, respectively. The excavation was carried out using the bottom-up method in 6 excavation stages, and the excavation depth was 17.1 m.

Since the excavation site is located in Taipei, the subsurface consists mostly of clayey soil. The soil stratigraphy of the site consists of eight soil layers underlain by a dense gravel layer at a depth of 56.1 m. The top layer is a 3.5-m thick clay layer. The second layer is a 5.8-m silty sand with a SPT-N value of 8. The third layer is a 14.9-m thick clay layer. The undrained shear strength (s_u) of the third layer is considered to increase with the effective overburden pressure (σ_v'), and a ratio of 0.18 is used between s_u and σ_v', i.e., $s_u = 0.18\sigma_v'$. The ratio is called the undrained shear strength ratio (s_u/σ_v'). The fourth layer is a 6.2-m thick clay with $s_u/\sigma_v' = 0.22$. The fifth layer is a 2.4-m thick silty sand with a SPT-N value of 9. The sixth layer is a 12.6-m thick clay with $s_u/\sigma_v' = 0.25$. The seventh layer is a 3-m clay with $s_u/\sigma_v' = 0.25$. The eighth layer is a 7.7-m clay with $s_u/\sigma_v' = 0.28$. Underlain the soft soil layer is a very dense layer comprises mainly of sandy gravel with a SPT-N value of more than 100. The simplified

doi:10.6342/NTU201900743

soil profile and soil parameters are presented in Table 3.1 and Table 3.2, respectively. The ground water level was at 2 m below the ground surface.

The diaphragm wall was 0.8 m in thickness and 34 m in depth together with five levels of H-steel bracing as the retaining system. The typical horizontal spacing of H-steel bracing is 6 m, and each level of bracing was preloaded to 50% of its allowable axial capacity. The horizontal bracings were installed stage by stage in a bottom-up excavation scheme and pre-stressed to design values immediately after installation. Auxiliary measure in the form of cross walls were adopted to reduce the wall deflection. Depth of the cross wall extended from GL. 0 m to GL. -34 m. The cross walls above the excavation surface would be removed by step-by-step excavation. There were six inclinometer casings installed in the perimeter diaphragm wall to monitor the wall deflection for each excavation stage. The layout of 4 cross walls and 6 inclinometer casings are shown in Figure 3.1. The excavation sequence of Case A is shown in Figure 3.2, including the sizes and preloads of horizontal struts.

3.1.2 PLAXIS simulation

1. Boundary condition

For the domain of the analysis model, there are two methods to calculate the domain size in the finite element software PLAXIS 3D. One is that the boundary of the domain in x-direction and y-direction extended seven times of the excavation depth suggested by

doi:10.6342/NTU201900743

Khoiri and Ou (2013). As shown in Figure 3.3, a full model was established, including the whole analysis domain and the excavation model. In Case A, the domain size is 400 m by 400 m, it is about eleven times of the excavation depth.

2. Soil parameters

The Mohr-Coulomb Model was used in the numerical analyses with the parameters listed in Table 3.1 and Table 3.2. An effective stress analysis under drained condition was used for sand layer, while a total stress analysis under undrained condition (*Undrained C*) was used for clay layer. The undrained condition in Mohr-Coulomb Model has three types, A, B and C, which are used for the undrained or short-term material. *Undrained A* is performed by the material behavior in which stiffness and strength are defined in terms of effective properties, while *Undrained B* is performed by the material in which stiffness is defined in terms of effective properties and strength is defined as undrained shear strength. *Undrained C* is performed by the material behavior in which stiffness and strength are defined in terms of undrained properties. In the drained condition, the material parameters for the Mohr-Coulomb Model are the effective Young's modulus (E'), effective Poisson ratio (ν'), effective cohesion (c') and effective friction angle (ϕ'). The effective Young's modulus of sand layer was determined by the following empirical equation, which was suggested by Hsiung (2009).

$$E' = 2000N \ \text{(kPa)} \tag{3.1}$$

doi:10.6342/NTU201900743

where N is the blow count of standard penetration test (SPT). For *Undrained C* of undrained condition, the parameters required are the undrained Young's modulus (E_u), undrained Poisson ratio (ν_u), undrained shear strength (s_u) and friction angle ($\phi_u = 0$). The undrained Young's modulus of clay layer was obtained by the following empirical equation reported by Bowles (1996), Lim et al. (2010), Likitlersuang et al. (2013), Khoiri and Ou (2013).

$$E_u = 500 s_u \ \text{(kPa)} \tag{3.2}$$

3. Structural parameters

Table 3.3 and Table 3.4 list the input parameters of the diaphragm wall, cross wall and floor slabs. Diaphragm wall, cross wall and floor slabs are regarded as plate elements in PLAXIS 3D. The Young's modulus of diaphragm wall, cross wall and floor slabs are estimated as suggested by ACI code or Construction and Planning Agency, MOI (2011):

$$E = 4700\sqrt{f_c'} \ \text{(MPa)} \tag{3.3}$$

$$E = 15000\sqrt{f_c'} \ \text{(kgf/cm}^2\text{)} \tag{3.4}$$

where f_c' is the compressive strength of the concrete.

Table 3.5 shows the input parameters of the H-steel bracing. In the numerical analyses, the H-steel bracings are regarded as node-to-node anchor elements. According to the AISC standard or Construction and Planning Agency, MOI (2011), the Young's modulus of the H-steel is 2.04×10^6 $\text{(kgf/cm}^2\text{)}$.

doi:10.6342/NTU201900743

3.1.3 Comparison of results

In Case A, there are a total of four cross walls within the excavation zone. It is obvious that the wall deflection would be larger than the excavation with cross walls if the cross walls are ignored in numerical analysis. Situations with and without cross walls are both analyzed by the numerical code PLAXIS 3D. Figure 3.4 summarizes all results including field observations, numerical results with and without cross walls. The red and blue curves respectively represent the wall displacements with and without the effect of cross walls, and the blue curve exhibits larger wall deflection than the others. The diaphragm wall deflection would be pronouncedly refrained if the cross walls are implemented in the numerical model. The effect of cross walls on the suppression of wall deflection is obvious once the two numerical results are compared.

Table 3.6 and Figure 3.5 compare the maximum wall displacements including field data, two numerical results and the predictions by Clough's chart. The predictions from Clough's chart overestimate the wall displacements compared with the field performance and numerical results. Essentially, the numerical results without cross wall should be similar to the estimated results by Clough's chart. However, there is an obvious difference between these two results. The difference could be attributed to the three-dimensional effect in the excavation zone, which could not be reflected by Clough's chart.

doi:10.6342/NTU201900743

3.2 Case B

3.2.1 Project overview

Case B locates at Hsinyi District of Taipei City, and details of this project can be found in Hsieh et al. (2017). The Uni-President International Building (UPIB) is a 35-story building with 7 levels of basement. The excavation zone is a polygon with a maximum length and width of 122 m and 66 m, respectively. The excavation was carried out using the top-down method in 9 excavation stages, and the excavation depth was 32.5 m.

The soil stratigraphy of the site consists of five soil layers underlain by bedrock at a depth of 66.7 m. The top layer is a 3-m thick fill layer. The second layer is a 29.6-m thick silty clay layer with undrained shear strength ratio (s_u/σ_v') of 0.30. The third layer is an 18.4-m thick silty clay with undrained shear strength ratio of 0.33. The fourth layer is a 15.7-m thick silty sand with a SPT-N value of 12. The ground water level was at 3 m below the ground surface.

The diaphragm wall was 1.5 m in thickness and 57.5 in depth. Moreover, auxiliary measures in the form of cross walls and buttress walls were adopted to reduce the wall deflection. The 1-m thick cross walls were extended from GL. -1.5 m to GL. -45 m, and the 1-m thick buttress walls with 6, 12 and 15 m in length were extended from GL. -1.5 m to GL. -55 m. The buttress walls and cross walls above the excavation surface would

doi:10.6342/NTU201900743

be removed by step-by-step excavation. There were four inclinometers, SID-2, SID-4, SID-7 and SID-9, installed in the diaphragm wall at midpoint of each side to monitor the wall displacement for each excavation stage. The layout of 3 cross walls, 10 buttress walls and 4 inclinometers are shown in Figure 3.6. The excavation sequence of Case B is shown in Figure 3.7.

3.2.2 PLAXIS simulation

1. Boundary condition

The domain boundary in x-direction and y-direction extended beyond seven times of the excavation depth as suggested by Khoiri and Ou (2013). A full model was established as shown in Figure 3.8, including the whole analysis domain and the excavation model. In Case B, the domain size is 350 m by 350 m, it is about ten times of the excavation depth.

2. Soil parameters

In Case B, the Mohr-Coulomb Model was selected with the input parameters listed in Table 3.7 and Table 3.8. An effective Young's modulus was used for sandy gravel layer, and undrained Young' modulus was used for clay layers. The determination of the Young's modulus has been described in section 3.1.2.

3. Structural parameters

Table 3.9 to Table 3.11 list the structural parameters of the diaphragm wall, buttress

doi:10.6342/NTU201900743

wall, cross wall, slabs and H-steel bracings. Diaphragm wall, buttress wall, cross wall and floor slabs are regarded as plate elements, and the H-steel bracings are regarded as node-to-node anchor elements. The estimation of Young's modulus has been described in section 3.1.2.

3.2.3 Comparison of the results

In Case B, there are three cross walls and ten buttress walls installed in the excavation zone. Numerical simulations with and without cross walls were both conducted. Figure 3.9 summarizes all results including the field observations, the numerical results with and without cross walls. The numerical results are the wall displacements at the location of the inclinometer casings. The red and blue curves respectively represent the excavation behavior with and without the effect of cross walls. The blue curve shows larger wall deflection than the others. However, the numerical results with cross walls are slightly smaller than field observation. Since the cross walls are simulated in the analyses, the diaphragm wall deflection should be pronouncedly refrained. However, at the location of SI-7, the numerical results deviate from the field observation by a wide margin at the depth of 5 m to 10 m under the ground surface, the field curve appeared unreasonably distorted. At the location of SI-9, it has the largest wall deflection than the others. It is evident that the cross walls are effective in suppressing the wall deflection by comparing the two numerical results. The amount of reduction for all

doi:10.6342/NTU201900743

locations is close to 50% to 60% as presented in Table 3.12, which is enough to justify the effect of cross walls on limiting the excavation induced wall displacement.

Table 3.12 and Figure 3.10 show the maximum values of all results including field data, two numerical results and the results predicted by Clough's chart. The predictions by Clough's chart overestimate the wall displacements compared with the field observation, whereas the numerical results with the cross walls are close to the field data. Essentially, the numerical results without cross wall should be similar to the estimated values by Clough's chart. However, there is an obvious difference between these two results. The difference can be attributed to the fact that Clough's chart ignores the three-dimensional effect of a project site.

doi:10.6342/NTU201900743

3.3 Case C

3.3.1 Project overview

Case C locates at Shih-Lin District of Taipei City. The excavation zone is an irregular polygon with a maximum length and width of 47 m and 18 m, respectively. The project site was originally occupied by a 7-story building that the owners decided to demolish and replace it with a 14-story high-rise building. To fulfill the parking requirement of the new building, a 4-level of basement was needed with an excavation depth of 16.1 m using the bottom-up method in 5 excavation stages.

The soil stratigraphy of the site consists of a 3-m thick surface fill, followed by a thick clay layer, and underlain by andesite debris. The top layer is a 3-m thick fill layer. The second layer is a thick soft clay deposit with a depth varying from GL. -20 m to GL. -30 m, and the undrained shear strength ratio is about 0.24. The SPT-N values of this clay deposit increase from 2 at GL.-3 m to about 4 at the bottom elevation. Underlain the soft clay layer is a very dense layer comprises mainly of andesite debris. Depth of the andesite debris varies greatly from GL. -20 m to GL. -30 m. The SPT-N values of the very dense layer are more than 50, and it is regarded as the bearing stratum of the project site. The elevation contour of the andesite is shown in Figure 3.11, and simplified soil profile and soil parameters are presented in Table 3.13 and Table 3.14. The ground water level was located at 0.5 m below the ground surface.

doi:10.6342/NTU201900743

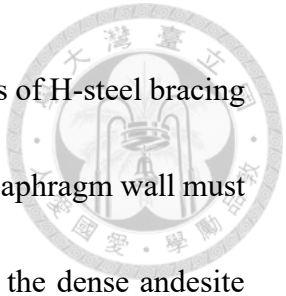

The diaphragm wall was 0.8 m in thickness together with 4 levels of H-steel bracing as the retaining system. It is worthy to mention that the depth of the diaphragm wall must be penetrated into the andesite debris at least 1.5 m. Embedment in the dense andesite debris is necessary as the diaphragm wall is required to provide adequate passive resistance to counter the active earth pressure on the retaining side. The diaphragm wall also serves as an integral part of the foundation system as it carries structural loads through columns embedded in the diaphragm wall. Four levels of horizontal bracing were installed stage by stage in the bottom-up method. The horizontal bracing consists of H-steel beams that were pre-stressed to design values immediately after installation. Moreover, auxiliary measures in the form of cross wall and buttress wall were adopted to reduce the wall deflection. The 0.8-m thick cross walls were extended from GL. -1.5 m to GL. -24.5 m, as a 0.8-m thick buttress wall was extended from GL. -1.5 m to GL. -23 m. The buttress walls and the cross walls above the excavation surface would be removed by step-by-step excavation. There were six inclinometer casings installed in the perimeter diaphragm wall to monitor the wall deflection for each excavation stage. The layout of 4 cross walls, 1 buttress wall, 6 inclinometer casings and the site plan are shown in Figure 3.12 and Figure 3.13. The structural parameters are listed in Table 3.15 and Table 3.16. As the existing adjacent buildings are at close proximity, the project owner and contractor were very conservative about the design and construction of the basement. Therefore, the

doi:10.6342/NTU201900743

structural engineers were asked to be cautious on the foundation and excavation design. The excavation sequence of Case C is shown in Figure 3.14, including the sizes and preloads of the horizontal struts.

3.3.2 PLAXIS simulation

1. Boundary condition

The domain boundaries in x-direction and y-direction should extend approximately seven times of the excavation depth as suggested by Khoiri and Ou (2013). A full model was established as shown in Figure 3.15, including the whole analysis domain and the excavation model. In Case C, the domain size is 350 m by 320 m, which is about eight times of the excavation depth, exceeding the requirements suggested by Khoiri and Ou (2013).

2. Soil parameters

In Case C, the Mohr-Coulomb Model was selected with the input parameters listed in Figure 3.13 and Figure 3.14. An effective Young's modulus was used for the first and third layer, while the undrained Young' modulus was used for the second clay layer. The estimation of the Young's modulus has been described in section 3.1.2.

3. Structural parameters

Table 3.15 and Table 3.16 summarized the input parameters of the diaphragm wall, buttress walls, cross walls and H-steel bracings. Diaphragm wall, buttress wall and cross

doi:10.6342/NTU201900743

wall are regarded as plate elements, and H-steel bracings are regarded as node-to-node anchor elements. The calculation of the Young's modulus has been described in section 3.1.2.

3.3.3 Comparison of results

In Case C, there are four cross walls installed within the excavation. Two conditions with and without the effect of cross walls are both considered in the numerical analyses. Figure 3.16 shows all results including the field observation, numerical results with and without cross walls. The numerical results are the wall displacements at the location of the inclinometer casings. The red and blue curves respectively represent the excavations with and without cross walls. The blue curve shows larger wall deflection than the others. With the cross walls incorporated in the numerical analyses, the diaphragm wall deflection should be refrained pronouncedly. At the locations of SI-1 and SI-4, the numerical results show very small wall movements. It is perhaps that SI-1 and SI-4 are significantly affected by corner effect, the wall deformations tend to be small anyway. It is evident that the cross walls are effective in suppressing the wall deflection by comparing the two numerical results. The amount of reduction is also presented in Table 3.18. The amount of reduction for most locations is close to 80% to 90% except for the locations of SI-1 and SI-4, which is enough to justify the effect of cross walls on limiting the excavation induced wall displacement.

doi:10.6342/NTU201900743

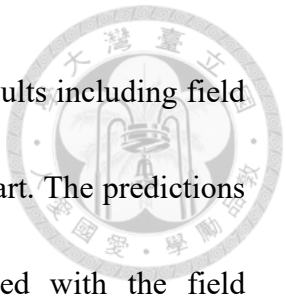

Table 3.18 and Figure 3.17 show the maximum values of all results including field data, two numerical results and the results predicted by Clough's chart. The predictions by Clough's chart overestimate the wall displacements compared with the field performance, whereas the numerical results with the cross walls are close to the field data. Essentially, the numerical results without cross wall should be similar to the estimated values by Clough's chart. However, there is an obvious difference between these two results. The difference can be attributed to that Clough's chart ignores the three-dimensional effect of a project site.

3.4 Summary

As revealed by the three case studies, the effect of cross wall plays an important role in limiting the wall displacements. However, the three-dimensional effect of cross wall can only be quantified by using the complex numerical analyses. In practice, one can use simplified methods to estimate the three-dimensional effect induced by cross walls, but the accuracies may be inadequate. The use of 3D numerical program requires a well-trained engineer to conduct the analyses, and it is not a feasible option for routine excavation designs. The Clough's chart is easy to use, but poor accuracies are observed if the presence of cross walls is ignored. It is believed that revising the Clough's chart to incorporate the effect of cross walls may serve as a good tool for engineers to deal with the task for estimating wall displacement when cross walls are implemented in the design.

doi:10.6342/NTU201900743

Table 3.1 Properties for undrained cohesive soils for Case A

Type	Depth from	Depth to	γ_s	N	s_u	ϕ'	E_u	ν_u	R_{int}
	m	m	kN/m^3	-	kPa	º	kPa	-	-
1CL	0.0	-3.5	18.7	5	54.0	0	27000	0.495	0.67
3CL	-9.3	-24.2	18.6	3	32.4	27	16200	0.495	0.67
4CL	-24.2	-30.4	18.6	6	58.9	30	37250	0.495	0.67
6CL	-32.8	-45.4	18.3	10	98.1	31	49050	0.495	0.67
7CL	-45.4	-48.4	18.2	15	107.9	0	53950	0.495	1
8CL	-48.4	-56.1	19.1	19	135.4	0	67700	0.495	1

Table 3.2 Properties for drained non-cohesive soils for Case A

Type	Depth from	Depth to	γ_s	N	c'	ϕ'	E'	ν'	R_{int}
	m	m	kN/m^3	-	kPa	º	kPa	-	-
2SM	-3.5	-9.3	20.0	8	0	31	16000	0.3	0.67
5SM	-30.4	-32.8	18.7	9	0	31	18000	0.3	0.67
9GM	-56.1	-59.9	21.6	>100	0	37	912000	0.3	1

doi:10.6342/NTU201900743

Table 3.3 Structural parameters for Case A

Type	Depth from	Depth to	t	γ_s	fc'	E	I	ν
	m	m	m	kN/m^3	MPa	kPa	m^4	-
DW	0.0	-34.0	0.8	23.56	27.5	2.46E+07	0.04267	0.2
CWa	0.0	-16.1	0.8	23.56	13.7	1.74E+07	0.04267	0.2
CWb	-16.1	-34.0	0.8	23.56	24.0	2.30E+07	0.04267	0.2

Note:
(1) DW: diaphragm wall
(2) CWa: cross wall above the excavation surface
(3) CWb: cross wall below the excavation surface

Table 3.4 Floors parameters for Case A

Type	Depth	t	fc'	E	I	ν
	m	m	MPa	kPa	m^4	-
F1	0.00	0.25	27.5	2.46E+07	0.00130	0.2
B1	-4.80	0.40	27.5	2.46E+07	0.00533	0.2
B2	-8.00	0.40	27.5	2.46E+07	0.00533	0.2
B3	-11.20	0.40	27.5	2.46E+07	0.00533	0.2
B4	-14.40	0.20	27.5	2.46E+07	0.00067	0.2
MAT	-17.10	0.60	27.5	2.46E+07	0.01800	0.2

doi:10.6342/NTU201900743

Table 3.5 Strut parameters for Case A

Type	Depth	E	A	EA	EA	Preload (each strut)
	m	kgf/cm^2	cm^2	kgf	kN	kN
H300 × 300 × 10 × 15	-1.0	2.04E+06	118.4	2.42E+08	2.37E+06	490
H400 × 400 × 13 × 21	-4.1	2.04E+06	218.7	4.46E+08	4.38E+06	980
2H400 × 408 × 21 × 21	-7.3	2.04E+06	501.4	1.02E+09	1.00E+07	980
2H400 × 408 × 21 × 21	-10.5	2.04E+06	501.4	1.02E+09	1.00E+07	980
2H400 × 408 × 21 × 21	-13.7	2.04E+06	501.4	1.02E+09	1.00E+07	980

Table 3.6 Comparison of estimated wall displacements for Case A

SI	F_b	S	δ_{Clough} / H_e	δ_{field} / H_e	δ_{3D_with} / H_e	$\delta_{3D\_without} / H_e$	Reduction (δ_{3D_with}&$\delta_{3D\_without}$)
	-	-	%	%	%	%	%
1	0.97	1022	1.050	0.009	0.021	0.119	82.29
3	0.96	1022	0.950	0.024	0.076	0.345	78.09
4	0.97	1022	1.050	0.023	0.105	0.370	71.72
5	0.95	1022	0.950	0.045	0.072	0.345	79.08

doi:10.6342/NTU201900743

Table 3.7 Properties for undrained cohesive soils for Case B

Type	Depth from	Depth to	γ_s	N	s_u	ϕ'	E_u	$E_{u,inc}$	$s_{u,inc}$	v_u	R_{int}
	m	m	kN/m^3	-	kPa	º	kPa	kPa/m	kPa/m	-	-
1CL	0	-3.0	18.25	>50	15	0	7500	-	-	0.495	0.67
2CL	-3.0	-32.6	18.05	4	34	0	17000	940	1.88	0.495	0.67
3CL	-32.6	-51.0	18.74	22	114	0	57000	1066	2.13	0.495	0.67

Table 3.8 Properties for drained non-cohesive soils for Case B

Type	Depth from	Depth to	γ_s	N	c'	ϕ'	E'	v'	R_{int}
	m	m	kN/m^3	-	kPa	º	kPa	-	-
4GW	-51.0	-67.0	19.62	>50	0	36.5	912000	0.3	0.67

Table 3.9 Structural parameters for Case B

Type	Depth from	Depth to	t	γ	fc'	E	I	v
	m	m	m	kN/m^3	MPa	kPa	m^4	-
DW	0.0	-57.5	1.5	23.56	27.5	2.46E+07	0.2813	0.2
CWa	-1.5	-32.5	1.0	23.56	13.7	1.74E+07	0.0833	0.2
CWb	-32.5	-45.0	1.0	23.56	24.0	2.30E+07	0.0833	0.2
BWa	-1.5	-32.5	1.0	23.56	13.7	1.74E+07	0.0833	0.2
BWb	-32.5	-55.0	1.0	23.56	24.0	2.30E+07	0.0833	0.2

doi:10.6342/NTU201900743

Table 3.10 Floor parameters for Case B

Type	Depth	t	γ	fc'	E	I	ν
	m	m	kN/m^3	MPa	kPa	m^4	-
F1	0.0	0.25	23.56	27.5	2.46E+07	0.0013	0.2
B1	-4.4	0.20	23.56	27.5	2.46E+07	0.0007	0.2
B2	-9.0	0.61	23.56	27.5	2.46E+07	0.0189	0.2
B3	-13.4	0.61	23.56	27.5	2.46E+07	0.0189	0.2
B4	-16.8	0.61	23.56	27.5	2.46E+07	0.0189	0.2
B5	-20.2	0.61	23.56	27.5	2.46E+07	0.0189	0.2
B6	-24.8	0.61	23.56	27.5	2.46E+07	0.0189	0.2
B7	-29.4	0.20	23.56	27.5	2.46E+07	0.0007	0.2
MAT	-32.5	0.60	23.56	27.5	2.46E+07	0.0180	0.2

Table 3.11 Strut parameters for Case B

Type	Depth from	Depth to	E	A	EA	Preload (each strut)
	m	m	kgf/cm^2	cm^2	kN	kN
H400 × 400 × 13 × 21	-24.8	-29.4	2.04E+06	218.7	4.38E+06	850

Table 3.12 Comparison of estimated wall displacements for Case B

SI	F_b	S	δ_{Clough} / H_e	δ_{field} / H_e	δ_{3D_with} / H_e	$\delta_{3D\_without} / H_e$	Reduction (δ_{3D_with}&$\delta_{3D\_without}$)
	-	-	%	%	%	%	%
2	0.96	2599	0.85	0.172	0.137	0.366	62.42
4	0.96	2599	0.85	0.170	0.131	0.260	49.55
7	0.96	2599	0.85	0.208	0.128	0.355	63.90
9	0.96	2599	0.85	0.270	0.170	0.333	48.84

doi:10.6342/NTU201900743

Table 3.13 Properties for undrained cohesive soils for Case C

Type	Depth from	Depth to	γ_s	N	s_u	ϕ'	E_u	v_u	R_{int}
	m	m	kN/m^3	-	kPa	º	kPa	-	-
2CL	-3.5	-4.0	16.87	2	7.79	0	3897	0.495	0.67
2CL	-4.0	-12.0	16.87	2	21.35	0	10677	0.495	0.67
2CL	-12.0	-18.0	16.87	2	31.53	0	15763	0.495	0.67
2CL	-18.0	-20.0	16.87	2	34.92	0	17458	0.495	0.67
2CL	-20.0	-23.0	16.87	2	40.00	0	20001	0.495	0.67

Table 3.14 Properties for drained non-cohesive soils for Case C

Type	Depth from	Depth to	γ_s	N	c'	ϕ'	E'	v'	R_{int}
	m	m	kN/m^3	-	kPa	º	kPa	-	-
1SF	0.0	-3.5	16.68	4	0	28	8000	0.3	0.67
3ROCK	-23.0	-30.0	22.56	>50	0	38	912000	0.3	0.67

Table 3.15 Structural parameters for Case C

Type	Depth from	Depth to	t	γ	fc'	E	I	v
	m	m	m	kN/m^3	MPa	kPa	m^4	-
DW	0	-	0.8	23.56	27.5	2.46E+07	0.04267	0.2
CWa	0	-16.1	0.8	23.56	13.7	1.74E+07	0.04267	0.2
CWb	-16.1	-24.5	0.8	23.56	27.5	2.46E+07	0.04267	0.2
BWa	0	-16.1	0.8	23.56	13.7	1.74E+07	0.04267	0.2
BWb	-16.1	-23.0	0.8	23.56	27.5	2.46E+07	0.04267	0.2

doi:10.6342/NTU201900743

Table 3.17 Strut parameters for Case C

Type	Depth	E	A	EA	EA	Preload (each strut)
	m	kgf/cm^2	cm^2	kgf	kN	kN
H400 × 400 × 13 × 21	-1.45	2.04E+06	218.7	4.46E+08	4.38E+06	740
2H400 × 400 × 13 × 21	-4.7	2.04E+06	437.4	8.92E+08	8.75E+06	1600
2H400 × 400 × 13 × 21	-8.1	2.04E+06	437.4	8.92E+08	8.75E+06	1600
2H400 × 408 × 21 × 21	-12.1	2.04E+06	501.4	1.02E+09	1.00E+07	2400

Table 3.18 Comparison of estimated wall displacements for Case C

SI	F_b	S	δ_{Clough} / H_e	δ_{field} / H_e	δ_{3D_with} / H_e	$\delta_{3D\_without} / H_e$	Reduction (δ_{3D_with}&$\delta_{3D\_without}$)
	-	-	%	%	%	%	%
1	0.94	675	1.30	0.024	0.051	0.055	7.69
2	0.92	675	1.10	0.026	0.120	0.538	77.74
3	0.87	675	1.28	0.023	0.077	0.407	80.98
4	0.91	675	1.10	0.005	0.043	0.063	32.82
5	0.82	675	1.30	0.019	0.092	0.547	83.12
6	0.82	675	1.30	0.019	0.043	0.490	91.24

doi:10.6342/NTU201900743

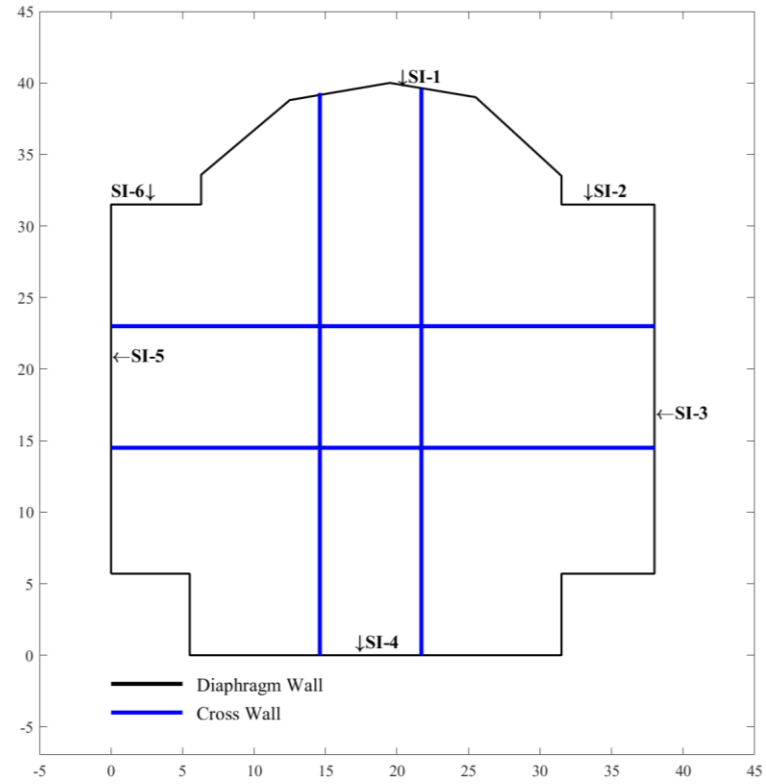

Figure 3.1 Site plan for Case A

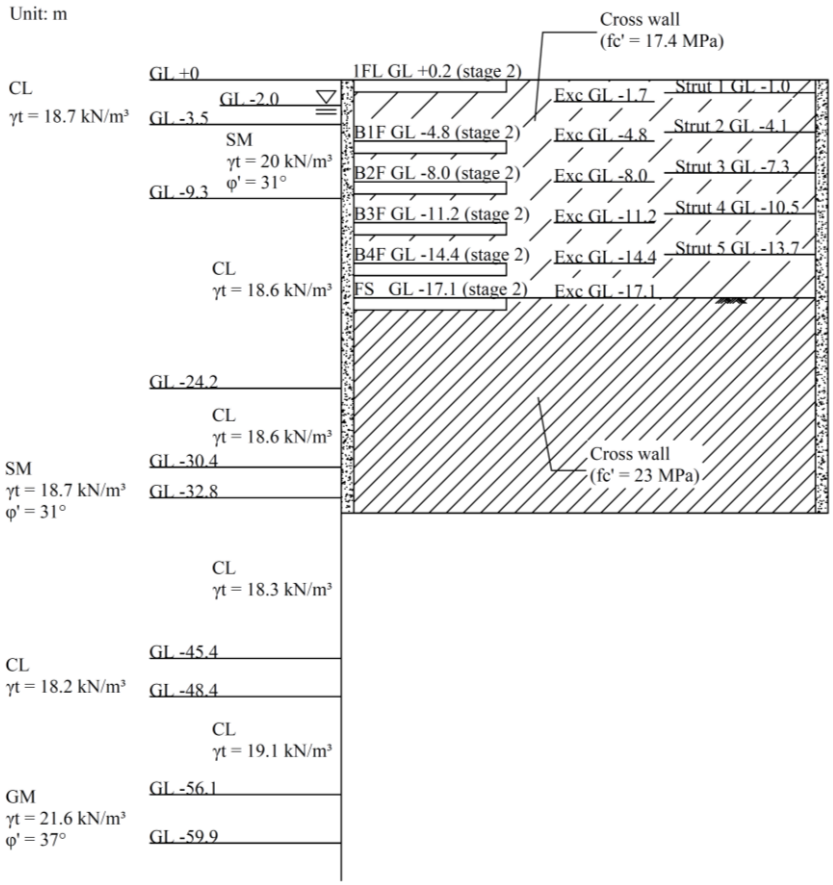

Figure 3.2 Soil stratigraphy and construction sequence for Case A

doi:10.6342/NTU201900743

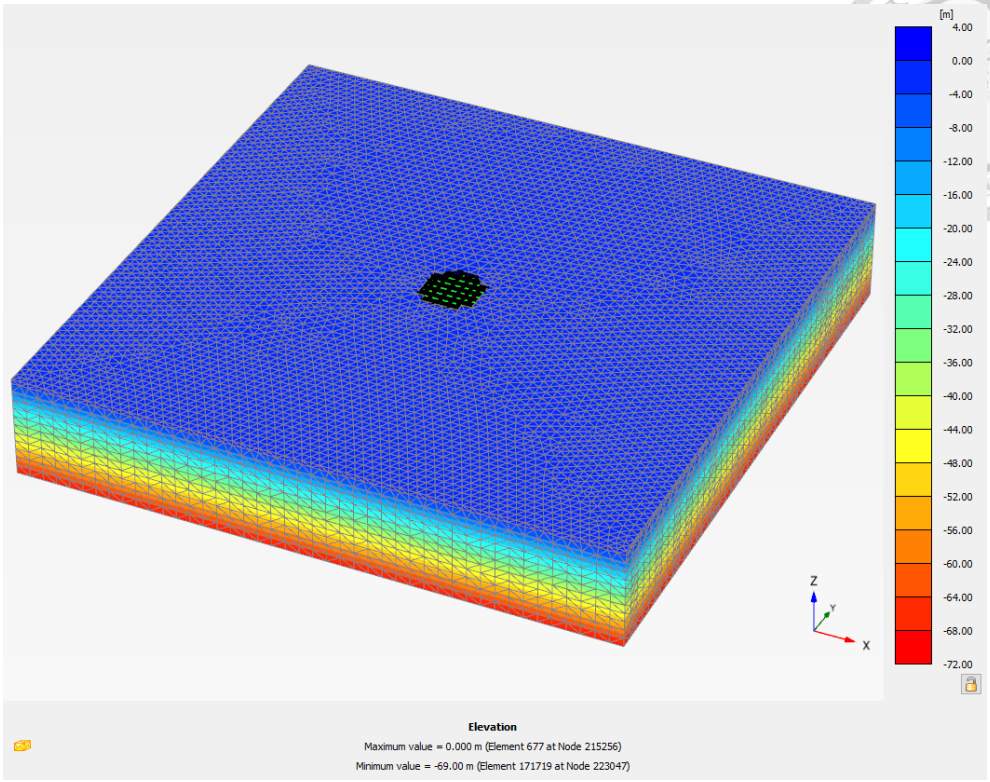

(a) Analysis domain

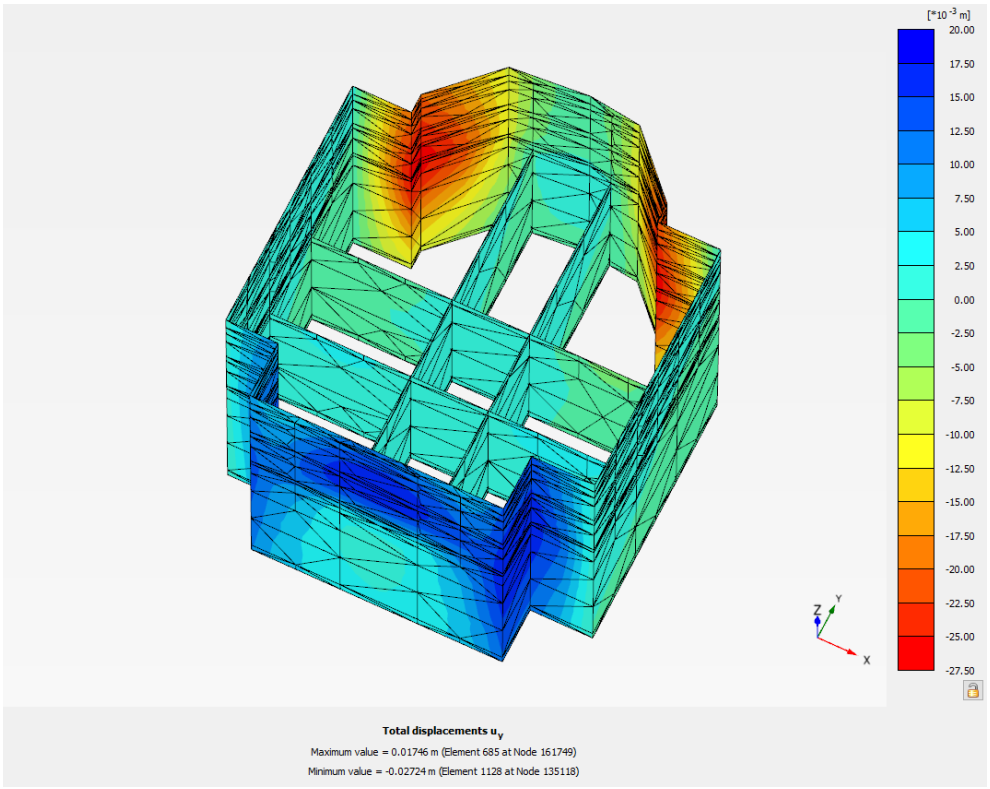

(b) Model of the excavation

Figure 3.3 Finite element model of Case A

doi:10.6342/NTU201900743

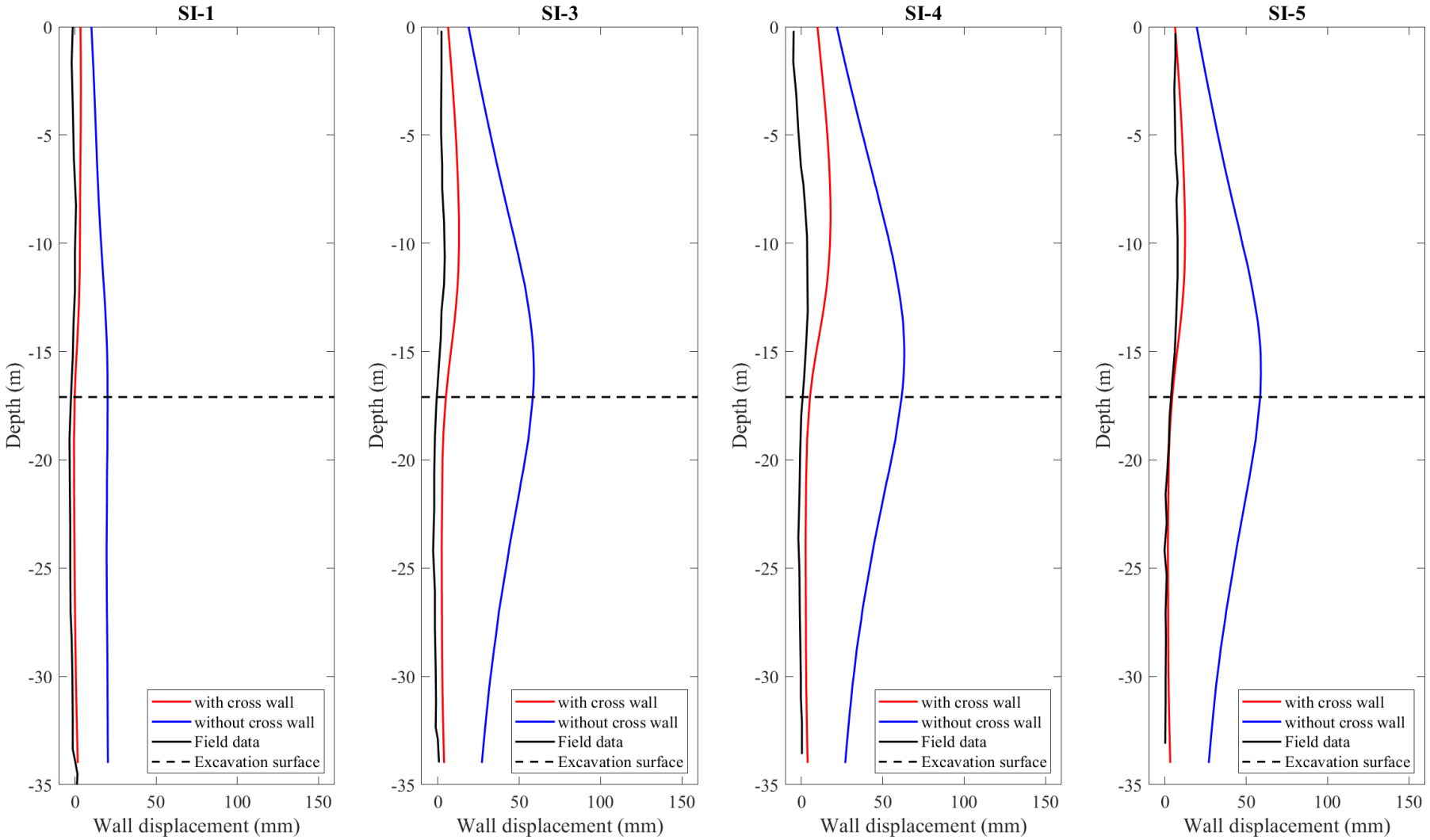

Figure 3.4 Comparison of numerical results with field data (Case A)

doi:10.6342/NTU201900743

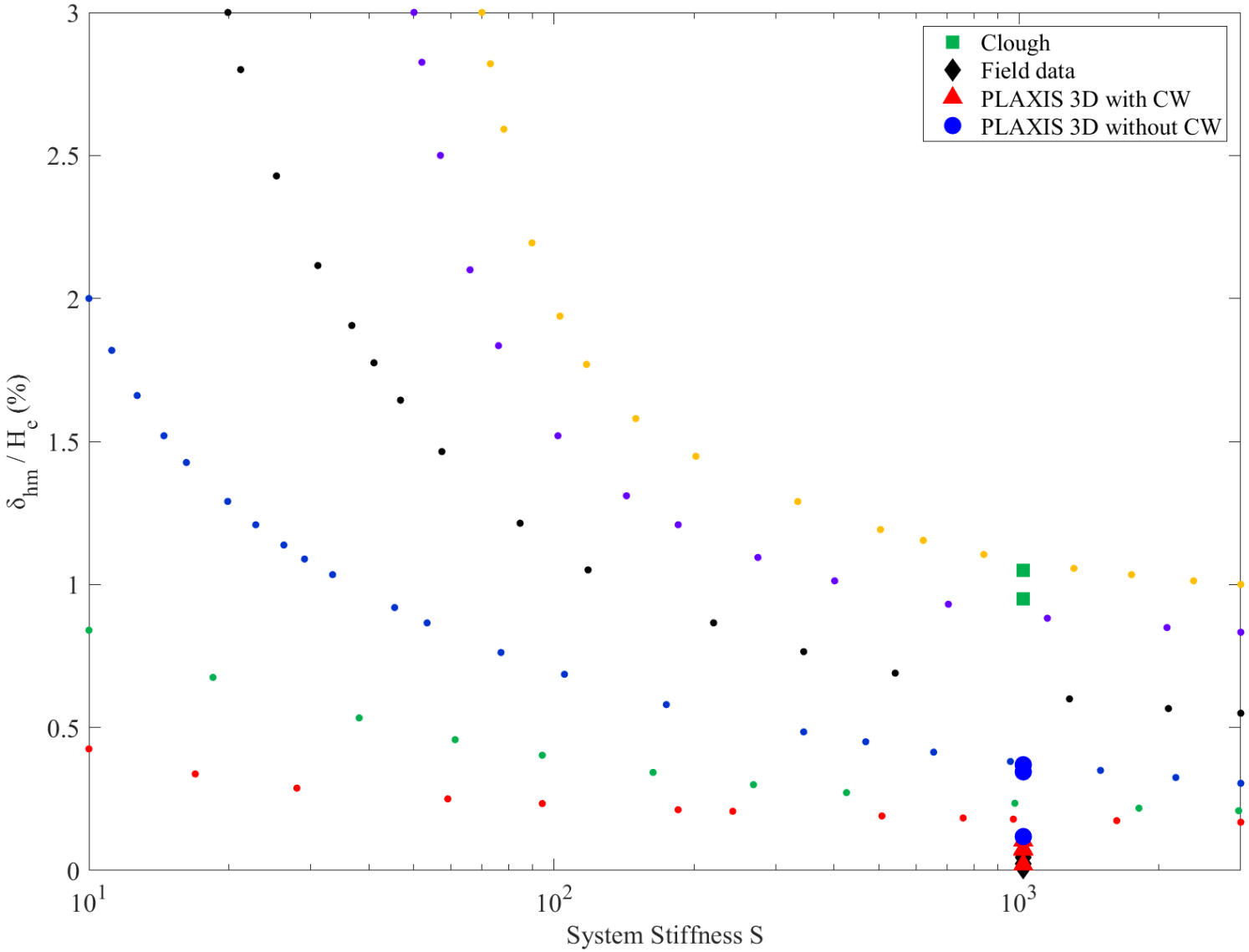

Figure 3.5 Comparison of estimated wall displacements for Case A

doi:10.6342/NTU201900743

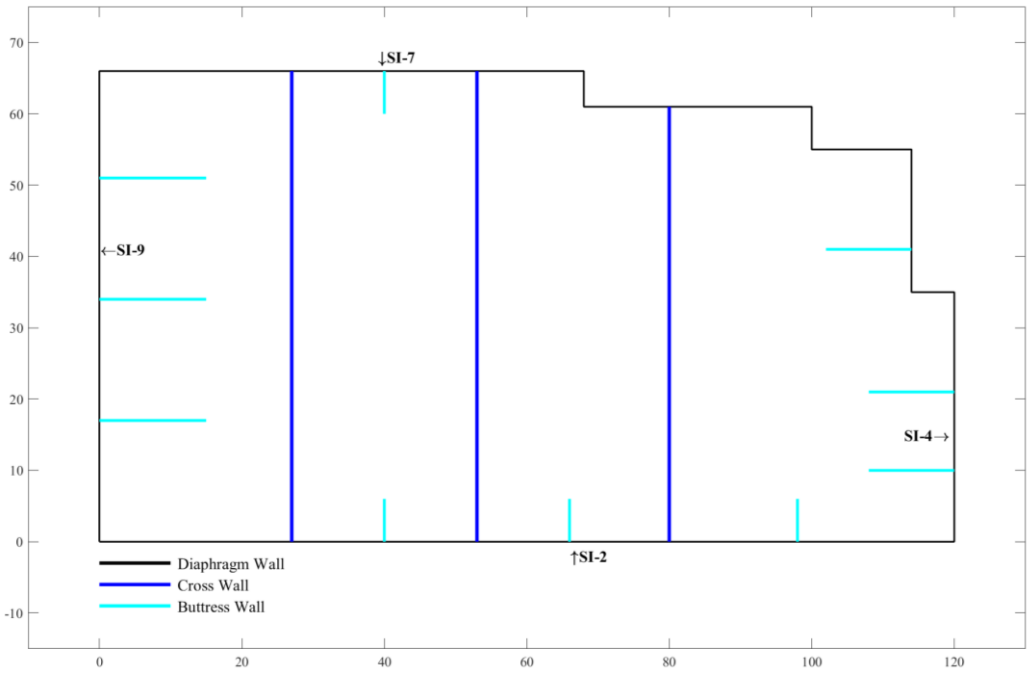

Figure 3.6 Site plan for Case B

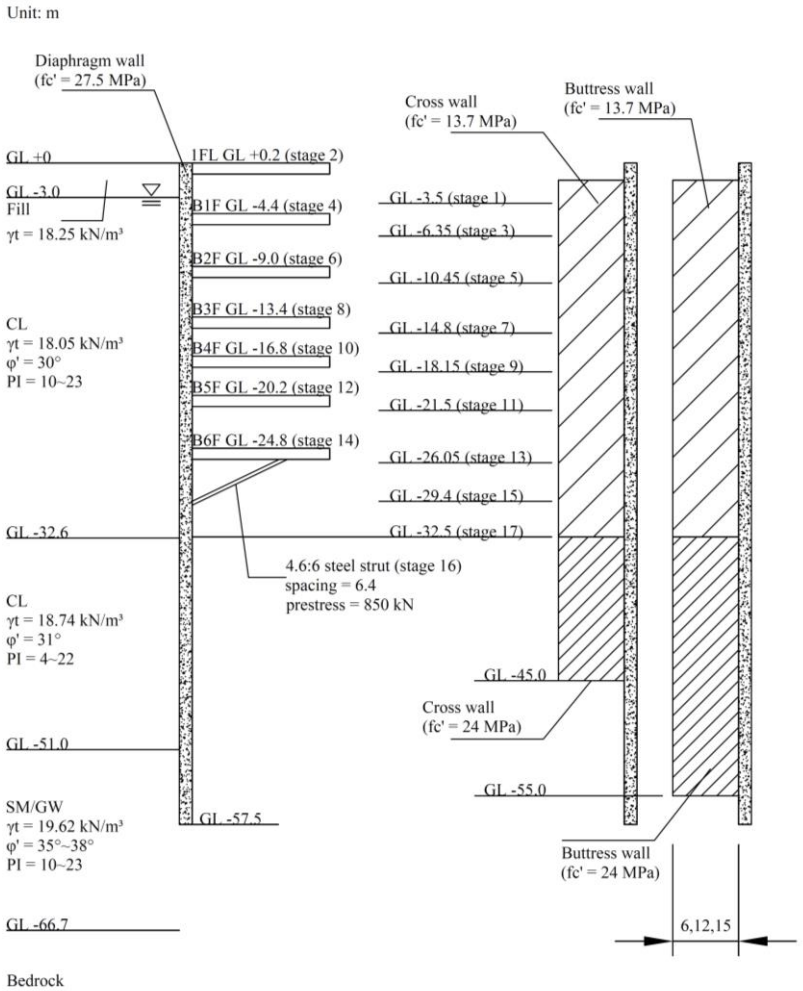

Figure 3.7 Soil stratigraphy and construction sequence for Case B

doi:10.6342/NTU201900743

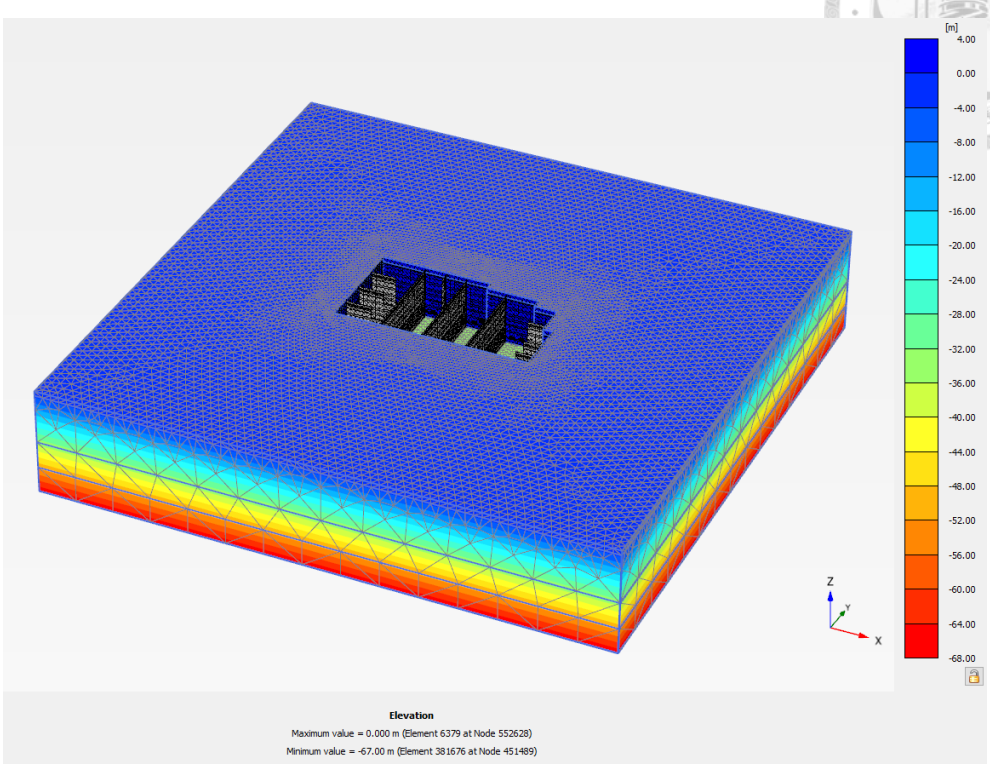

(a) Analysis domain

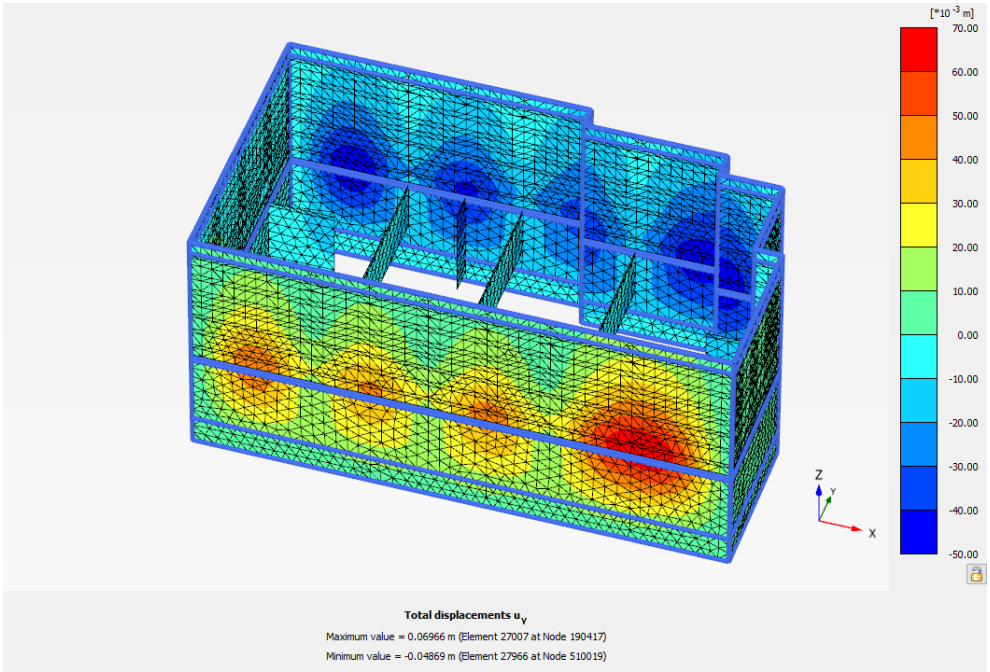

(b) Model of the excavation

Figure 3.8 Finite element model of Case B

doi:10.6342/NTU201900743

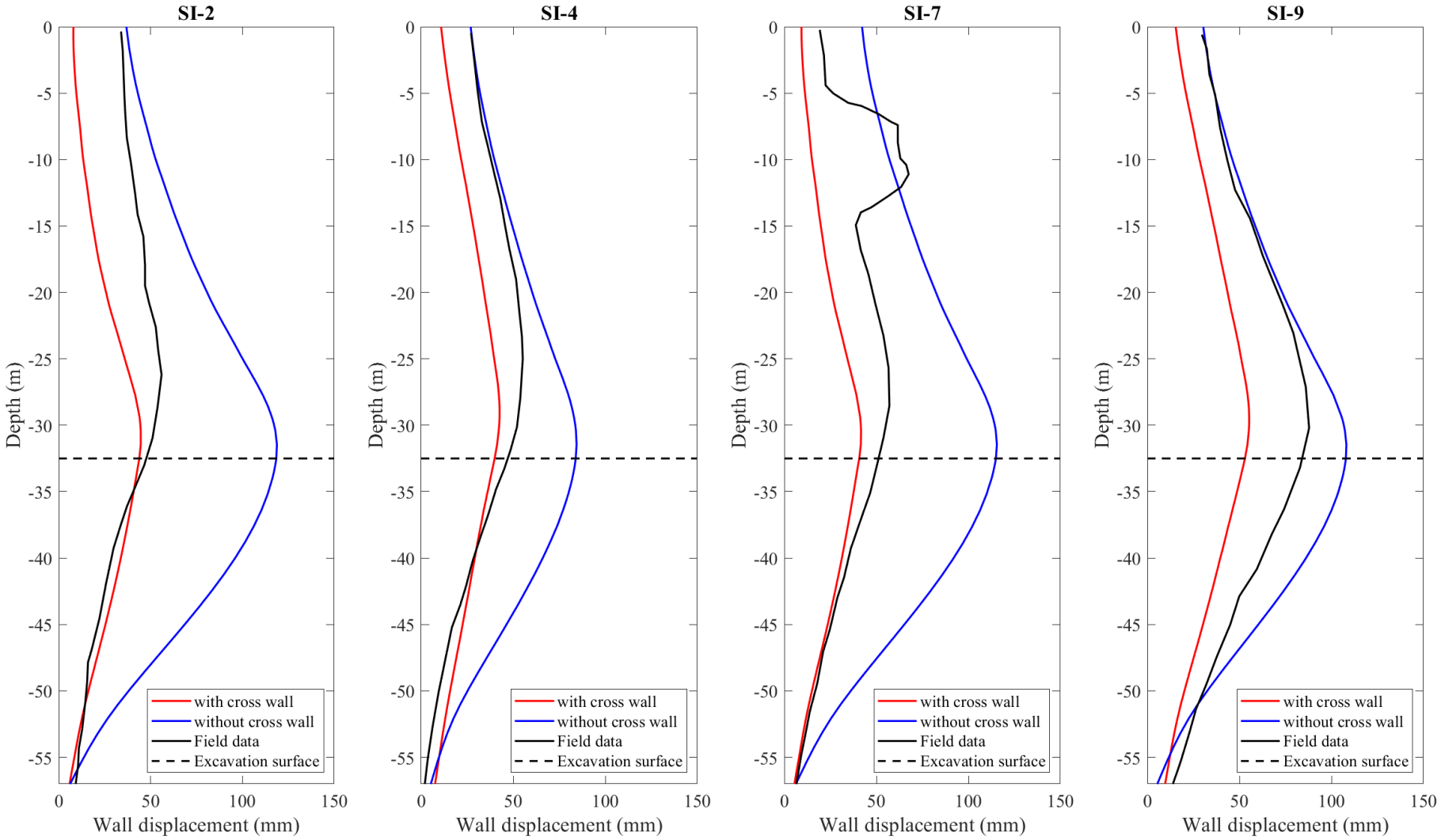

Figure 3.9 Comparison of numerical results with field data (Case B)

doi:10.6342/NTU201900743

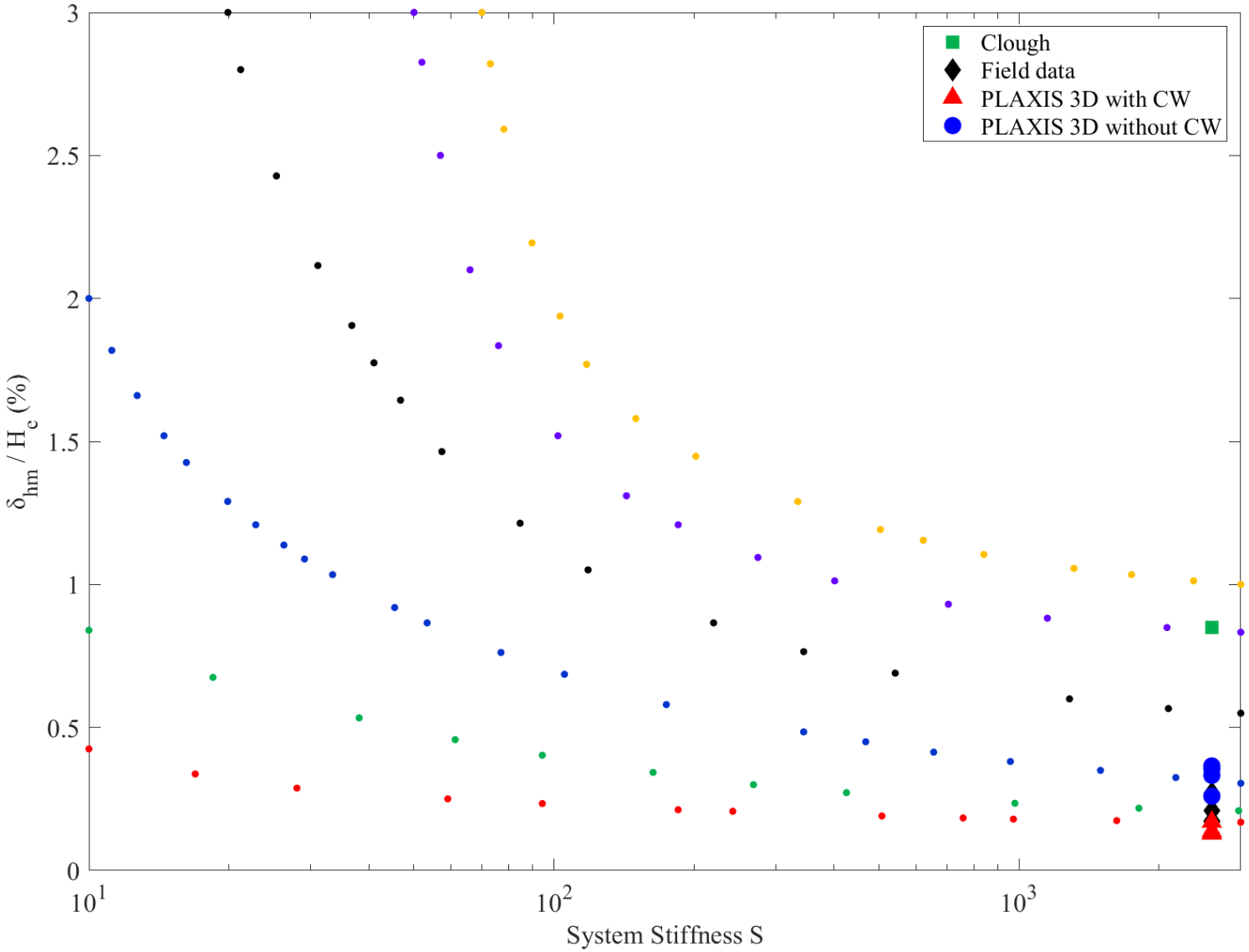

Figure 3.10 Comparison of estimated wall displacements for Case B

doi:10.6342/NTU201900743

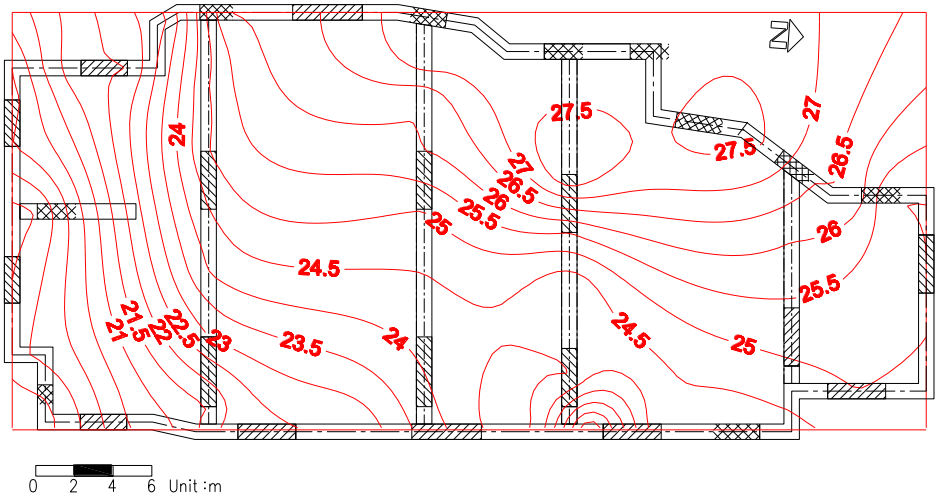

Figure 3.11 Elevation contour of the andesite for Case C

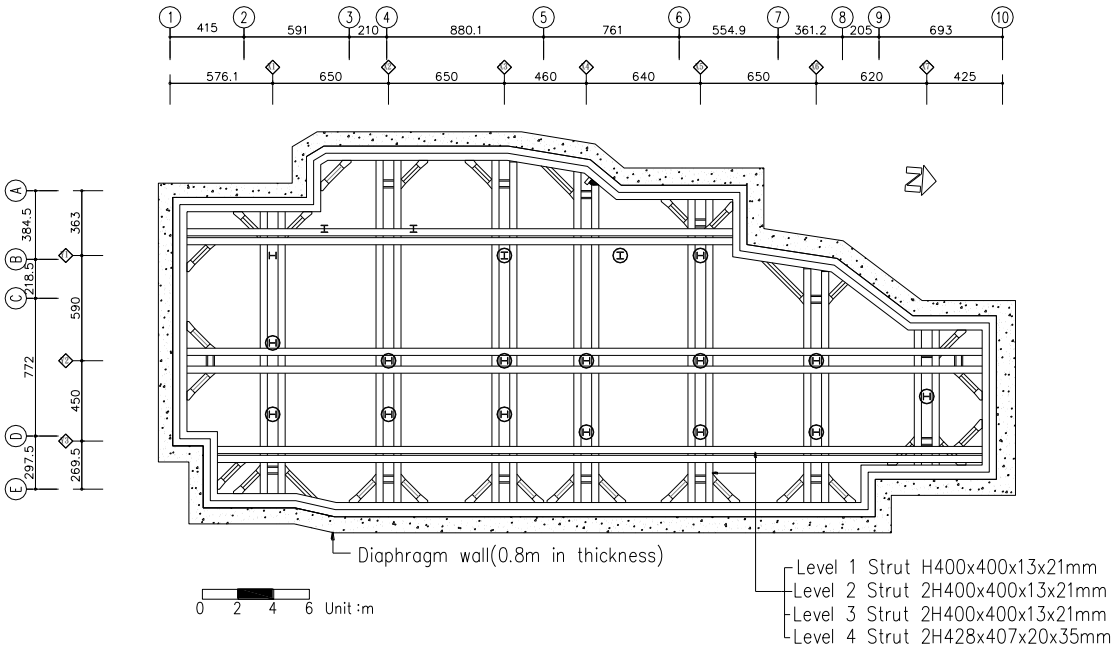

Figure 3.12 Layout of horizontal supports for Case C

doi:10.6342/NTU201900743

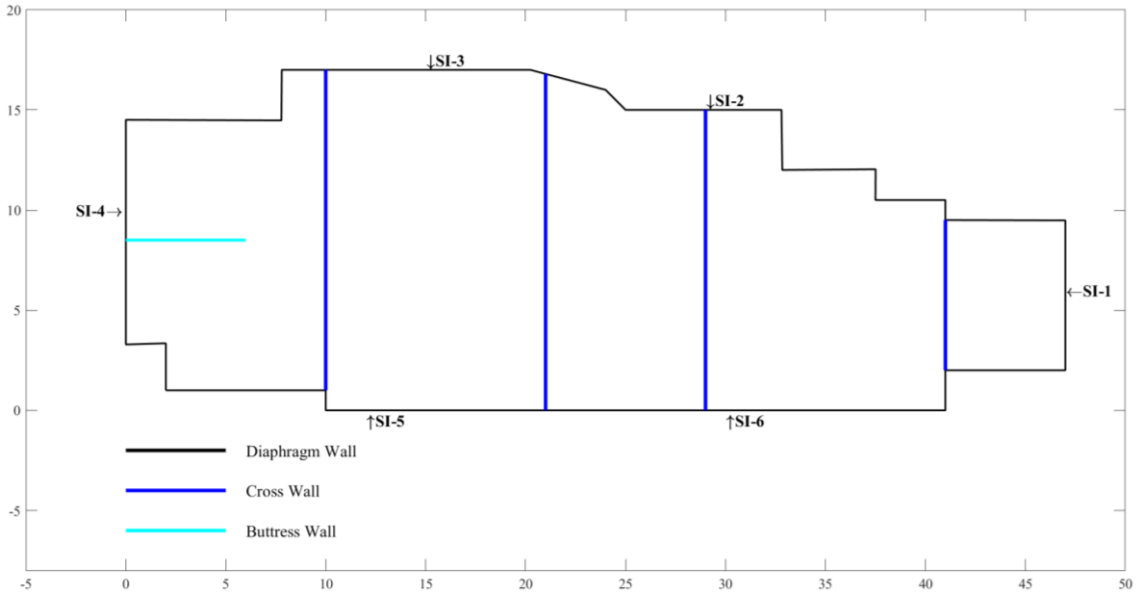

Figure 3.13 Site plan for Case C

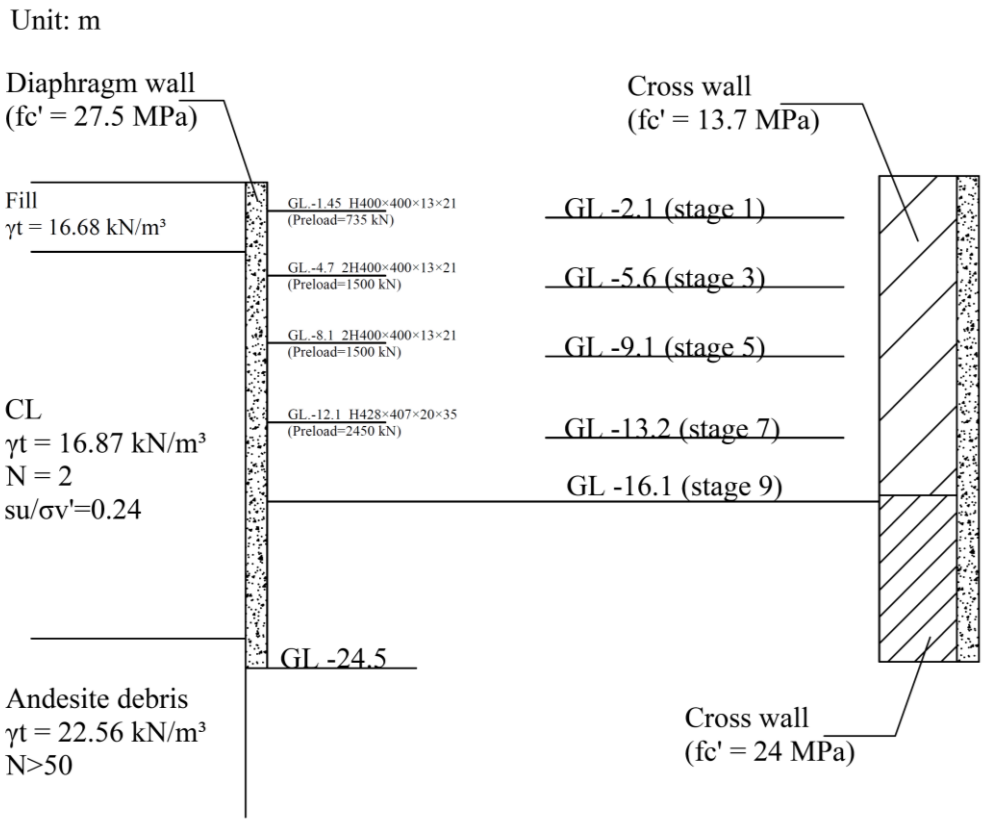

Figure 3.14 Soil stratigraphy and construction sequence for Case C

doi:10.6342/NTU201900743

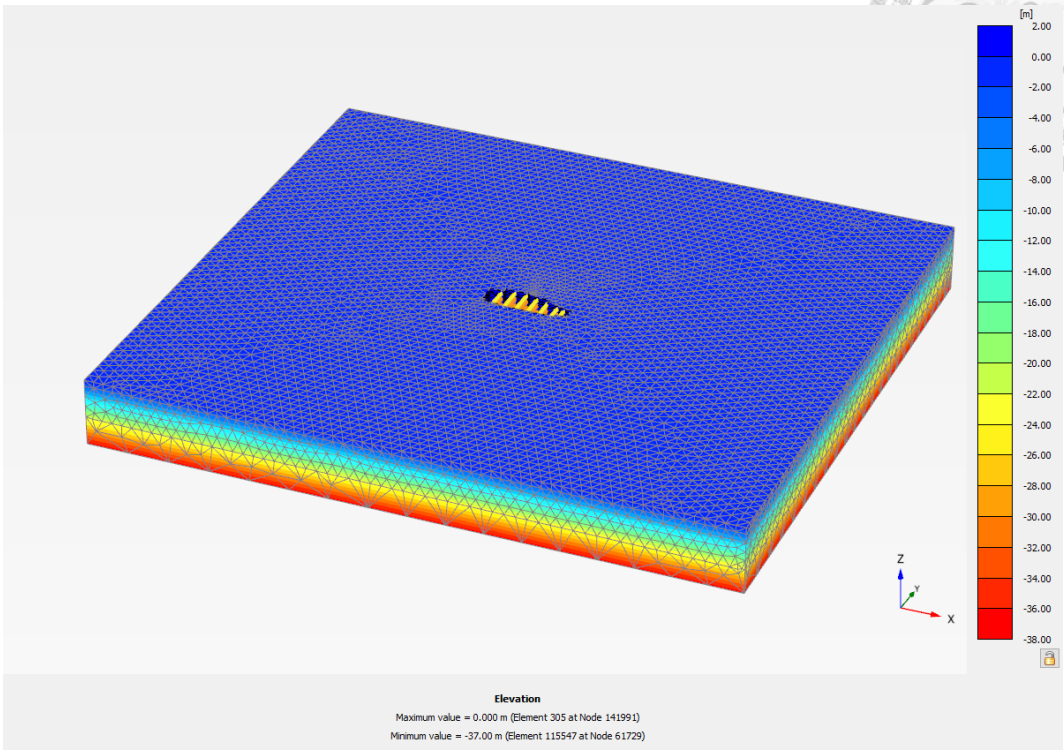

(a) Analysis domain

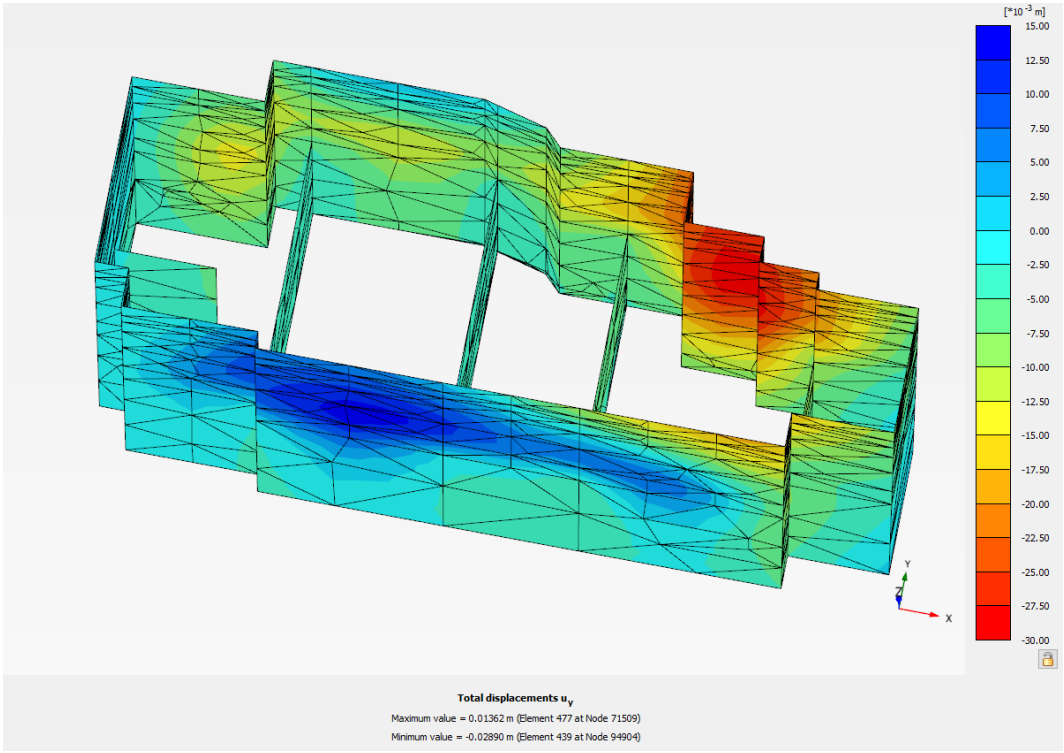

(b) Model of the excavation

Figure 3.15 Finite element model of Case C

doi:10.6342/NTU201900743

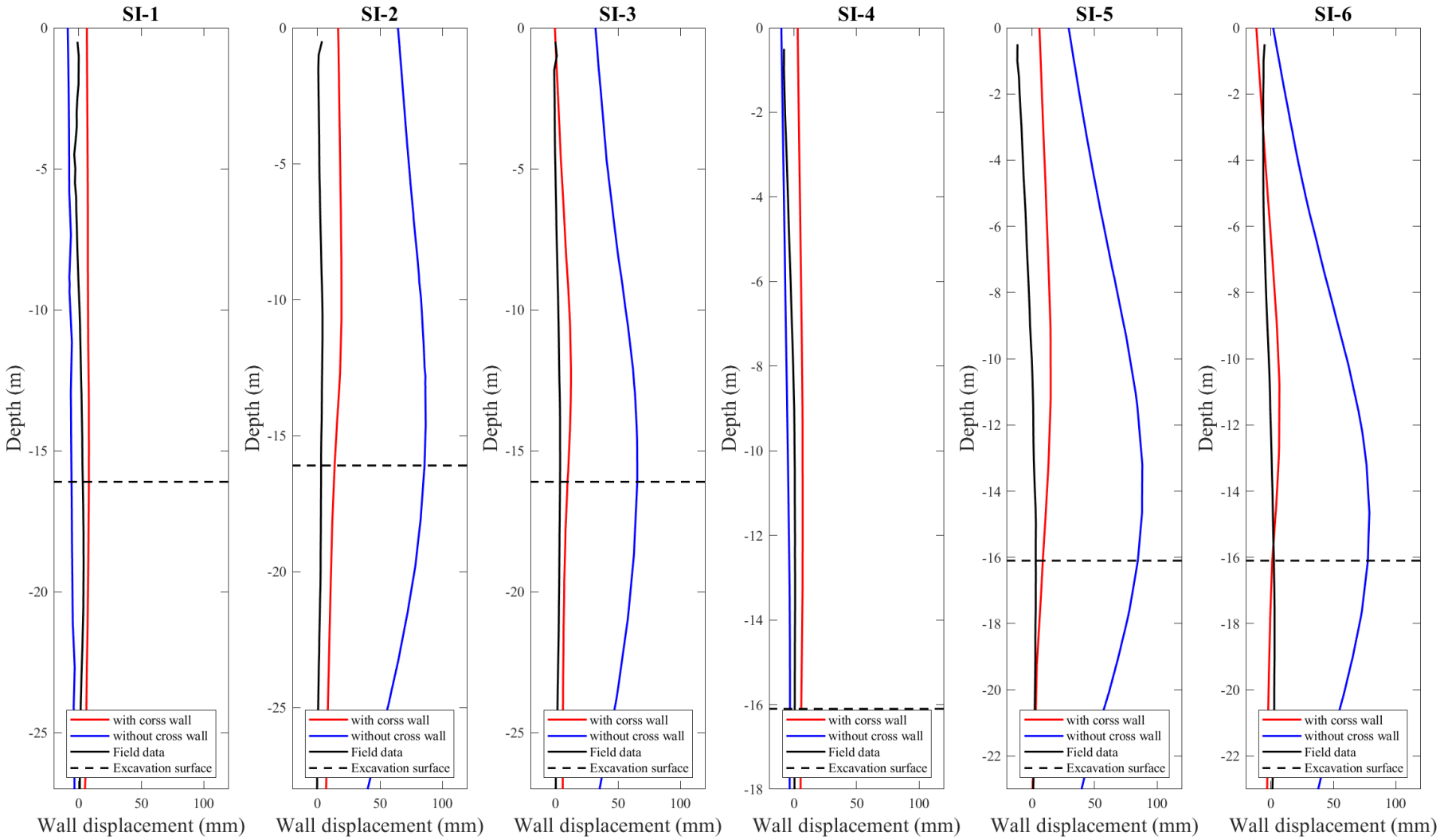

Figure 3.16 Comparison of numerical results with field data (Case C)

doi:10.6342/NTU201900743

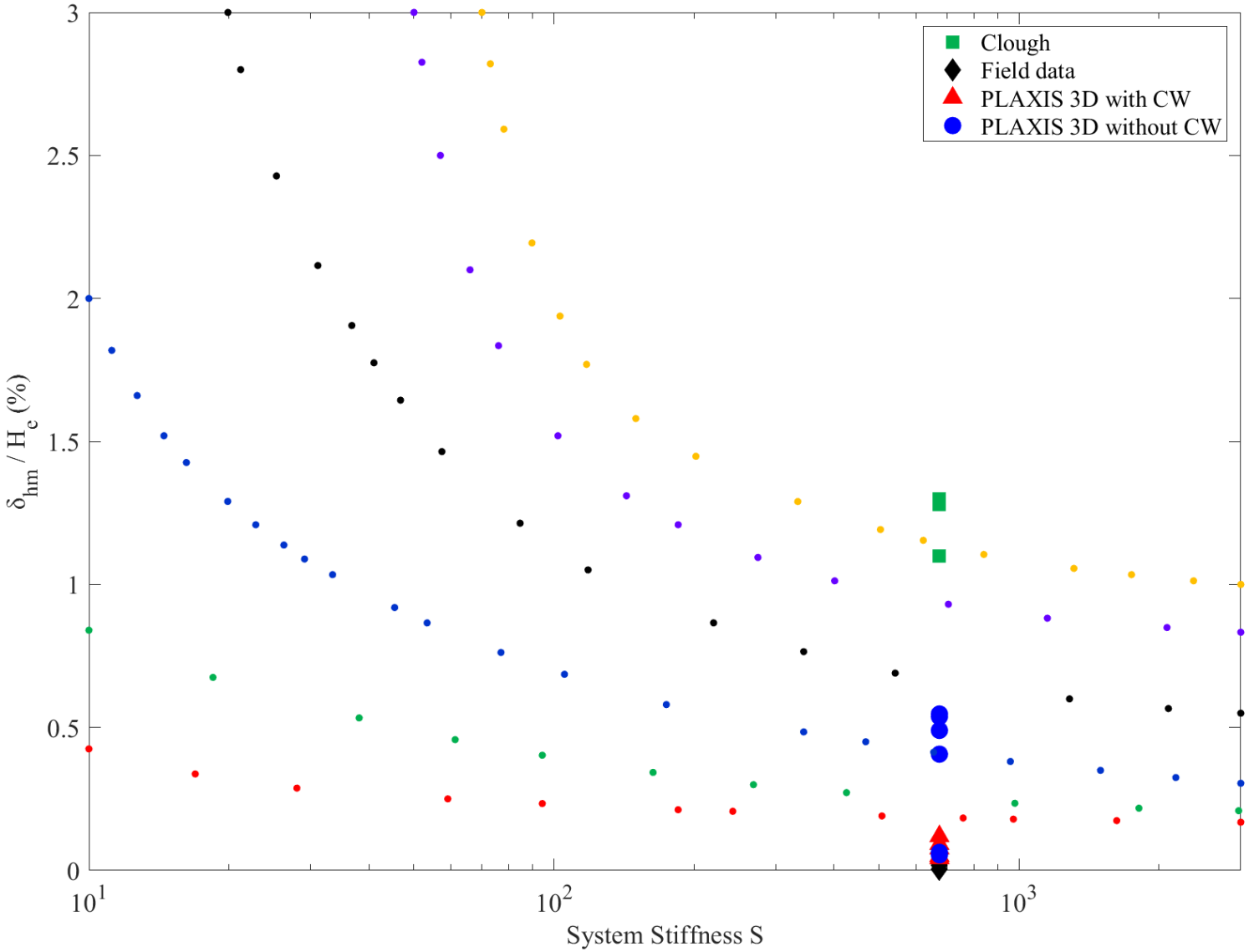

Figure 3.17 Comparison of estimated wall displacements for Case C

doi:10.6342/NTU201900743

Chapter 4 Revision of the Clough's Curves

As revealed by the case histories in previous chapter, it is known that the effect of cross wall is important in restraining the wall deflection to an extremely low level. In addition, the results estimated by Clough's chart is overly excessive when compared with field observation as the Clough's chart ignores the effect of cross walls in its present form. Therefore, it is a major objective of this chapter to incorporate the effect of cross walls in Clough's chart, and that would allow the engineers to evaluate the wall displacement when cross walls are used in the excavation design.

In this chapter, the curves in Clough's chart are extended to high stiffness area by regression technique. In conjunction with the extension of the design curves, the two factors S and F_b are modified to incorporate the effect of cross walls. The case histories outlined in previous chapters are then used to verify the applicability of the extended curves as well as the simplified approaches to evaluate the strengthening effect of cross walls.

doi:10.6342/NTU201900743

4.1 Revised scheme

4.1.1 Use of the original scheme

The Clough's chart was often adopted to estimate the maximum wall displacement for excavation in soft clays. However, the present form of Clough's chart consists of curves with limited S and F_b values, it is not fully applicable for modern excavations with cross walls. The use of cross walls tends to increase the system stiffness and factor of safety against basal heave by a significant amount, which is obviously not revealed in the original scheme. Take Case A for instance, inserting the required parameters presented in Table 3.6 in Equation (2.1). The dimensionless system stiffness (S) is 1022 for any location of Case A. The factors of safety against basal heave are different at each side as the width factor is different for each side when divided by cross walls. The factor of safety against basal heave is therefore not a fixed value for Case A. The system stiffness, factor of safety against basal heave together with the maximum wall displacement estimated by Clough's chart (δ_{clough}) and field observation (δ_{field}) are summarized in Table 3.6. It can be seen that the estimated wall displacement is large compared with the field observation. Using the Clough's chart to estimate the wall displacement is not a suitable approach as there are cross walls in the excavation zone. The original Clough's chart is unable to incorporate the effect of cross walls in limiting wall displacement that certain revisions have to be added to the original scheme.

doi:10.6342/NTU201900743

In essence, cross walls provide extra passive resistance to the retaining system, so that the overall system stiffness and factor of safety against basal heave should both increase as a result. In other words, the system stiffness and factor of safety against basal heave have to be increased when considering the effect of cross walls. If the effect of the cross wall can be reasonably quantified in evaluating the system stiffness and factor of safety against basal heave, then the Clough's chart can be extended into the high system stiffness and low displacement levels, which are more useful for excavation designs.

4.1.2 Extension of the design curves

The original curves shown in Figure 2.1 are applicable for projects with system stiffness less than 3000 and factor of safety against basal heave less than 3. For excavation projects with cross walls, the curves must be extended into the high system stiffness and high factor of safety zone as needed. For the required extension, the curves in Figure 2.1 are first digitized and redrawn as shown in Figure 4.1. To focus on the low displacement area, only data points with system stiffness larger than 300 are discussed. Using F_b as the x-coordinate instead, the relationship among F_b, S and δ_{hm}/H_e is redrawn and presented in Figure 4.2. Curves represent different levels of system stiffness and the same color points represent the same system stiffness. It can be seen that the data points in Figure 4.2 are congested within a small zone while the factor of safety was taken as the x-axis, it appears that a simple regression equation can be derived to represent the

doi:10.6342/NTU201900743

relationship among F_b, S and δ_{hm}/H_e. To do so, curve fitting technique is used and these curves can be extrapolated to high factor of safety values as shown in Figure 4.3. It is interesting to note that those curves in Figure 4.3 can be represented by a simple equation with exponential type as shown in the following form:

$$\delta_{hm}/H_e = \mu {F_b}^{-1.55} \tag{4.1}$$

where μ is a factor depending on the value of system stiffness. It is worthy to mention that the exponential coefficient is about -1.55 for different values of system stiffness. The relationship between μ and system stiffness is further defined by a best fit relationship shown in Figure 4.4, and a simple relationship can be obtained:

$$\mu = 2.17S^{-0.143} \tag{4.2}$$

Combining Equations (4.1) and (4.2), a new equation representing the ratio of maximum wall displacement to the excavation depth can be obtained. The wall displacement calculated by this regression equation is called the revised wall displacement (δ_{rev}). The new equation is shown in Equation (4.3), which only considers two parameters, and is graphically shown in Figure 4.5.

$$\delta_{rev}/H_e = 2.17S^{-0.143}{F_b}^{-1.55} \tag{4.3}$$

It is noted that Equation (4.3) can only be applied with the system stiffness larger than 300 and the factor of safety larger than 0.9. Moreover, the exponential equation is applicable in the area of high system stiffness and factor of safety against basal heave,

doi:10.6342/NTU201900743

especially for $F_b > 3$, which may be more suitable for modern excavations with cross walls. The curves calculated by the regression equation can be compared with the original data points as shown in Figure 4.6. The curves with lower factor of safety tend to underestimate the wall displacement, while at high F_b, the curves slightly overestimate the wall displacement. It is considered that this regression equation provides reasonable results for estimating wall displacement. In order to better use of the regression equation, three more curves with $F_b = 5, 7$ and 10 are also sketched in Figure 4.6. However, these three curves are too close to each other, so they are redrawn in Figure 4.7 to provide better resolution. In Figure 4.7, it appears that the curves with high factor of safety are more or less independent with system stiffness. These curves with $F_b = 5, 7$ and 10 are almost straight lines, which are coincided with the idea proposed by Long (2001).

A closer look at the curves shows another interesting point. Besides of the independence with high system stiffness, it seems that the ratio of the wall displacement to the excavation depth has a limited value. The ratio would fall within a certain range between 0.02% and 0.12% when system stiffness is larger than 3000 and factor of safety is larger than 3.0. The ratio of 0.02% is the minimal value, even with a very high factor of safety if the excavation is heavily strengthened with many cross walls. In other words, the minimum lateral wall displacement is 0.02% of the excavation depth even if the excavation is heavily reinforced with many cross walls. This observation seems

doi:10.6342/NTU201900743

reasonable in the actual cases.

4.1.3 Revision of the system stiffness

With the presence of the cross walls in Case A, the excavation zone is divided by the cross walls into 4 small zones marked respectively with A to D, and the plan layout is shown in Figure 4.8. Since each zone is small so that the three-dimensional effect or corner effect is pronounced. In other words, the presence of the cross wall strengthens the overall system stiffness and reduces the wall deflection by increasing three-dimensional or corner effect. In the past, estimating the influence of three-dimensional effect of the project site can only be achieved by using a complex and time-consuming numerical analyses. Though there are many simplified methods by Hsieh and Lu (1999) available to simplify the three-dimensional behavior of the cross walls into 1D or 2D situation, these approaches still involve the use of one-dimensional (1D) numerical program, which may be difficult for inexperienced engineers.

As for revising the system stiffness, one may use a simple approach to quantify the three-dimensional effect or corner effect induced by the presence of the cross walls. According to the chart proposed by Ou et al. (1996), inputting the length and width of each zone and the distance from the midpoint to the corner, a PSR can be acquired for estimating the reduced wall displacement. The reciprocal of PSR is considered as the magnification factor of the original system stiffness in this study. The combined system

doi:10.6342/NTU201900743

stiffness (S_c) as a combination of the original system stiffness and the corner or three-dimensional effect induced by cross wall is defined as:

$$S_c = S/PSR \tag{4.4}$$

where the combined system stiffness (S_c) is a dimensionless factor similar to the original system stiffness.

4.1.4 Revision of the factor of safety against basal heave

In fact, cross walls not only provide extra passive resistance to the system stiffness but also restrain the development of the basal heave. During excavation, the surface friction of the cross walls would provide additional resistance to restrain the heaving of the soft clay between the cross wall. So, the factor of safety against basal heave should also be adjusted if cross walls exist in the project site. The details on the derivation of equivalent undrained shear strength (s_u^*) can be found in section 2.4 or Hsieh and Lu (1999). Herein, the adjusted factor of safety against basal heave (F_{b_adj}) is calculated by Equations (4.5) and (4.6) similar to Equations (2.2) and (2.3) for each small zone divided by the cross walls instead of using the dimension of the whole site.

$$F_{b\_adj} = \frac{N_c \times s_{ub\_adj} \times B/\sqrt{2}}{(\gamma H_e + q) \times B/\sqrt{2} - s_{uu} H_e} \tag{4.5}$$

$$F_{b\_adj} = \frac{N_c \times s_{ub\_adj} \times D}{(\gamma H_e + q) \times D - s_{uu} H_e} \tag{4.6}$$

where s_{ub_adj} is the average of s_{ub} and s_{ub}^*, which are respectively the original s_{ub} and the revised s_{ub}^* subjected to the influence of cross walls. Since the cross walls only

doi:10.6342/NTU201900743

affect the clay strength in the excavation zone and clay on the retaining side would remain the same, so an average value of undrained shear strength (s_{ub_adj}) should be used in calculating the factor of safety against basal heave. Equation (2.15) should be changed slightly as shown below:

$$I_{CL} = 1 + \kappa \times L_{CW} \times N_{CW}/B \tag{4.7}$$

where B is the wall length of that small zone, which is connected with the cross walls. L_{CW} is the length of cross walls. N_{CW} is the number of cross walls, which is usually taken as 2 because of the amount of the secondary wall of a small zone. κ is either 1 or 2, as κ equals 1 is for situation when a cross wall is shared by two adjacent zones; while κ equals 2 is when there are no adjacent zones.

doi:10.6342/NTU201900743

4.2 Review of the previous case histories

According to the results shown in previous chapter, it is shown that the maximum wall displacement can be estimated by the regression equation. If the regression equation can be applied to other cases and obtained an appropriate prediction, then the equation can be regarded as a representative equation and be pervasive for any excavation. In this section, the predictions of wall displacements in Cases A, B and C are reviewed. The maximum wall displacement can be rapidly calculated with the regression equation, there is no need to use the complicated finite-element software to solve such problem.

4.2.1 Review of Case A

The revised wall displacement (δ_{rev}) were recalculated based upon the revised scheme outlined in previous section. The project site was divided into small zones by 4 cross walls as shown in Figure 4.8. Table 4.1 shows the width and length of each small zone, and its PSR can be found accordingly. It can be observed that each zone has pronounced three-dimensional effect with the PSR close to 0.1. In addition, the original factor of safety (F_b) is approximately 1. Using the Equations 4.4 and 4.5, the combined system stiffness (S_c) and the revised factor of safety against basal heave (F_{b_adj}) can be calculated and listed in Table 4.2 and Table 4.3, respectively. The comparison of predicted wall displacements by various methods are summarized in Table 4.4 and Table 4.5. Considering the cross wall effect, the combined system stiffness and factor of safety

doi:10.6342/NTU201900743

increase about 5 times and 3 times than the original values, respectively. Moreover, δ_{rev} are in better agreement with the field data. Despite δ_{rev} is about 10 times of the field data, it did significantly improve the prediction capability of Clough's original scheme.

4.2.2 Review of Case B

The layout and basic parameters of each small zone divided by the cross walls of Case B is shown in Figure 4.9 and Table 4.6, respectively. Following the same steps for the review of Case A, the combined system stiffness and the revised factor of safety against basal heave can be calculated and listed in Table 4.7 and Table 4.8, respectively. The comparison of predicted wall displacements by various methods are summarized in Table 4.9 and Table 4.10. By considering the cross wall effect, the combined system stiffness and factor of safety increased by 2.7 times and 2.2 times than the original values, respectively. Two of inclinometers, SI-4 and SI-9, did not have the obvious three-dimensional effect which means the PSR is close to 1, so the system stiffness remains about the same. Again, δ_{rev} are in better agreement with the field data. In Case B, δ_{rev} is about 1.2 times higher than field data, it is considered as a very good prediction.

4.2.3 Review of Case C

The layout and basic parameters of each small zone divided by the cross walls of Case C is shown in Figure 4.10 and Table 4.11, respectively. The original factor of safety against basal heave is approximately to 1. Following the same steps for the review of

doi:10.6342/NTU201900743

Case A, the combined system stiffness and the revised factor of safety against basal heave can be calculated and listed in Table 4.12 and Table 4.13, respectively. The comparisons of predicted wall displacements by various methods are summarized in Table 4.14 and Table 4.15. By considering the cross wall effect, the combined system stiffness and factor of safety against basal heave increased by 6.6 times and 3.4 times than the original values, respectively. Again, δ_{rev} are in better agreement with the field data. Despite δ_{rev} are almost about 10 times higher than field data, the revised predictions are much improved than the predictions by original scheme. It is interesting to note that the field data are smaller than 10 mm, which is an extremely low wall displacement for excavations in soft clay, which makes a close prediction almost impossible.

4.2.4 Summary

Though the effect of cross walls are incorporated in this study, the difference still exist about one order of magnitude between δ_{rev} and δ_{field}. The possible reason for the difference between δ_{rev} and δ_{field} can perhaps be attributed to certain factors. One obvious reason is the three-dimensional effect induced by cross walls is underestimated in the revised scheme. The other one, not all factors are considered in this regression equation, resulting in δ_{rev} larger than δ_{field}. Therefore, more field data and numerical results are required to quantify the effects of cross wall on the retaining wall. The numerical simulation of cross walls will be further discussed in the next chapter.

doi:10.6342/NTU201900743

Table 4.1 Basic parameters for each zone of Case A

SI	Zone	B	L	D	PSR_{Ou}	PSR_{Finno}	s_{uu}	s_{ub}	d_T	F_b	S
		m	m	m	-	-	kPa	kPa	m	-	-
1	A	17.3	6.9	39.0	0.16	0.16	19.62	51.08	12.23	0.97	1022
3	B	16.1	8.6	39.0	0.21	0.21	19.62	50.26	11.38	0.96	1022
4	C	17.3	6.9	39.0	0.16	0.16	19.62	51.08	12.23	0.97	1022
5	D	14.4	8.6	39.0	0.21	0.21	19.62	49.09	10.18	0.95	1022

Table 4.2 Revision of the system stiffness of Case A

SI	Zone	B	L	S	PSR_{Ou}	$S_{c,Ou}$	PSR_{Finno}	$S_{c,Finno}$
		m	m	-	-	-	-	-
1	A	17.3	6.9	1022	0.16	6386	0.16	6330
3	B	16.1	8.6	1022	0.21	4865	0.21	4915
4	C	17.3	6.9	1022	0.16	6386	0.16	6330
5	D	14.4	8.6	1022	0.21	4865	0.21	4887

Table 4.3 Revision of the factor of safety against basal heave of Case A

SI	Zone	N_{cw}	L_{cw}	κ	B	s_{uu}	s_{ub}	I_{CL}	s_{ub}*	s_{ub_adj}	F_{b_adj}
		m	m	-	m	kPa	kPa	kPa	kPa	kPa	-
1	A	2	17.3	1	6.9	19.62	51.08	6.01	307.20	179.14	3.41
3	B	2	16.1	1	8.6	19.62	50.26	4.74	238.42	144.34	2.77
4	C	2	17.3	1	6.9	19.62	51.08	6.01	307.20	179.14	3.41
5	D	2	14.4	1	8.6	19.62	49.09	4.35	213.50	131.30	2.55

Table 4.4 Estimation of wall displacements of Case A

SI	S	$S_{c,Ou}$	$S_{c,Finno}$	F_b	F_{b_adj}	δ_{clough}	$\delta_{rev,Ou}$	$\delta_{rev,Finno}$	δ_{3D_with}	δ_{field}
	-	-	-	-	-	mm	mm	mm	mm	mm
1	1022	6386	6330	0.97	3.41	179.55	15.80	15.82	3.59	1.49
3	1022	4865	4915	0.96	2.77	162.45	22.72	22.69	12.93	4.18
4	1022	6386	6330	0.97	3.41	179.55	15.80	15.82	17.88	3.87
5	1022	4865	4887	0.95	2.55	162.45	25.84	25.82	12.34	7.76

Table 4.5 Comparison of wall displacements of Case A

SI	δ_{Clough} / H_e	$\delta_{rev,Ou}$ / H_e	$\delta_{rev,Finno}$ / H_e	δ_{3D_with} / H_e	δ_{field} / H_e	$\delta_{spacing}$ / H_e
	%	%	%	%	%	%
1	1.05	0.092	0.093	0.021	0.0087	0.0169
3	0.95	0.133	0.133	0.076	0.0244	0.0284
4	1.05	0.092	0.093	0.105	0.0226	0.0169
5	0.95	0.151	0.151	0.072	0.0454	0.0321

doi:10.6342/NTU201900743

Table 4.6 Basic parameters for each zone of Case B

SI	Zone	B	L	D	PSR_{Ou}	PSR_{Finno}	s_{uu}	s_{ub}	d_T	F_b	S
		m	m	m	-	-	kPa	kPa	m	-	-
2	B	61	27	18.5	0.39	0.27	35.74	88.50	18.50	0.96	2599
4	A	40	61	18.5	0.91	0.58	35.74	88.50	18.50	0.96	2599
7	C	66	26	18.5	0.37	0.26	35.74	88.50	18.50	0.96	2599
9	D	27	66	18.5	0.95	0.65	35.74	88.50	18.50	0.96	2599

Table 4.7 Revision of the system stiffness of Case B

SI	Zone	B	L	S	PSR_{Ou}	$S_{c,Ou}$	PSR_{Finno}	$S_{c,Finno}$
		m	m	-	-	-	-	-
2	B	61	27	2599	0.39	6664	0.27	9538
4	A	40	61	2599	0.91	2856	0.58	4481
7	C	66	26	2599	0.37	7025	0.26	9968
9	D	27	66	2599	0.95	2736	0.65	3971

Table 4.8 Revision of the factor of safety against basal heave of Case B

SI	Zone	N_{cw}	L_{cw}	κ	B	s_{uu}	s_{ub}	I_{CL}	s_{ub}*	s_{ub_adj}	F_{b_adj}
		m	m	-	m	kPa	kPa	kPa	kPa	kPa	-
2	B	2	61	1	27	35.74	88.50	5.52	488.40	288.45	3.14
4	A	2	40	2	61	35.74	88.50	3.62	320.64	204.57	2.22
7	C	2	66	1	26	35.74	88.50	6.08	537.82	313.16	3.40
9	D	2	27	2	66	35.74	88.50	2.64	233.32	160.91	1.75

Table 4.9 Estimation of wall displacements of Case B

SI	S	$S_{c,Ou}$	$S_{c,Finno}$	F_b	F_{b_adj}	δ_{clough}	$\delta_{rev,Ou}$	$\delta_{rev,Finno}$	δ_{3D_with}	δ_{field}
	-	-	-	-	-	mm	mm	mm	mm	mm
2	2599	6664	9538	0.96	3.14	276.25	34.07	32.37	44.65	55.98
4	2599	2856	4481	0.96	2.22	276.25	65.51	61.42	42.58	55.18
7	2599	7025	9968	0.96	3.40	276.25	29.77	28.32	41.70	67.59
9	2599	2736	3971	0.96	1.75	276.25	95.62	90.66	55.32	87.87

Table 4.10 Comparison of wall displacements of Case B

SI	δ_{Clough} / H_e	$\delta_{rev,Ou}$ / H_e	$\delta_{rev,Finno}$ / H_e	δ_{3D_with} / H_e	δ_{field} / H_e	$\delta_{spacing}$ / H_e
	%	%	%	%	%	%
2	0.85	0.105	0.100	0.137	0.1722	0.1413
4	0.85	0.202	0.189	0.131	0.1698	0.2838
7	0.85	0.092	0.087	0.128	0.2080	0.1107
9	0.85	0.294	0.279	0.170	0.2704	0.4312

doi:10.6342/NTU201900743

Table 4.11 Basic parameters for each zone of Case C

SI	Zone	B	L	D	PSR_{Ou}	PSR_{Finno}	s_{uu}	s_{ub}	d_T	F_b	S
		m	m	m	-	-	kPa	kPa	m	-	-
1	E	6	7.5	8.9	0.15	0.21	14.15	31.89	4.24	0.84	675
2	D	15	11	13.9	0.24	0.27	14.15	37.28	10.61	0.85	675
3	B	18	10	11.9	0.20	0.24	14.15	38.38	11.90	0.87	675
4	A	10	14.5	2.9	0.35	0.40	14.15	30.75	2.90	0.91	675
5	B	18	10	6.4	0.20	0.23	14.15	33.72	6.40	0.82	675
6	D	15	11	7.9	0.24	0.26	14.15	34.99	7.90	0.82	675

Table 4.12 Revision of the system stiffness of Case C

SI	Zone	B	L	S	PSR_{Ou}	$S_{c,Ou}$	PSR_{Finno}	$S_{c,Finno}$
		m	m	-	-	-	-	-
1	E	6	7.5	675	0.15	4497	0.21	3150
2	D	15	11	675	0.24	2811	0.27	2485
3	B	18	10	675	0.20	3373	0.24	2765
4	A	10	14.5	675	0.35	1927	0.40	1706
5	B	18	10	675	0.20	3373	0.23	2897
6	D	15	11	675	0.24	2811	0.26	2546

Table 4.13 Revision of the factor of safety against basal heave of Case C

SI	Zone	N_{cw}	L_{cw}	κ	B	s_{uu}	s_{ub}	I_{CL}	s_{ub}*	s_{ub_adj}	F_{b_adj}
		m	m	-	m	kPa	kPa	kPa	kPa	kPa	-
1	E	2	6	2	7.5	14.15	31.89	4.20	133.95	82.92	2.18
2	D	2	15	1	11	14.15	37.28	3.73	138.97	88.12	2.01
3	B	2	18	1	10	14.15	38.38	4.60	176.54	107.46	2.43
4	A	2	10	2	14.5	14.15	30.75	3.76	115.59	73.17	2.17
5	B	2	18	1	10	14.15	33.72	4.60	155.11	94.41	2.29
6	D	2	15	1	11	14.15	34.99	3.73	130.42	82.70	1.95

doi:10.6342/NTU201900743

Table 4.14 Estimation of wall displacements of Case C

SI	S	$S_{c,Ou}$	$S_{c,Finno}$	F_b	F_{b_adj}	δ_{Clough}	$\delta_{rev,Ou}$	$\delta_{rev,Finno}$	δ_{3D_with}	δ_{field}
	-	-	-	-	-	mm	mm	mm	mm	mm
1	675	4497	3150	0.84	2.18	209.30	31.45	33.10	8.15	3.90
2	675	2811	2485	0.85	2.01	177.10	37.93	38.60	19.28	4.11
3	675	3373	2765	0.87	2.43	206.08	27.57	28.36	12.45	3.78
4	675	1927	1706	0.91	2.17	177.10	35.70	36.33	6.85	0.83
5	675	3373	2897	0.82	2.29	209.30	30.34	31.01	14.87	3.01
6	675	2811	2546	0.82	1.95	209.30	39.95	40.52	6.91	3.04

Table 4.15 Comparison of wall displacements of Case C

SI	δ_{Clough} / H_e	$\delta_{rev,Ou} / H_e$	$\delta_{rev,Finno} / H_e$	δ_{3D_with} / H_e	δ_{field} / H_e	$\delta_{spacing} / H_e$
	%	%	%	%	%	%
1	1.30	0.195	0.206	0.051	0.0242	0.0265
2	1.10	0.236	0.240	0.120	0.0255	0.0529
3	1.28	0.171	0.176	0.077	0.0235	0.0221
4	1.10	0.222	0.226	0.043	0.0052	0.1444
5	1.30	0.188	0.193	0.092	0.0187	0.0310
6	1.30	0.248	0.252	0.043	0.0189	0.0417

doi:10.6342/NTU201900743

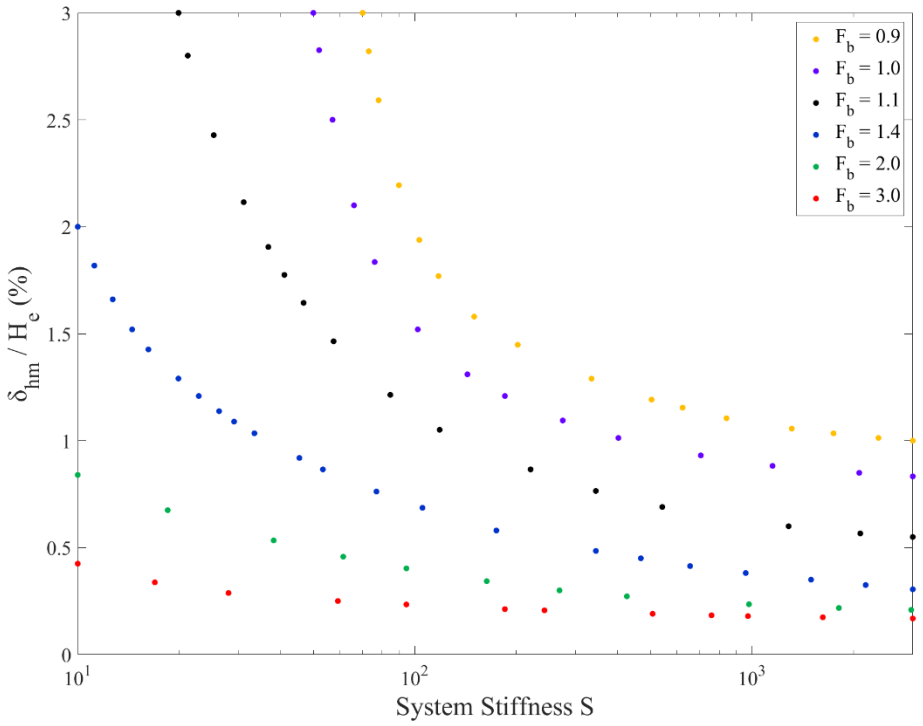

Figure 4.1 Redrawn relationship between maximum wall movement and system stiffness
(Clough et al., 1989)

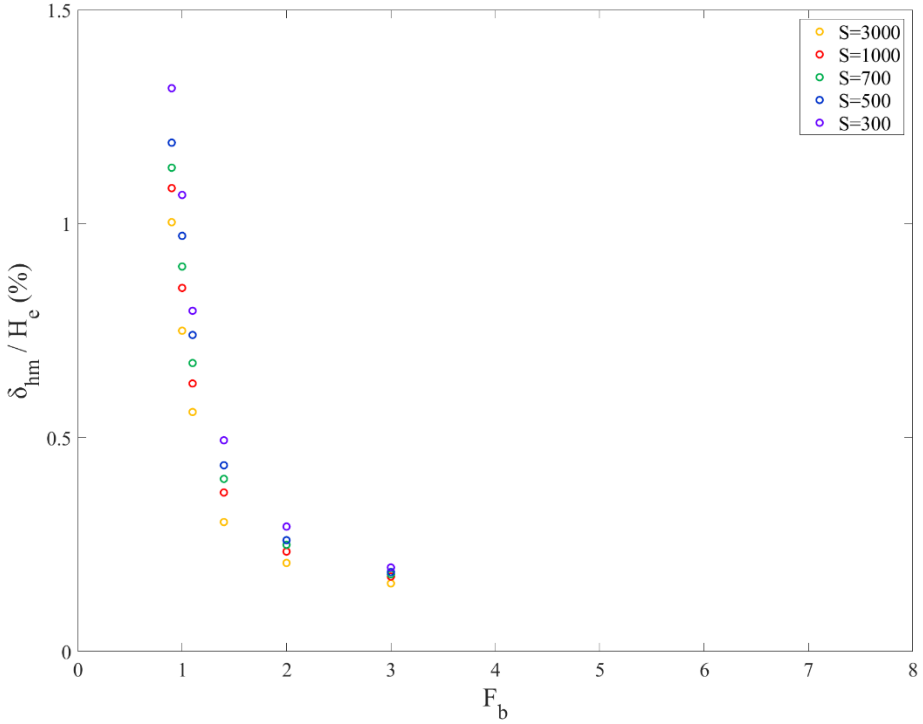

Figure 4.2 Relationship between maximum wall movements and factor of safety against basal heave

doi:10.6342/NTU201900743

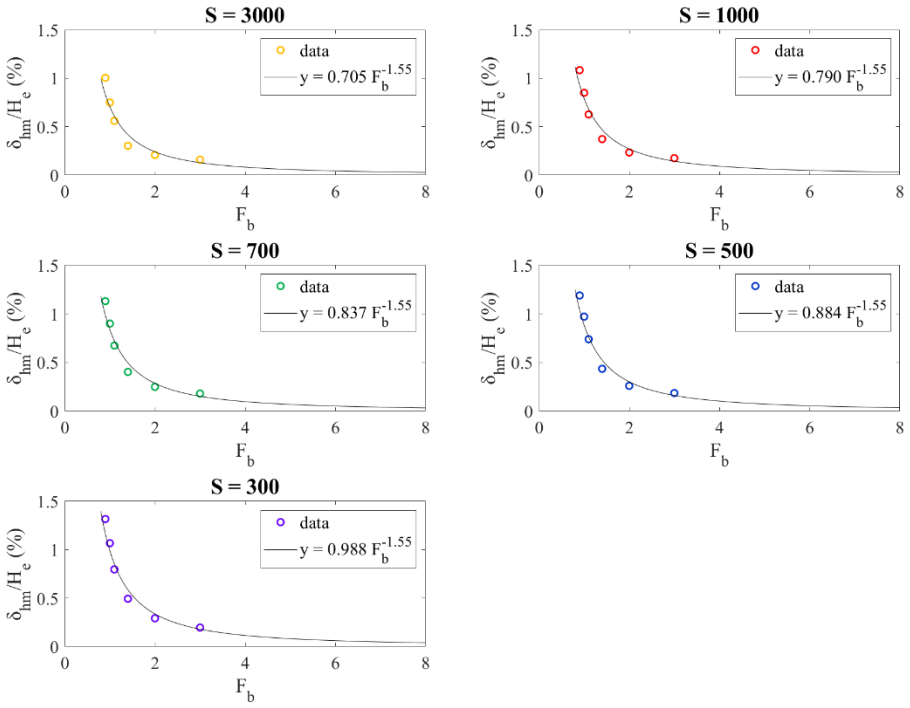

Figure 4.3 Regression equations for various system stiffness

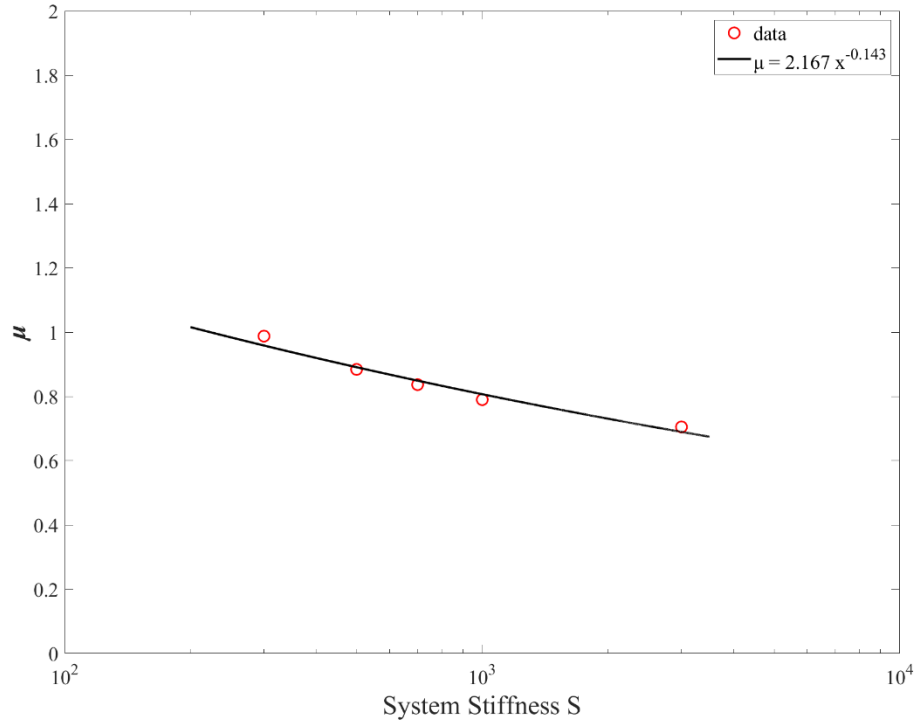

Figure 4.4 Relationship between μ and system stiffness

doi:10.6342/NTU201900743

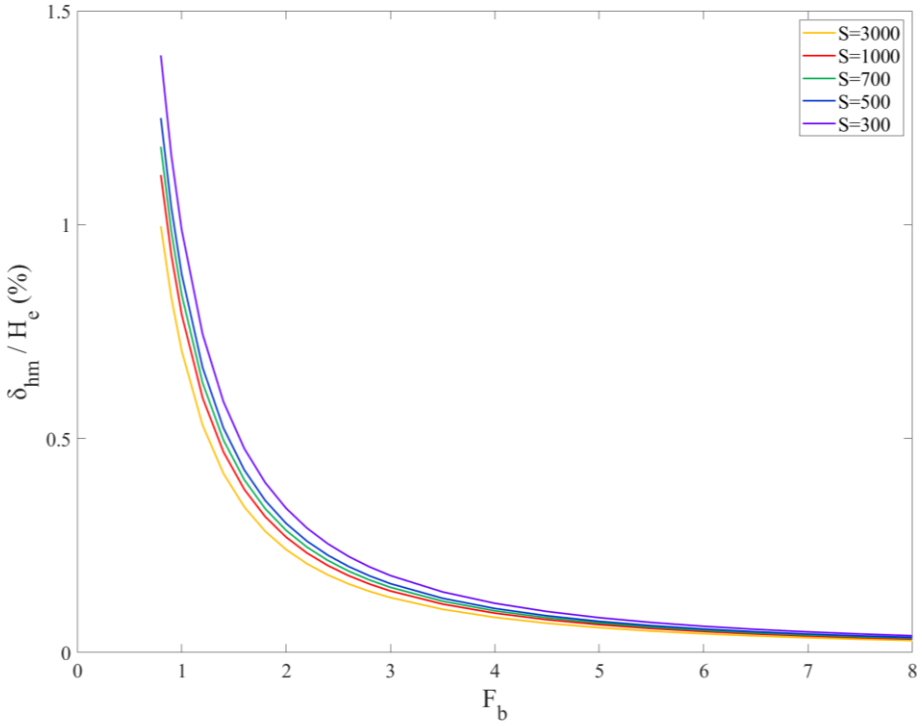

Figure 4.5 Regression curves with different system stiffness

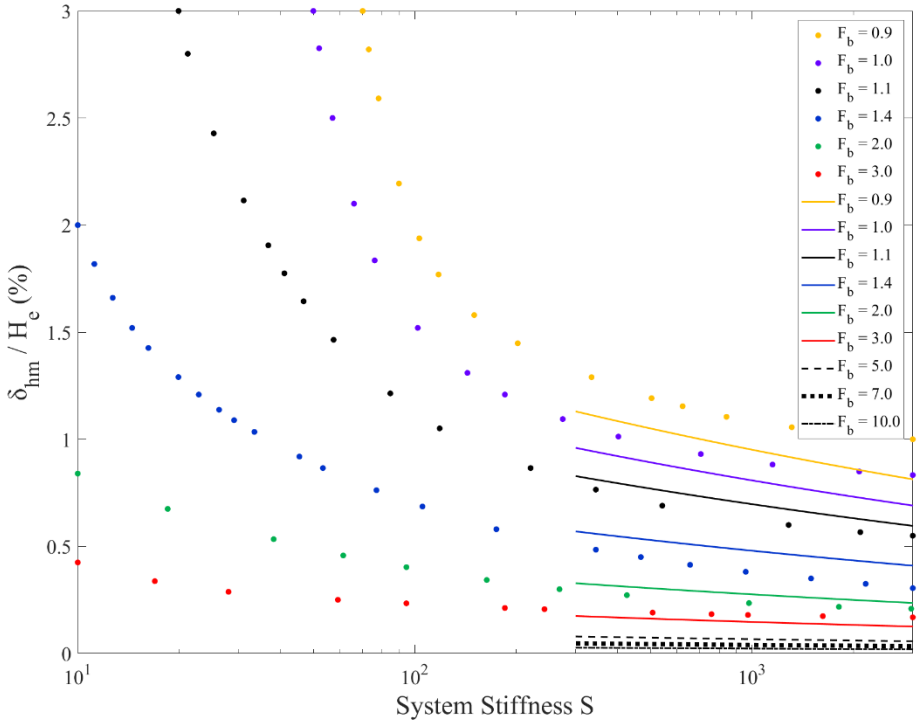

Figure 4.6 Comparison of original data with regression curves

doi:10.6342/NTU201900743

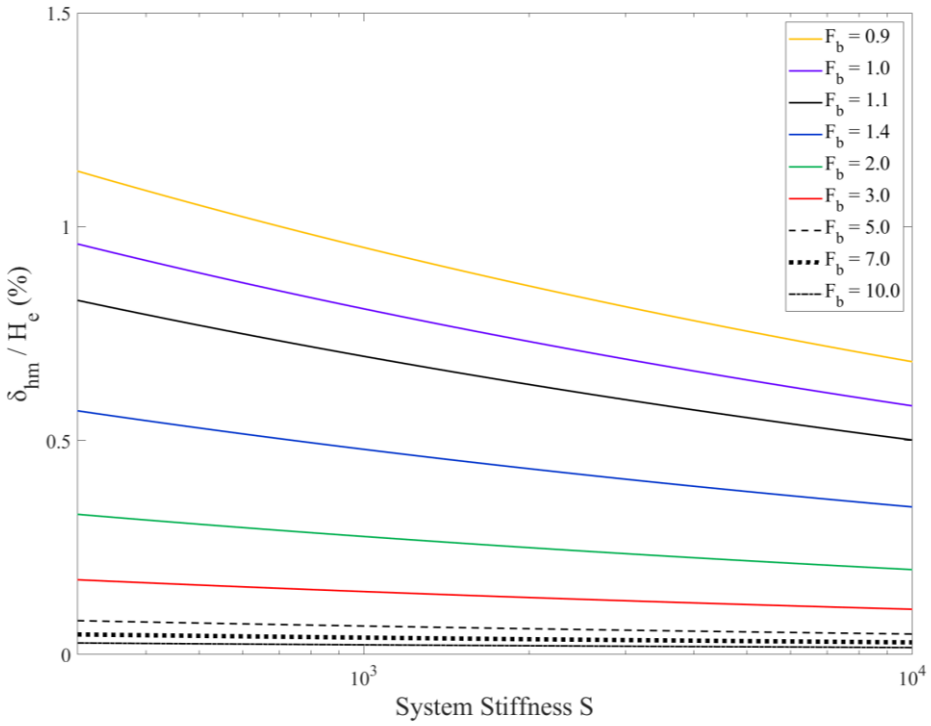

Figure 4.7 Regression curves for $S > 300$

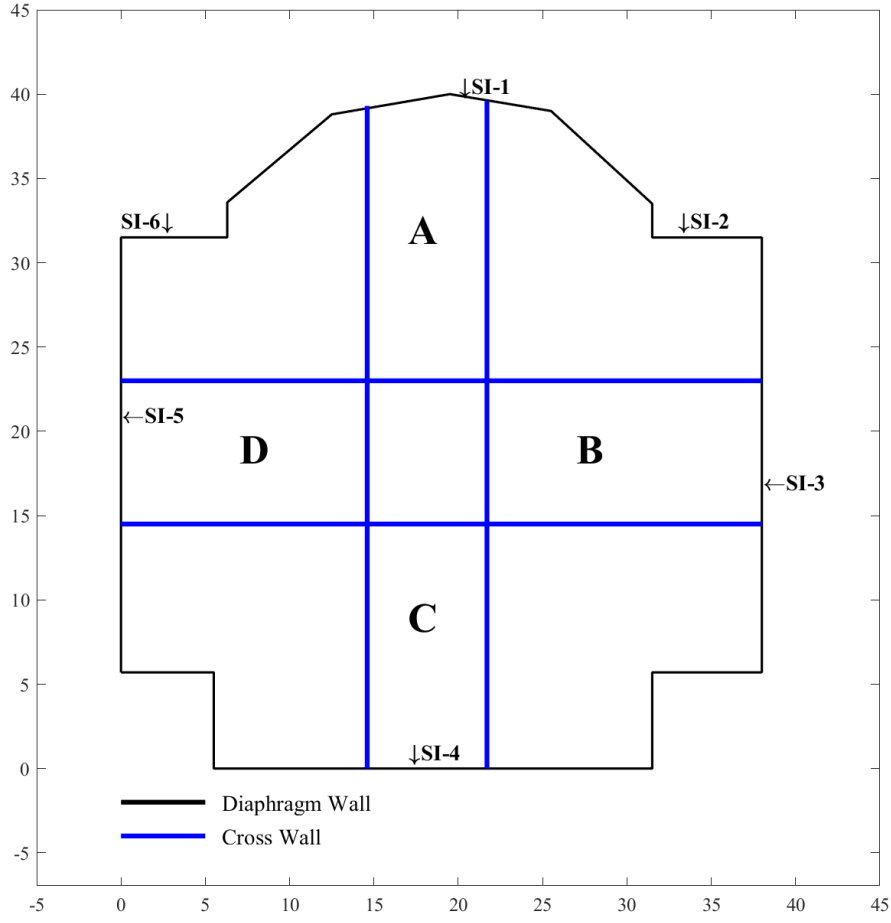

Figure 4.8 Small zones of Case A

doi:10.6342/NTU201900743

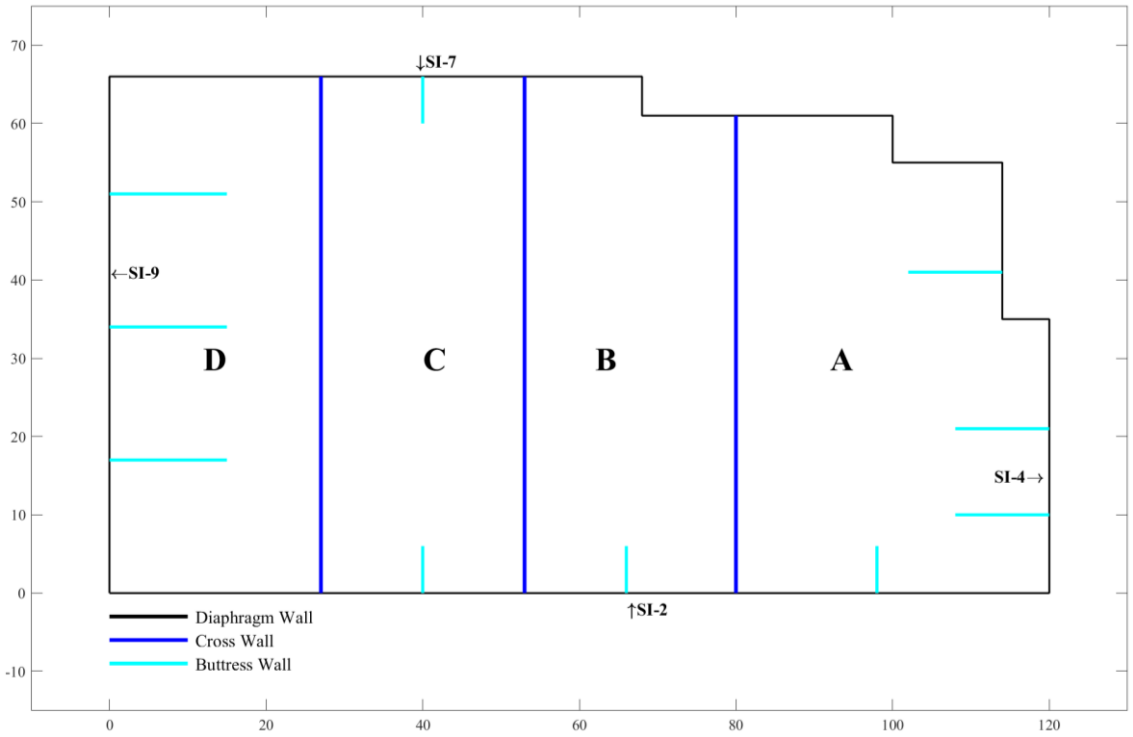

Figure 4.9 Small zones of Case B

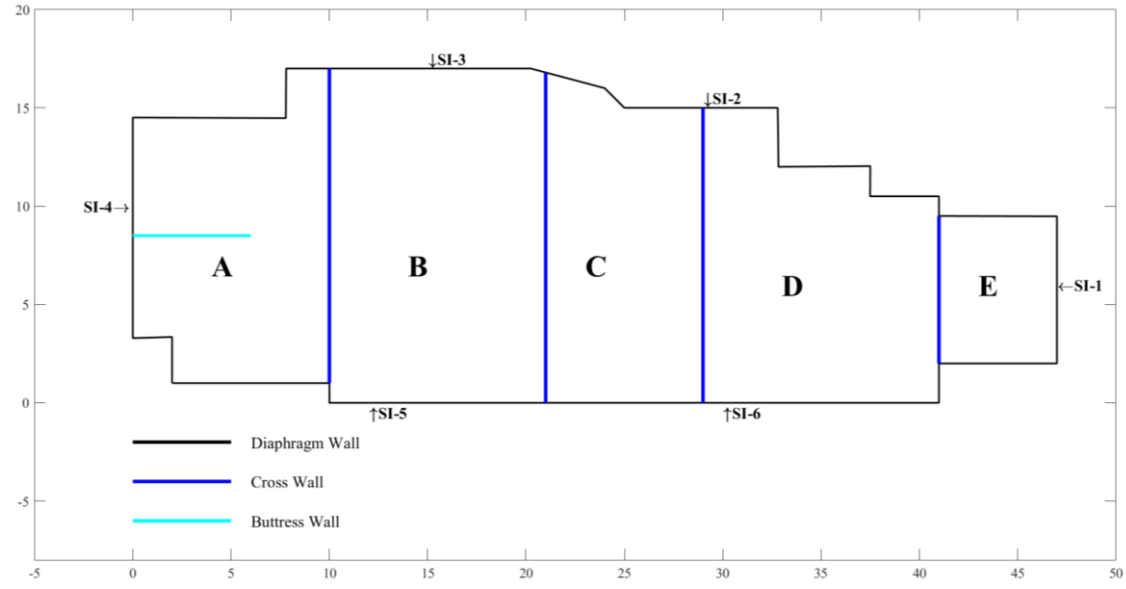

Figure 4.10 Small zones of Case C

doi:10.6342/NTU201900743

Chapter 5 Effects of Cross Walls on Wall Displacement

According to the outcomes of previous parametric studies, the effects of cross walls were underestimated by the simplified approach. The reason for such underestimation should be further investigated. More data and more numerical results are required to quantify the effects of cross walls on the retaining wall, and numerical simulations are conducted by PLAXIS 3D herein. The numerical analysis is considered as a better method to simulate the behavior of cross walls, which can model the full excavation site to investigate the effect of cross walls. Judging from the results of case histories, it appears that the spacing and the number of cross walls are the most important factors in limiting wall displacement. Therefore, a series of numerical analyses are carried out focusing on such factors.

A thick clay layer is adopted in the numerical analyses, which is an ideal soil condition. The undrained shear strength of clay is assumed to increase with depth. Despite of being ideal, it can simplify complex issues such as the effects of mixed layers. The finite element code, PLAXIS 3D, is adopted to simulate the effect of cross walls and calculate the wall displacement. It is noted that varying the number of cross walls is the same as varying the spacing of cross walls. Therefore, only the spacing of cross walls is addressed in this chapter. Afterwards, an equation is established by using these results to

doi:10.6342/NTU201900743

quantify the relationship between the spacing of cross walls, the strength of soil and the maximum wall displacement.

5.1 Spacing of Cross Walls

If cross walls are used in excavation project, the wall deformation can be reduced as a result. It is intuitive that as the number of the cross walls increases, the wall deformation would further reduce to a lower value. Since the cross walls are constructed before the excavation, the supporting effect of cross walls on the retaining wall is more pronounced than the horizontal supports. The spacing of the cross walls is a vital factor to control the magnitude of the wall deformation. Of course, the spacing has a limited value if cost and construction stability of cross walls construction are of concern. It implies that there is an optimal spacing of cross walls. In other words, if the spacing is further reduced after a certain wall displacement, the reduction in wall displacement is no longer significantly. Exactly, how much the wall displacement can be effectively reduced due to the decreasing in spacing of the cross walls will be discussed in this chapter.

It is of great interest to find out if there exists optimal spacing that yields a wall displacement of minimal value. Once the optimal spacing is found, there is no need to further reduce the spacing between cross walls, as the wall displacement can no longer be effectively reduced. In next section, it would be described in detail how the spacing of cross walls is simulated, and the selection of the material parameters including the soil,

doi:10.6342/NTU201900743

the diaphragm walls, the cross walls and the horizontal supports.

5.2 Refined Analysis

The finite element program, PLAXIS 3D is used to simulate the effect of cross walls at different spacing. For simplicity, the shape of the excavation zone is square with four different sizes, which are 60 m by 60 m, 42 m by 42 m, 30 m by 30 m and 20 m by 20 m, while the excavation depth is a fixed value of 14 m. The cross walls are either installed in one direction or in both horizontal and vertical directions. The direction issue could be simplified as the excavation zone is square, which means that installing horizontal cross wall is similar with installing vertical cross wall. Installing cross walls in both directions helps to reduce the effort in conducting numerical analyses as the excavation is symmetry in both directions. The number of the cross wall at each direction is two to seven depends on the excavation size. For instance, there are five different spacing for a 60 m by 60 m site, which are 60 m, 30 m, 20 m, 15 m and 10 m. The total number of analysis models is 25 as shown in Figure 5.1. Due to the symmetrical characteristics of the square, the number of models can be reduced to 15. For the 20 m by 20 m site, two spacing values of 20 m and 10 m are specified. The total number of analysis models is 4, and it can be reduced to 3 due to symmetry. The spacing used in analyses for various project size are listed in Table 5.1, including the full domain size in the 3D numerical analyses. The assumed bottom-up excavation sequence is presented in Table 5.2. The diaphragm wall

doi:10.6342/NTU201900743

is 0.8 m in thickness and 28 m in depth, the cross wall is 0.8 m in thickness and 25 m in depth. Details of the structural parameters are presented in Table 5.3. There are 3 levels of horizontal supports in the assumed excavation zone, the material properties are presented in Table 5.4. Though, the thickness and depth of the cross walls could also affect the displacement of perimeter diaphragm wall, these two factors are not investigated herein.

In the assumed analysis domain, the subsurface consist of a thick clay layer to a depth of 60 m. The assumption is an ideal condition, but it serves as a baseline condition to study the effect of cross walls. For the parametric studies, the undrained shear strength of the thick clay layer is assumed to increase with depth. The undrained shear strength ratio varies from 0.18 to 0.33. To be specific, six undrained shear strength ratio of 0.18, 0.22, 0.24, 0.27, 0.30 and 0.33 are used in the parametric studies, the per meter increment of both Young's modulus and undrained shear strength for six soil conditions are listed in Table 5.5. Generally, the undrained shear strength ratio of normally consolidated clay is 0.24, and the parametric studies cover clay layer with different consistencies. The ground water level was assumed at 3 m below the ground surface.

doi:10.6342/NTU201900743

5.3 Numerical Results and Comparisons

5.3.1 Results of numerical analyses

Summarizing the numerical results, the ratio of the maximum wall displacement divided by the excavation depth (δ_{hm}/H_e) versus the spacing of cross wall (d_c) are shown in Figure 5.2 to Figure 5.5 and these figures respectively represent a specific site dimension with different soil strength. For example in Figure 5.2, the numerical results are for 60 m by 60 m site with different soil strength. It can be seen that the ratio of the maximum wall displacement divided by the excavation depth reduces significantly as the spacing is decreased from 60 m to 20 m. Especially for the weaker soil, the reduction rate is more obvious. In addition, these results can be redrawn with site dimension as variable, the results are shown in Figure 5.6 to Figure 5.11.

All numerical results can be summarized in a single chart to show the effect of the spacing, which is shown in Figure 5.12. It is observed that the wall displacement decreases linearly with the spacing of cross walls, and it might be able to draw a straight line to describe the relationship between the spacing and the wall displacement ratio. In other words, there is a unique relationship between the wall displacement ratio and its corresponding spacing of cross walls. It is also observed that a same spacing of cross walls would result in a similar displacement of diaphragm wall regardless the size of these excavation zones. For instance, for strength ratio of 0.18, the 30 m spacing of Square60

doi:10.6342/NTU201900743

and Square30 models had similar maximum wall displacement of about 0.58% and 0.56% of the excavation depth, respectively. In addition, for the same soil strength, the 10 m spacing of the Square60, Square30 and Square20 models did not have the similar maximum wall displacement though the maximum wall displacement ratio is below 0.2%.

A larger excavation zone will result in a larger maximum wall displacement. This can be attributed to the cross walls above the excavation surface are removed by step-by-step excavation. In addition, the maximum wall displacement would usually happen at the center section of diaphragm wall or the middle of the two adjacent cross walls, so that the possible location of the maximum wall displacement would be more further away from the corner of the diaphragm wall for the larger excavation zone. The site dimension of Square60 is larger than those of Square30 and Square20, resulting in a larger maximum wall displacement despite the spacing of cross walls are the same for sites with different size.

Linear relationship between the spacing of cross walls and wall displacement ratio are presented in Figure 5.13 for various soil strength. Lines shown in Figure 5.13 are for the undrained shear strength ratio equals to 0.18, 0.22, 0.24, 0.27, 0.30 and 0.33, respectively. The slope and the intercept of these lines depend on the undrained shear strength ratio. It is interesting to note that the slope and the intercept of those lines could be represented by a simple equation in exponential form as shown in the following.

doi:10.6342/NTU201900743

$$A = 0.0011 \times m^{-1.87}$$

$$B = -0.0001 \times m^{-4.4}$$

$$\delta_{hm}/H_e\,(\%) = (0.0011 \times m^{-1.87}) \cdot x + (-0.0001 \times m^{-4.4}) \quad (5.1)$$

where A and B are the slope and the intercept of the lines, respectively; m is the undrained shear strength ratio; x is the spacing of cross walls.

In Figure 5.13, it is noted that these lines seems to have a limited cut-off line at about 15 m, which is the spacing of cross walls that develops the best efficiency in limiting wall displacement. Once reached the cut-off line, decreasing the spacing further has very limited effect on reducing the displacement of diaphragm wall. An optimal spacing of 15 m is in agreement with current design practice that the best spacing of cross walls should be around 15 m.

Using undrained shear strength ratio of 0.18 and 0.33 as the lower and upper boundaries of soil strength, the range of possible wall displacement ratio can be defined in Figure 5.14. The boundaries of displacement ratios can be applied in other cases to verify its applicability, which is discussed in the next chapter.

doi:10.6342/NTU201900743

5.3.2 Comparing the numerical results with predictions by the regression equation

The numerical results are further discussed in this section. As shown in Appendix A, the system stiffness (S), combined system stiffness (S_c), factor of safety against basal heave (F_b) and adjusted factor of safety against basal heave (F_{b_adj}) are calculated for all numerical results. The combined system stiffness and adjusted factor of safety against basal heave can further be used in conjunction with the regression equation to predict the corresponding wall displacements (δ_{rev}) under the influence of cross walls. If the regression equation is valid to certain extent, the predictions (δ_{rev}) by regression equation should be close to the numerical results (δ_{3D}).

Unfortunately, the comparison shows the opposite. It is found that most of the predictions by regression equation are far smaller than the numerical results. In addition, some of the adjusted factor of safety against basal heave are unreasonably high as the small zones divided by cross walls may have an extremely high length to width ratio. For instance, the adjusted factor of safety against basal heave is 11.21 for case "S60, m033, 5h0v", which is an unreasonably high value induced by a length to width ratio of 6 as shown in Table 5.6 extracted from Appendix A. The high length to width ratio results in an overestimation of the cross wall effect.

More often than not, the full length of cross walls is used in estimating its strengthening effect, but it may lead to an overestimation of the strengthening effect by

doi:10.6342/NTU201900743

cross walls. There is doubt that if the full length of cross walls should be used in estimating the associated strengthening effect. From a theoretical point of view, the development of basal heave failure surface is subdued by the friction between cross walls and soil, this is a concept also shared by Hsieh and Lu (1999). Since the potential basal heave failure surface is limited by the dimension of the project site, perhaps an equivalent length (L_e) of cross walls should be used instead of the full length of cross walls. In this study, L_e is taken as the radius of the potential failure surface, which in turn is a function depending on the width of the excavation zone or the distance between the excavation surface and the stiff soil layer as proposed by Terzaghi (1943). As shown in Appendix B, it appears that an equivalent length (L_e) should be used in estimating the effect of cross wall. Replacing the full length of cross wall with the equivalent length seems be better to calibrate the adjusted factors of safety against basal heave. Instead of an excessive value of 11.21, the maximum adjusted factor of safety against basal heave is now 4.3 as shown in Table 5.7 extracted from Appendix B.

It is also noted that the applicability of regression equation has its limit. First, if the cross walls spacing is larger than 30 m or the undrained shear strength ratio is higher than 0.30, the predictions by regression equation is not very reasonable. Second, another interesting aspect to note is the adjusted factor of safety against basal heave will reach a peak value as the spacing of cross walls assumes a value of 20 m. As the spacing of cross

doi:10.6342/NTU201900743

wall is reduced or the number of cross walls increased, the adjusted factor of safety against basal heave is found to be lower as shown in Table 5.7. This observation is against basic cognitions that the adjusted factor of safety against basal heave should increase with the number of cross walls. One possible explanation for this phenomenon is that the adjusted factor of safety against basal heave is a function of site dimension. As the spacing of cross walls reduced, the depth of potential failure surface is limited to a shallower depth and the undrained shear strength ratio is smaller, resulting in an adjusted factor of safety against basal heave that has a smaller value than expected.

In summary, as the spacing of cross walls approaches 15 m, the effect will reach its peak value. Further reducing the spacing between cross walls will not effectively result in further reduction on wall deflection. Therefore, the effects of cross walls on retaining wall would not develop infinitely to an extremely low level. It appears that there is an ultimate low value of wall displacement even if the spacing of cross walls is reduced to a very small number. Hence, the regression equation is most suitable for excavations with cross wall spacing less than 15 m and the undrained shear strength ratio less than 0.30.

doi:10.6342/NTU201900743

Table 5.1 Domain size and spacing of cross walls

Type	Spacing	x_{min}	x_{max}	y_{min}	y_{max}
-	m	m	m	m	m
Square 60×60	60 30 20 15 10	-120	180	-120	180
Square 42×42	42 21 14 10.5	-114	156	-114	156
Square 30×30	30 15 10	-75	105	-75	105
Square 20×20	20 10	-65	85	-65	85

Table 5.2 Assumed excavation sequence of the parametric studies

Phase	Type	depth	Remark
-	-	m	-
1	Exc	-3.5	First exc. Stage
2	Strut	-2.8	H400 × 400 × 13 × 21 Preload: 490 kN/ea
3	Exc	-7.0	Second exc. Stage
4	Strut	-6.3	H400 × 400 × 13 × 21 Preload: 980 kN/ea
5	Exc	-11.0	Third exc. Stage
6	Strut	-10.3	H400 × 400 × 13 × 21 Preload: 980 kN/ea
7	Exc	-14.0	Fourth exc. Stage
10	Slab	-14.0	Cast FS
		-11.0	Cast B3F
11	Strut	-10.5	Remove Strut 3
	Slab	-8.0	Cast B2F
12	Strut	-6.5	Remove Strut 2
	Slab	-4.0	Cast B1F
13	Strut	-3.0	Remove Strut 1
	Slab	0.0	Cast 1F

Note: “ea” denotes “each strut”

doi:10.6342/NTU201900743

Table 5.3 Structural parameters of the parametric studies

Type	Depth from	Depth to	t	γ	fc'	E	ν
Unit	m	m	m	kN/m^3	MPa	kPa	-
DW	0	-28	0.8	23.56	27.5	2.46E+07	0.2
CW	0	-25	0.8	23.56	27.5	2.46E+07	0.2
1F	0	0	0.25	23.56	27.5	2.46E+07	0.2
B1	-4	-4	0.4	23.56	27.5	2.46E+07	0.2
B2	-8	-8	0.4	23.56	27.5	2.46E+07	0.2
B3	-11	-11	0.4	23.56	27.5	2.46E+07	0.2
FS	-14	-14	0.6	23.56	27.5	2.46E+07	0.2

Table 5.4 Strut parameters of the parametric studies

Type	Depth	E	A	EA	EA	Preload
Unit	m	kgf/cm^2	cm^2	kgf	kN	kN
H400 × 400 × 13 × 21	-	2.04E+06	218.7	4.46E+08	4.38E+06	490

Table 5.5 Assumed soil parameters of the parametric studies

Type	depth to	γ_s	E_u	$s_{u,ref}$	ν_u	$E_{u,inc}$	$s_{u,inc}$	z_{ref}	R_{int}
	m	kN/m^3	kPa	kPa	-	kPa/m	kPa /m	m	-
m=033	-60	18.15	14000	5	0.495	1415.4	2.83	0	0.67
m=030	-60	18.15	14000	5	0.495	1282.9	2.57	0	0.67
m=027	-60	18.15	14000	5	0.495	1150.5	2.30	0	0.67
m=024	-60	18.15	14000	5	0.495	1018.0	2.04	0	0.67
m=022	-60	18.15	14000	5	0.495	929.7	1.86	0	0.67
m=018	-60	18.15	14000	5	0.495	753.1	1.51	0	0.67

Note: m is the undrained shear strength ratio, $m = s_u/\sigma'_v$

doi:10.6342/NTU201900743

Table 5.6 The parameters and predictions for S60/m033 models by using the full length of cross walls

Type	Spacing y (L, B')	Spacing x (B, L')	PSR_x	PSR_y	S	F_{bx}	F_{by}	S_{cx}	S_{cy}	F_{bx_adj}	F_{by_adj}	δ_{3Dx} / H_e (%)	δ_{3Dy} / H_e (%)	δ_{revx} / H_e (%)	δ_{revy} / H_e (%)
S60, m033, 2h0v	20	60	0.28	0.92	542	1.68	2.47	1935	589	7.09	3.40	0.20	0.52	0.04	0.13
S60, m033, 2h1v	20	30	0.38	0.65	542	1.68	1.85	1426	833	5.26	3.64	0.21	0.36	0.06	0.11
S60, m033, 2h2v	20	20	0.42	0.42	542	1.68	1.68	1290	1290	4.65	4.65	0.21	0.21	0.07	0.07
S60, m033, 2h3v	20	15	0.45	0.20	542	1.68	1.61	1204	2709	4.35	3.76	0.21	0.14	0.08	0.09
S60, m033, 3h0v	15	60	0.19	0.94	542	1.61	2.47	2851	576	8.06	3.37	0.13	0.52	0.03	0.13
S60, m033, 3h1v	15	30	0.27	0.69	542	1.61	1.85	2007	785	4.83	3.51	0.14	0.35	0.06	0.12
S60, m033, 3h2v	15	20	0.20	0.45	542	1.61	1.68	2709	1204	3.76	4.35	0.14	0.21	0.09	0.08
S60, m033, 3h3v	15	15	0.35	0.35	542	1.61	1.61	1548	1548	3.22	3.22	0.14	0.14	0.12	0.12
S60, m033, 5h0v	10	60	0.12	0.96	542	1.60	2.47	4515	564	**11.21**	3.34	0.13	0.48	0.02	0.14

Table 5.7 The parameters and predictions for S60/m033 models by using the equivalent length of cross walls

Type	Spacing y (L, B')	Spacing x (B, L')	PSR_x	PSR_y	S	F_{bx}	F_{by}	S_{cx}	S_{cy}	F_{bx_adj}	F_{by_adj}	δ_{3Dx} / H_e (%)	δ_{3Dy} / H_e (%)	δ_{revx} / H_e (%)	δ_{revy} / H_e (%)
S60, m033, 2h0v	20	60	0.28	0.92	542	1.68	2.47	1935	589	4.29	3.54	0.20	0.52	0.08	0.12
S60, m033, 2h1v	20	30	0.38	0.65	542	1.68	1.85	1426	833	4.29	3.67	0.21	0.36	0.08	0.11
S60, m033, 2h2v	20	20	0.42	0.42	542	1.68	1.68	1290	1290	4.29	4.29	0.21	0.21	0.08	0.08
S60, m033, 2h3v	20	15	0.45	0.20	542	1.68	1.61	1204	2709	4.29	2.75	0.21	0.14	0.08	0.15
S60, m033, 3h0v	15	60	0.19	0.94	542	1.61	2.47	2851	576	2.75	3.54	0.13	0.52	0.14	0.12
S60, m033, 3h1v	15	30	0.27	0.69	542	1.61	1.85	2007	785	2.75	3.67	0.14	0.35	0.15	0.11
S60, m033, 3h2v	15	20	0.20	0.45	542	1.61	1.68	2709	1204	2.75	4.29	0.14	0.21	0.15	0.08
S60, m033, 3h3v	15	15	0.35	0.35	542	1.61	1.61	1548	1548	2.75	2.75	0.14	0.14	0.16	0.16
S60, m033, 5h0v	10	60	0.12	0.96	542	1.60	2.47	4515	564	2.73	3.54	0.13	0.48	0.14	0.12

doi:10.6342/NTU201900743

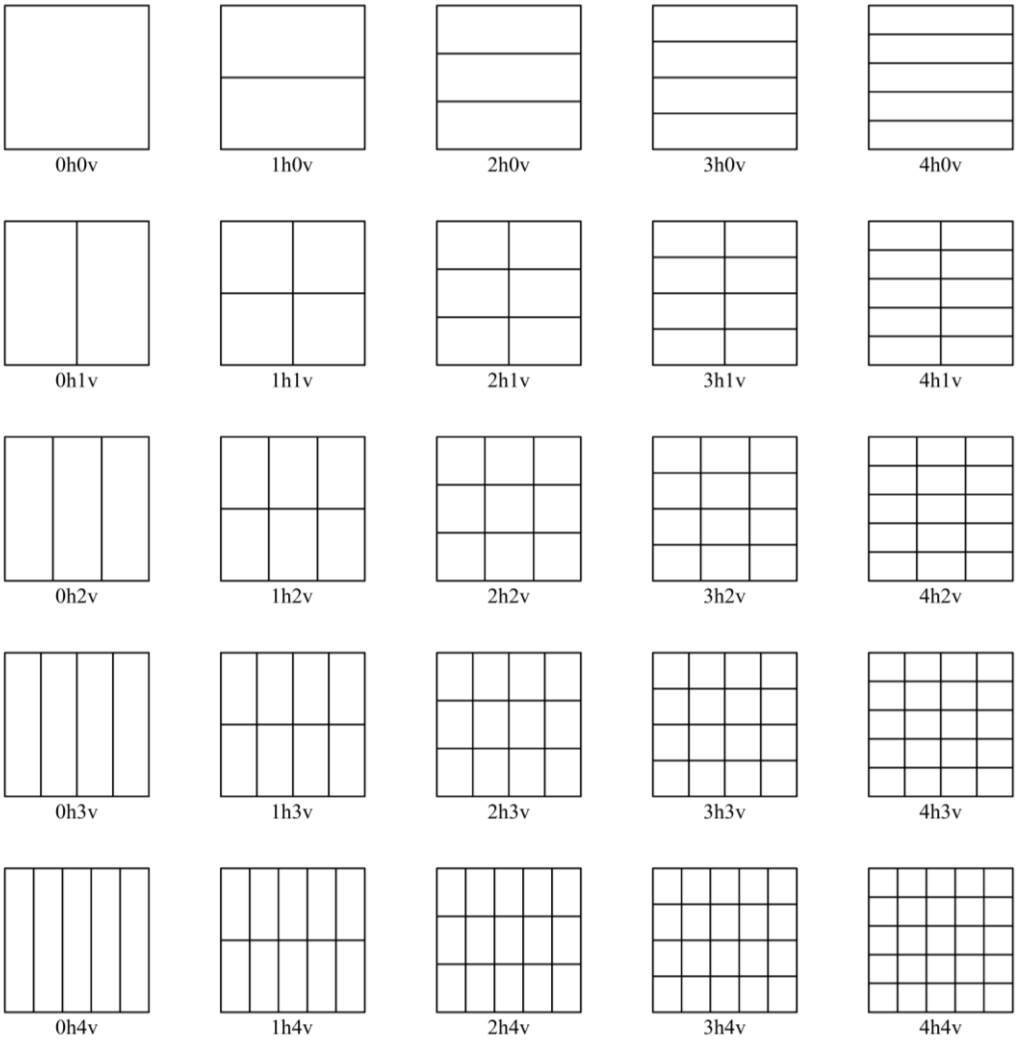

Figure 5.1 Plan layout of the cross walls

doi:10.6342/NTU201900743

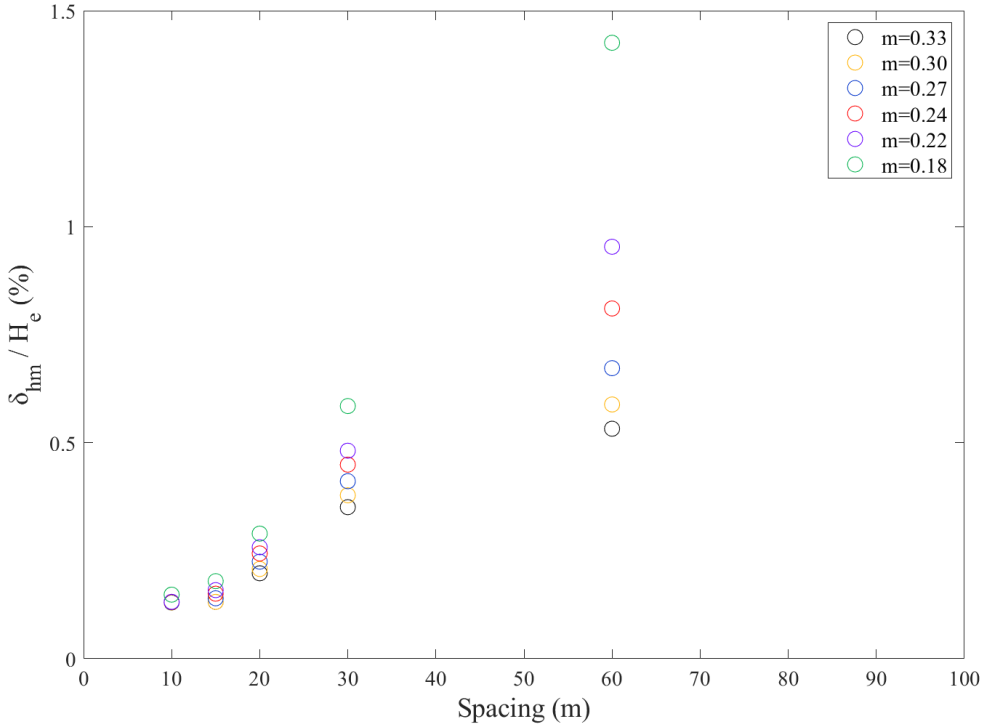

Figure 5.2 δ_{hm}/H_e versus cross wall spacing for Square 60

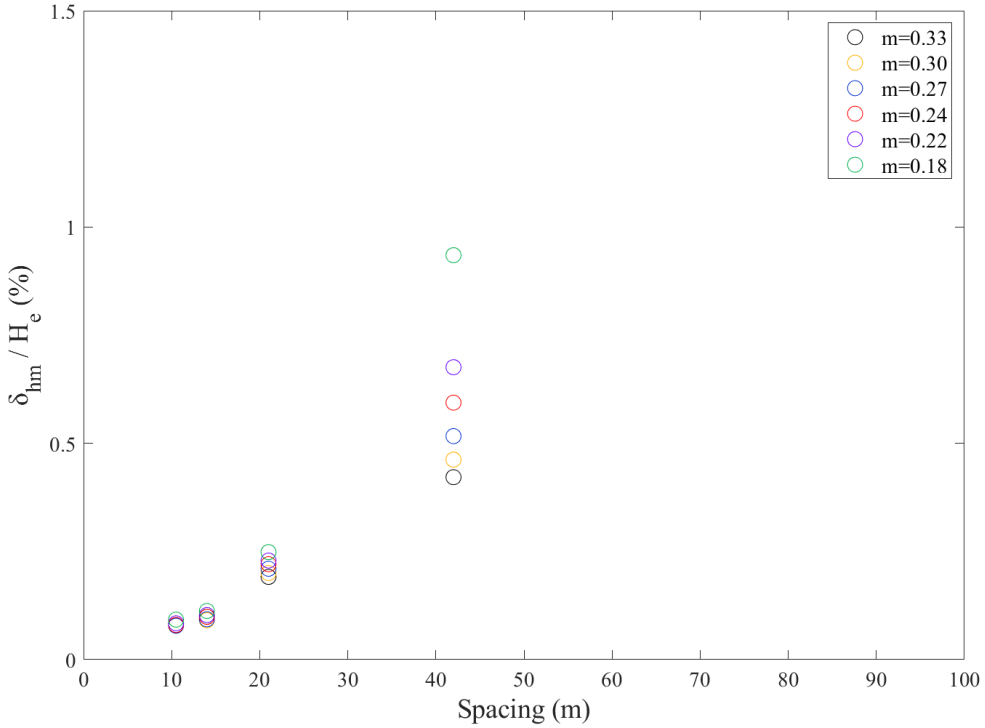

Figure 5.3 δ_{hm}/H_e versus cross wall spacing for Square 42

doi:10.6342/NTU201900743

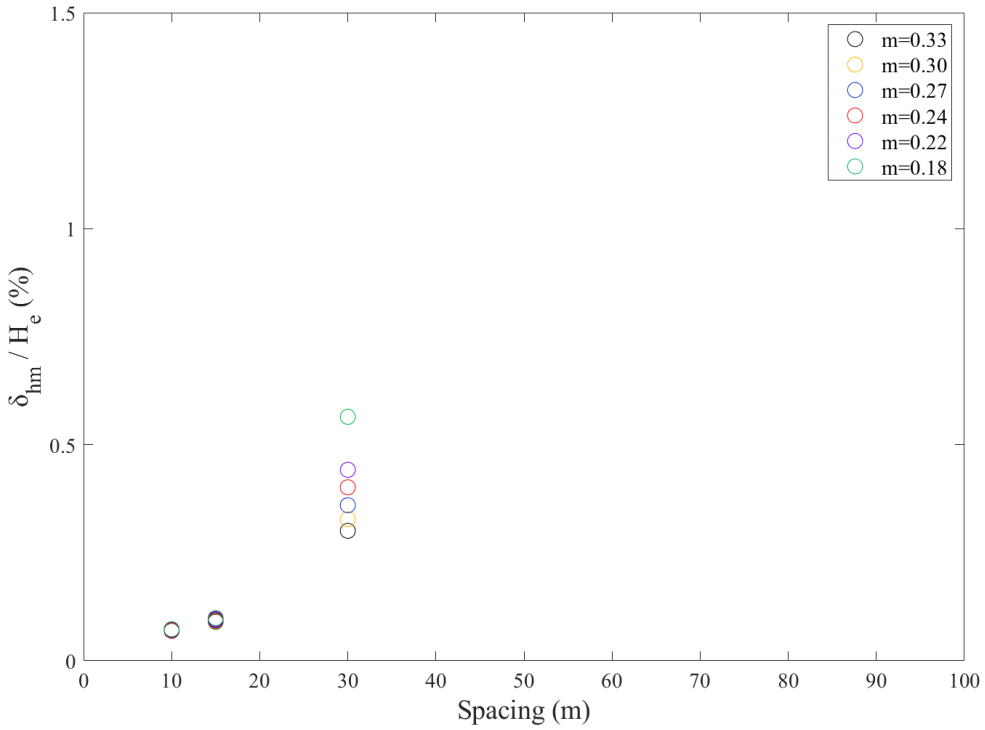

Figure 5.4 δ_{hm}/H_e versus cross wall spacing for Square 30

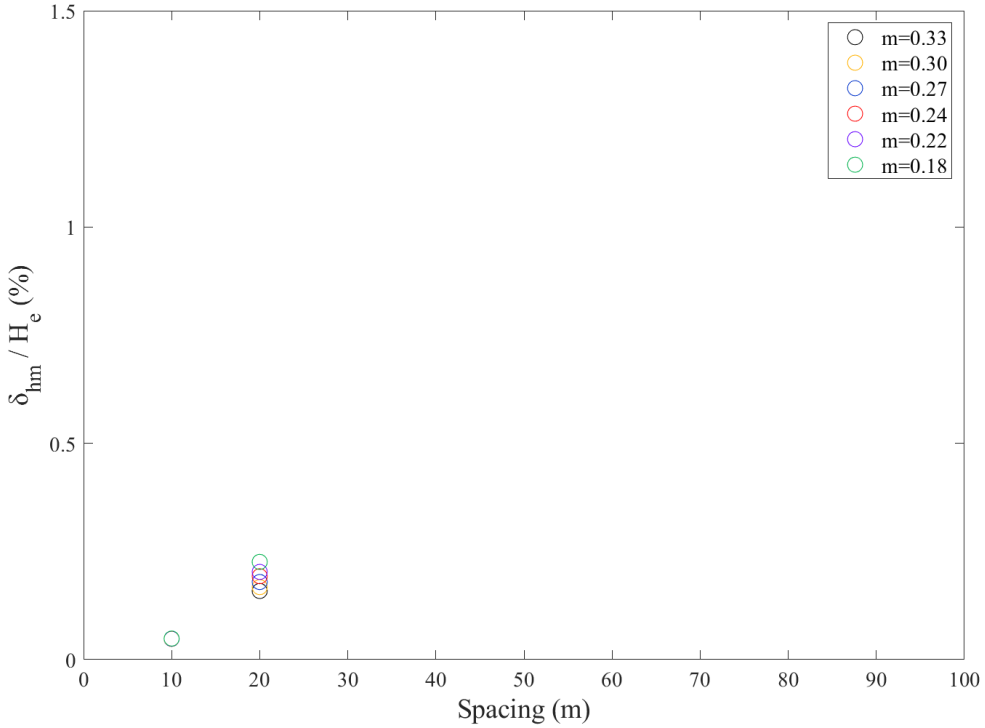

Figure 5.5 δ_{hm}/H_e versus cross wall spacing for Square 20

doi:10.6342/NTU201900743

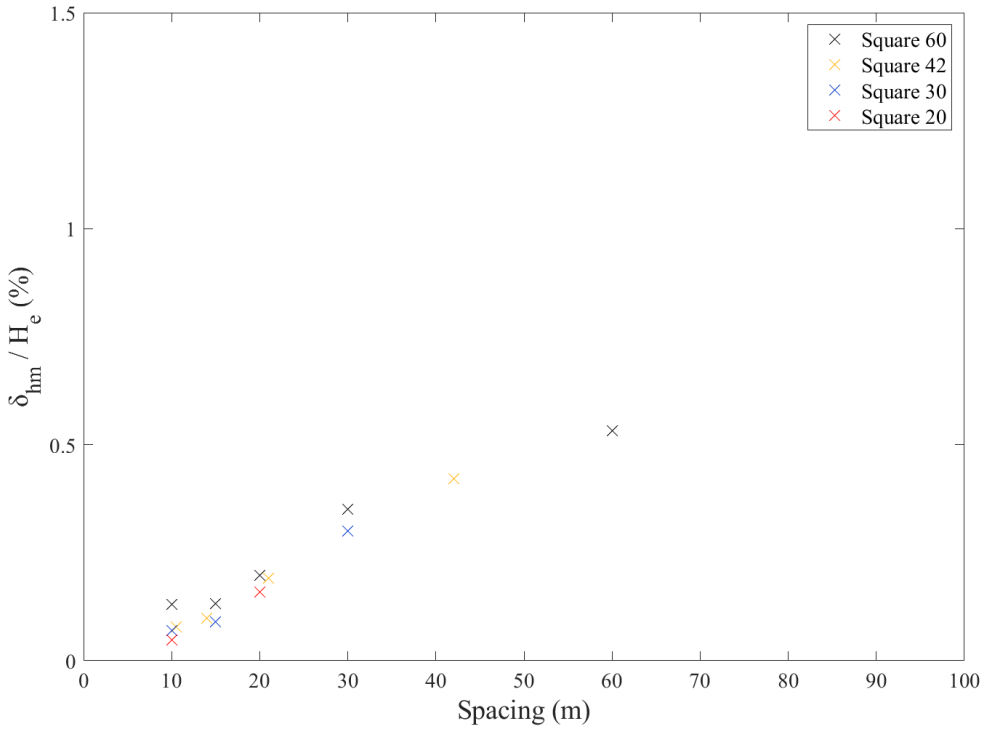

Figure 5.6 δ_{hm}/H_e versus cross wall spacing (m=0.33)

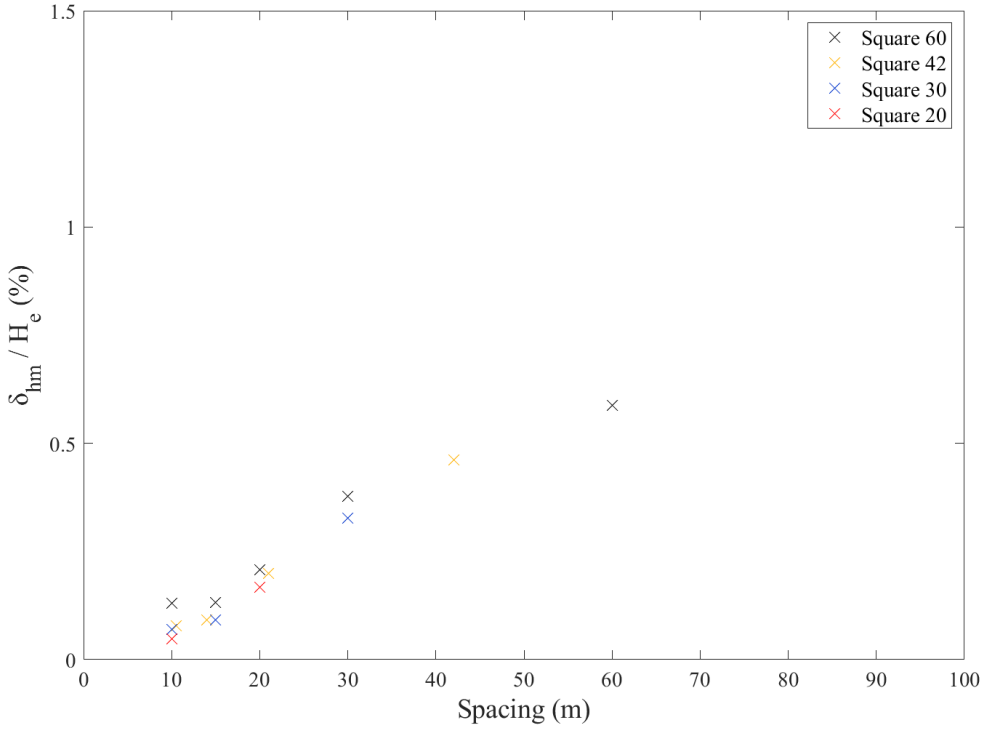

Figure 5.7 δ_{hm}/H_e versus cross wall spacing (m=0.30)

doi:10.6342/NTU201900743

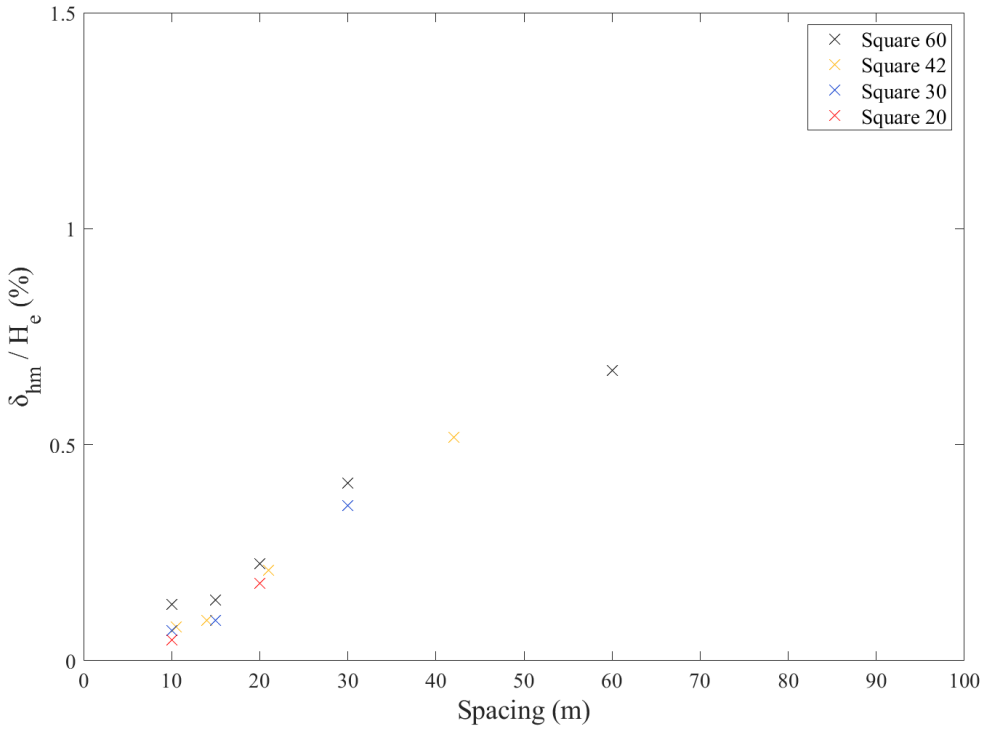

Figure 5.8 δ_{hm}/H_e versus cross wall spacing (m=0.27)

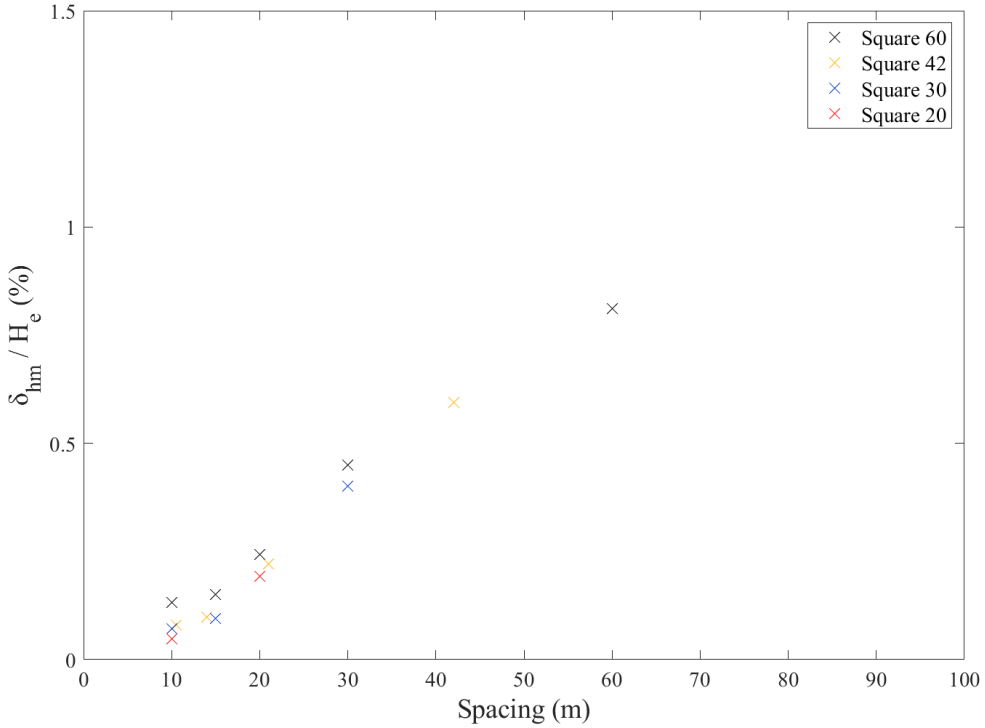

Figure 5.9 δ_{hm}/H_e versus cross wall spacing (m=0.24)

doi:10.6342/NTU201900743

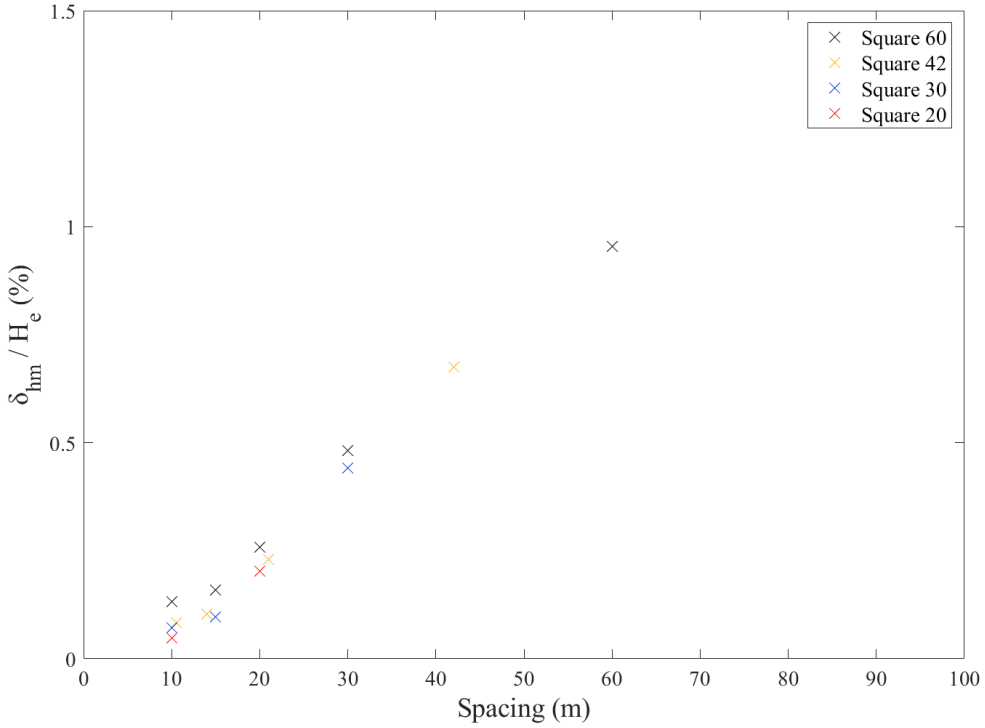

Figure 5.10 δ_{hm}/H_e versus cross wall spacing (m=0.22)

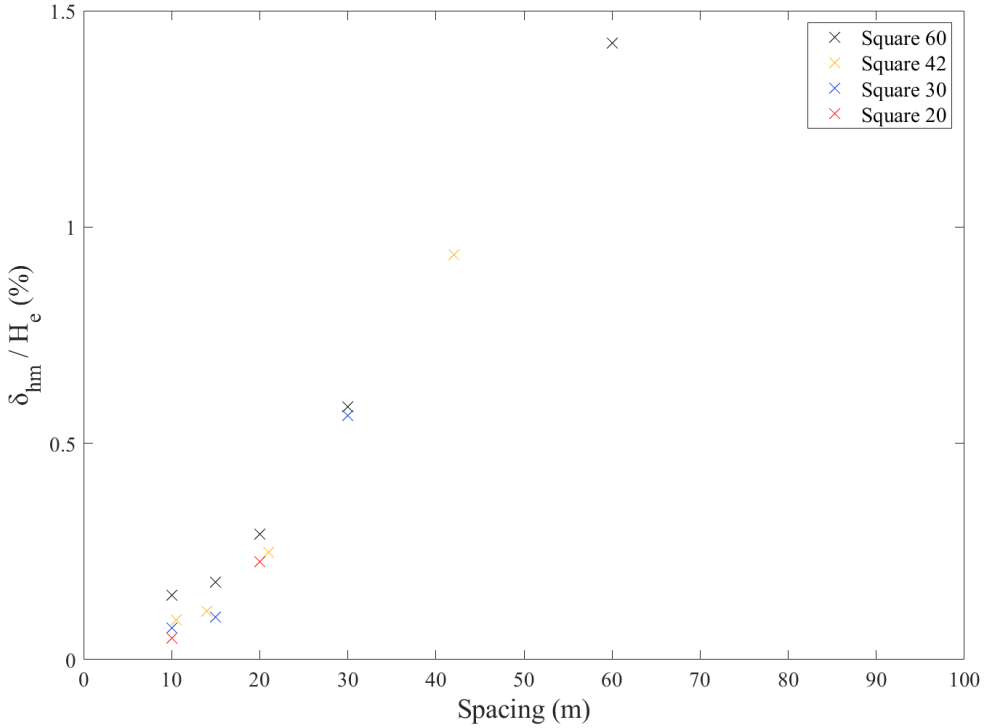

Figure 5.11 δ_{hm}/H_e versus cross wall spacing (m=0.18)

doi:10.6342/NTU201900743

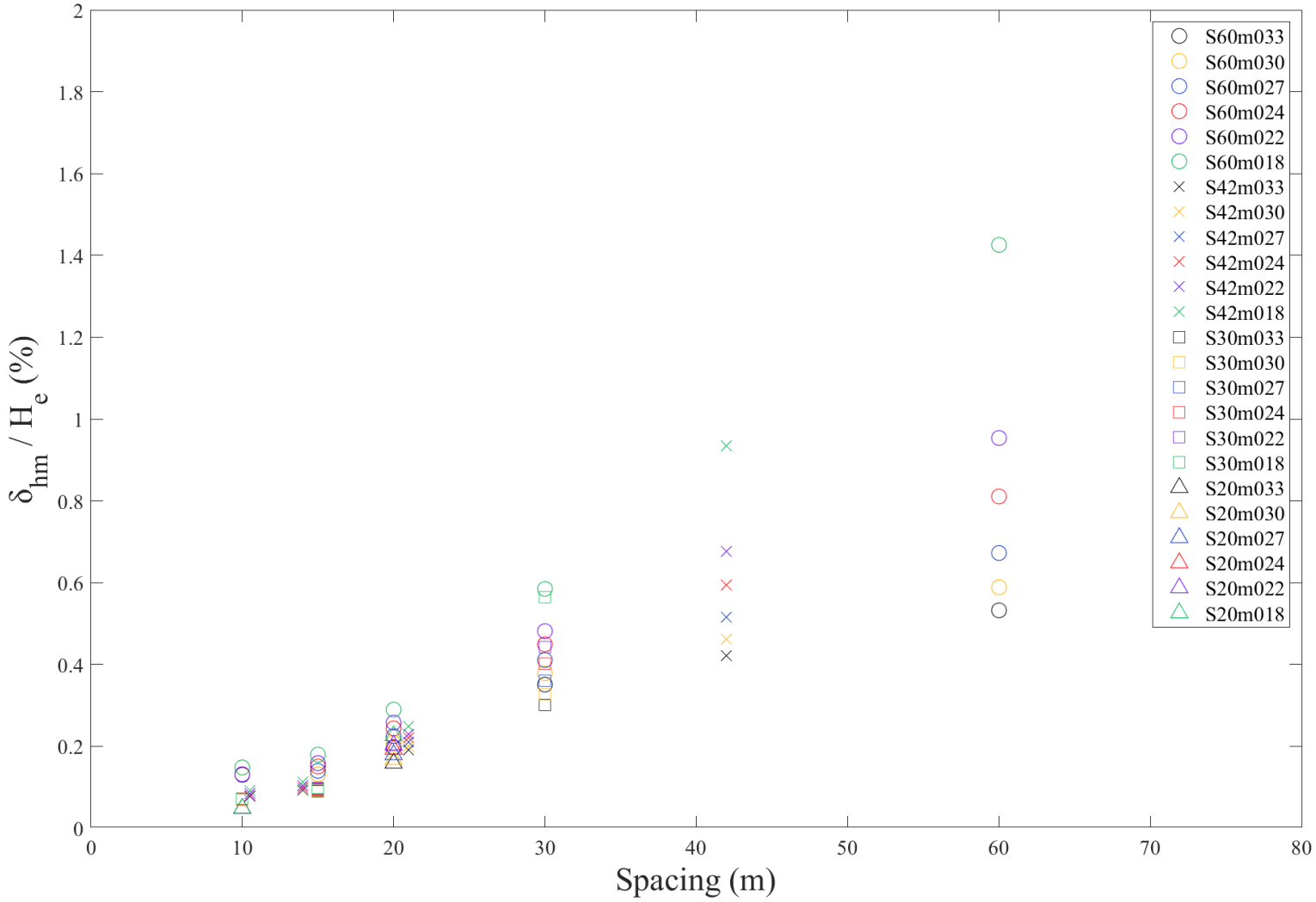

Figure 5.12 Relationship between wall displacement ratio and spacing of cross walls

doi:10.6342/NTU201900743

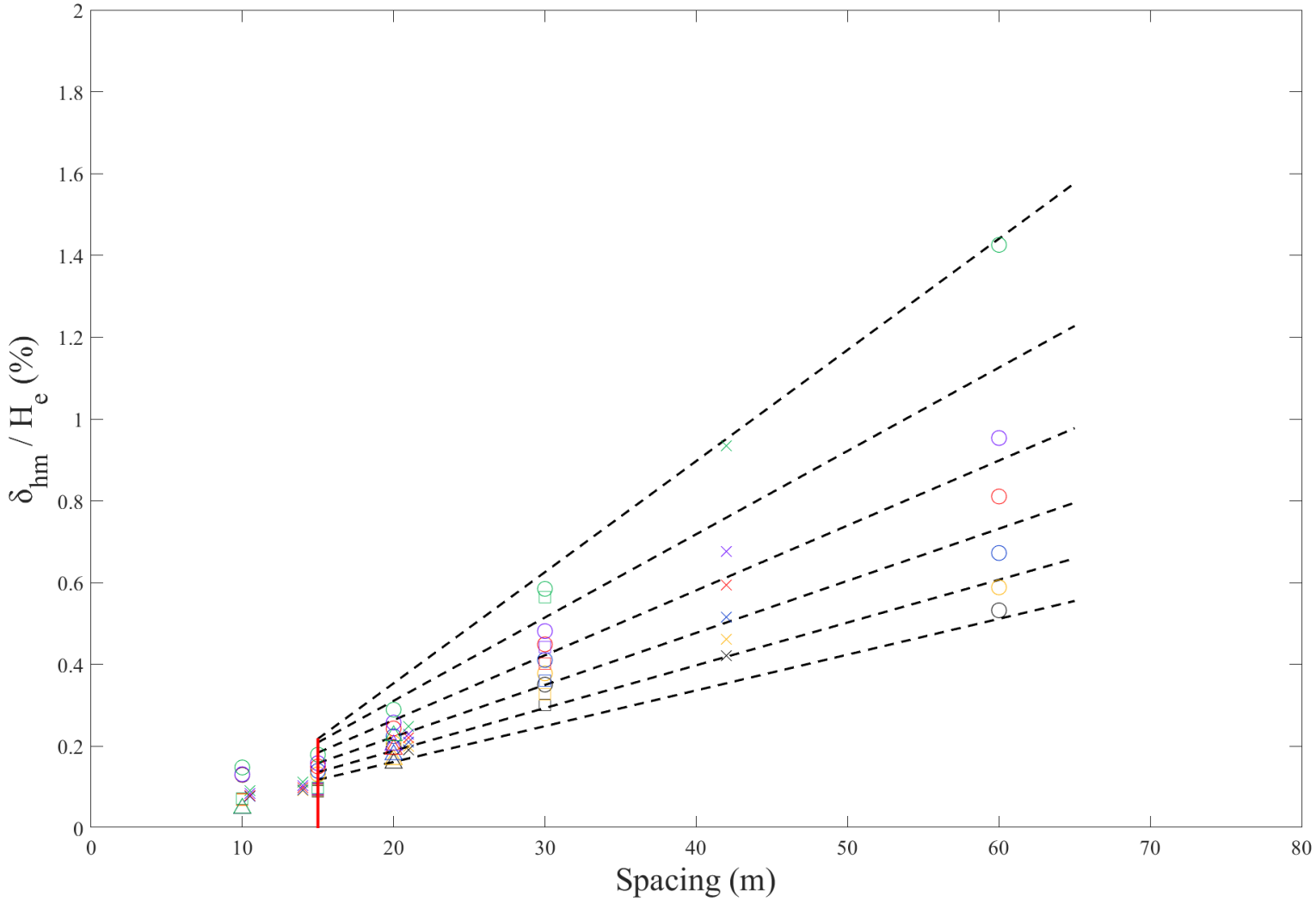

Figure 5.13 Linear relationship between displacement ratio and spacing of cross walls

doi:10.6342/NTU201900743

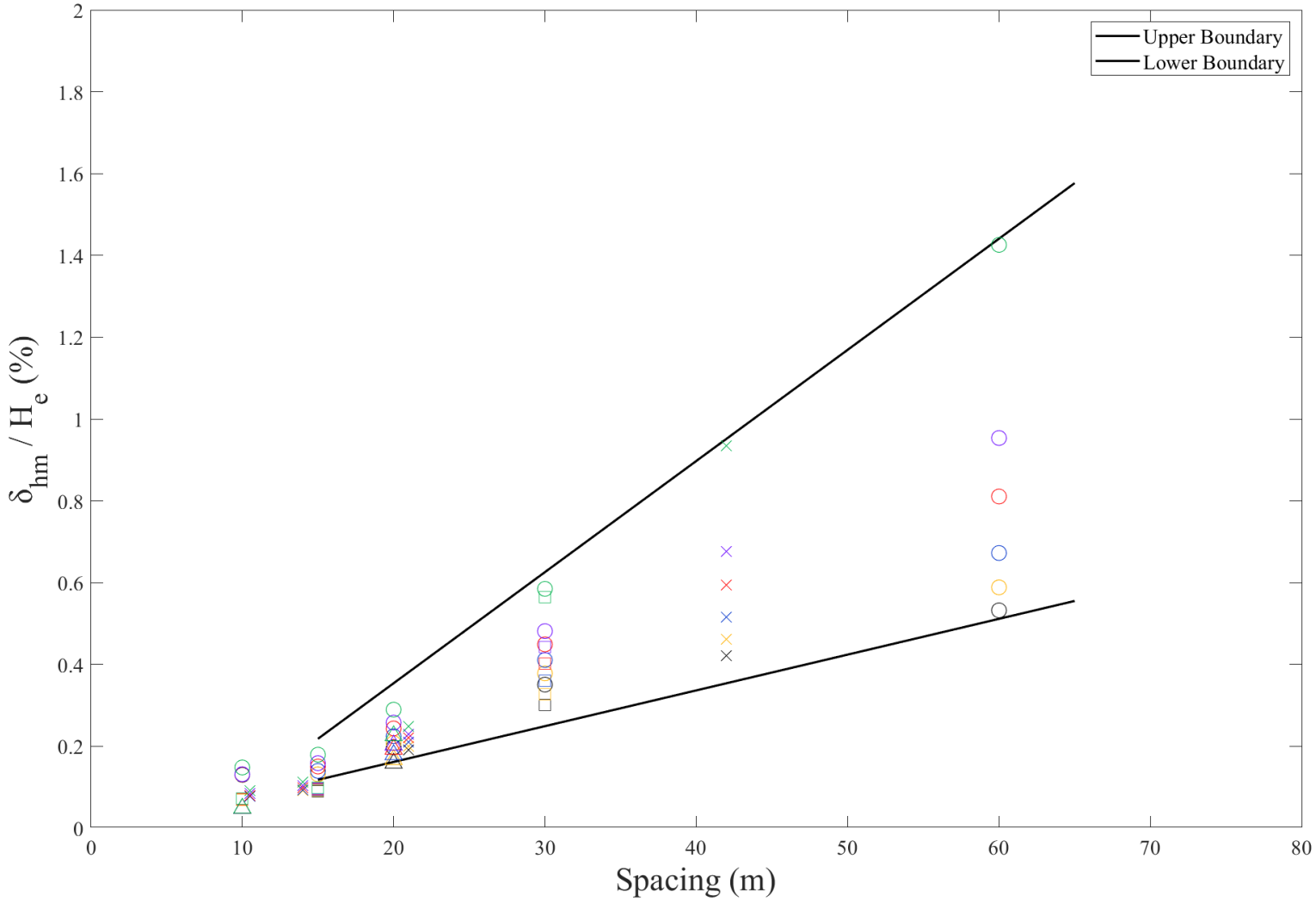

Figure 5.14 Boundaries of displacement ratios

doi:10.6342/NTU201900743

Chapter 6 Application of the Results of Parametric Studies

6.1 Application of the Regression Equation

The parametric studies conducted in chapter 4 showed that the maximum wall displacement of the retaining system estimated by the regression equation was satisfactory. In this section, the regression equation is applied to four additional case histories, which can be found in Wu (2017) and Chang (2016) that had enough inclinometer casings to measure the wall displacement. If reasonable predictions were achieved, the regression equation may be considered as a representative equation and is applicable for excavations in soft clay. The cumbersome task of using complicated finite element code to calculate the wall displacements can therefore be alleviated.

6.1.1 Case Z1

This case is located at Taipei and its detail can be found in Wu (2017). The excavation zone of Case Z1 was a rectangle with a maximum length and width of 76 m and 25 m, respectively. The soil stratigraphy of the site consists of eight layers underlain by a dense gravel at a depth of 52.5 m. The parameters of each soil layer are presented in Table 6.1. The ground water level is at 1.7 m below the ground surface. The excavation was carried out using the bottom-up method in 5 excavation stages, and the excavation depth was 13.5 m. The diaphragm wall was 0.7 m in thickness and 27 m in depth together

doi:10.6342/NTU201900743

with 3 levels of horizontal supports as the retaining system. In addition, there were two cross walls installed within excavation zone to reduce the wall deflection. The plan layout including the diaphragm wall, cross walls and locations of inclinometer casings are shown in Figure 6.1. It can be seen that the excavation zone was divided into three smaller zones by the cross walls, which are identified as zone A, B and C, respectively.

With all information at hand, the maximum wall displacement can be rapidly calculated. Knowing the width and length of each small zone, the factor of safety against basal heave and system stiffness can be calculated and listed in Table 6.2. The combined system stiffness and adjusted factor of safety against basal heave considering the cross wall effect can then be calculated. The details of both parameters are respectively presented in Table 6.3 and Table 6.4. With the S_c and F_{b_adj} being calculated, the regression equation is used to evaluate δ_{rev}. The comparison between δ_{rev}, δ_{Clough} and δ_{field} is summarized in Table 6.5. It can be seen that the δ_{rev} is much closer to δ_{field} than δ_{Clough}, which clearly indicates that the revised scheme is much better than the original scheme.

6.1.2 Case Z2

Case Z2 is located in Taipei and its detail can be found in Chang (2016). The excavation zone is an irregular shape with a maximum length and width of 50.5 m and 34 m, respectively. The soil stratigraphy of the site consists of six layers underlain by the

doi:10.6342/NTU201900743

dense gravel layer at a depth of 41.4 m. The parameters of each soil layer are presented in Table 6.7. The ground water level is at 1.7 m below the ground surface. The excavation was carried out using the top-down method in 6 excavation stages, and the excavation depth was 19.6 m. The diaphragm wall was 1.0 m in thickness and 36 m in depth together with 5 levels of slabs as the retaining system. This case was adjacent to Taipei MRT system; therefore, the wall deflection was strictly regulated by law. According to *Regulation on Building Restrictions along MRT Facilities* by Construction and Planning Agency, MOI (2013), any excavation near the MRT system must not induce deflection of tunnel exceeding 20 mm and settlement of rails must be less than 10 mm. This case was constructed with a much stiffer retaining system to guard against the lateral deformation. The retaining system includes 4 buttress walls and 3 cross walls, and its plan layout is shown in Figure 6.2. It can be seen that the excavation zone was divided into four smaller zones by the cross walls, which were defined as zone A, B, C and D.

Having acquired the basic information, the maximum wall displacement for each small zone can be rapidly calculated. Knowing the width and length of each small zone, the factor of safety against basal heave and system stiffness can be calculated, which are shown in Table 6.8. It has to be mentioned that though stratified soil layers with sand and clay exist in the excavation zone, it is considered that the strength of clay layer controls the excavation behavior. Therefore, the strength ratio of the weakest clay layer is used to

doi:10.6342/NTU201900743

calculate the undrained shear strength of each soil layer. The combined system stiffness and adjusted factor of safety against basal heave considering the cross walls effect can be calculated, and the details are presented in Table 6.9 and Table 6.10, respectively. Following the approach outlined in chapter 4, δ_{rev} can be calculated and compared with δ_{Clough} and δ_{field}, and the comparison is summarized in Table 6.11 and Table 6.12. Once again, it can be seen that δ_{rev} is in much better agreement with δ_{field}, while δ_{Clough} well overestimates the wall displacements.

6.1.3 Case Z3

Case Z3 is located in Kaohsiung and its detail can be found in Chang (2016). The excavation zone was a rectangular shape with a maximum length and width of 70 m and 20 m, respectively. The soil stratigraphy of the site consists of nine layers. Though the subsurface consists mainly of sandy soil, it can nevertheless be used to test the limits of the regression equation. The parameters of each soil layer were presented in Table 6.12. The ground water level is at 2 m below the ground surface. The excavation was carried out using the bottom-up method in 5 excavation stages, and the excavation depth was 16.8 m. The diaphragm wall was 0.9 m in thickness and 32 m in depth together with 4 levels of slabs as the retaining system. There were 4 inclinometer casings installed in the middle of each side of the site to monitor the wall deflection, the plan layout is indicated in Figure 6.3. There were no cross walls in the project site, and the secondary wall or side

doi:10.6342/NTU201900743

walls can be regarded as the cross walls.

Having acquired the basic information, the maximum wall displacement at each side can be rapidly calculated by the regression equation. Knowing the width and length of each side, the factor of safety against basal heave and system stiffness can be calculated as shown in Table 6.14. It has to be mentioned that though the subsurface layers consist mainly of sandy layers, a small undrained shear strength ratio is used to calculate the strength of all layers. The weakest clay of Case Z3 is the third layer, whose undrained shear strength is about 21 kPa, which means the undrained shear strength is increased with the effective overburden stress with a ratio of about 0.22. Having made the major assumption, both the combined system stiffness and adjusted factor of safety against basal heave can be calculated and listed in Table 6.15 and Table 6.16. It is worthy to mention that the length of the equivalent cross walls is not the full length of the secondary wall in the calculation at SI-2 and SI-4, and half length of the secondary wall of 35 m is actually used. If the full length is used, the revised wall displacement (δ_{rev}) would be a very low value of less than 9 mm, which is not a reasonable value. Following the approach outlined in previous chapter, δ_{rev} based on the revised scheme can be evaluated. Comparison was made between δ_{rev}, δ_{Clough} and δ_{field}, and the results are summarized in Table 6.17 and Table 6.18. It can be seen that δ_{rev} is in better agreement with the δ_{field}, though the revised scheme had been used within sandy layers.

doi:10.6342/NTU201900743

6.1.4 Case Z4

Case Z4 is located in Taipei, and its excavation zone was a rectangle with a maximum length and width of 47 m and 36 m, respectively. The soil stratigraphy of the site consists of ten layers underlain by a dense gravel layer at a depth of 57.9 m. The parameters of each soil layer were presented in Table 6.19. The ground water level was at 3.5 m below the ground surface. The excavation was carried out using the top-down method in 9 excavation stages, and the excavation depth was 21.6 m. The diaphragm wall was 1.0 m in thickness and 44 m in depth. There are six cross walls deployed in this site to reduce the wall deflection. Plan layout including the diaphragm wall, cross walls, adjacent buildings load and locations of inclinometer casings are shown in Figure 6.4. It can be seen that the excavation zone was divided into three smaller zones by the cross walls, which are called as A, B and C, respectively.

Having acquired the basic information, the maximum wall displacement could be calculated rapidly by the regression equation. Knowing the width and length of each small zone. The factor of safety against basal heave and system stiffness in their original forms were calculated and shown in Table 6.20. Both the combined system stiffness and adjusted factor of safety against basal heave can be evaluated and presented in Table 6.21 and Table 6.22, respectively. Following the approach outlined in previous chapter, δ_{rev} based on the revised scheme can be evaluated. Comparison was made between δ_{rev},

doi:10.6342/NTU201900743

δ_{Clough} and δ_{field}, and the results are summarized in Table 6.23 and Table 6.24. Once again, it can be seen that δ_{rev} is in much better agreement with δ_{field}, while δ_{Clough} well overestimates the wall displacements.

doi:10.6342/NTU201900743

6.2 Spacing Effect of Cross Walls

The parametric studies conducted in section 5.3 showed that there appears to have an upper and lower boundary for the displacement of diaphragm wall depending on the spacing of cross walls. In this section, the field data (δ_{field}) and the predictions ($\delta_{spacing}$) calculated by the Equation (5.1) are further examined to check if they fall within the bounded area.

6.2.1 Case A

The equivalent results ($\delta_{spacing}$) are calculated by Equation (5.1), the outcomes of chapter 5. δ_{field} and $\delta_{spacing}$ are listed in Table 4.5, and plotted in Figure 6.5 together with the two boundaries. The undrained shear strength ratio (m) is decided by the real soil condition and the effect of cross walls, which is similar with the s_u^* concept proposed by Hsieh and Lu (1999). The cross walls spacing in Case A are all smaller than 10 m, δ_{field} and $\delta_{spacing}$ both fall outside the lower boundary and the cut-off line. Since the spacing of cross walls is smaller than 15 m, the upper and lower boundaries fail to cover δ_{field} and $\delta_{spacing}$. Therefore, the improvement on the boundary lines may be required.

6.2.2 Case B

The calculation of equivalent results had been described in Case A of previous section. δ_{field} and $\delta_{spacing}$ are listed in Table 4.10, and plotted in Figure 6.6 together

doi:10.6342/NTU201900743

with the two boundaries. The cross walls spacing in Case B is about 20 m and 60 m. For Case B, $\delta_{spacing}$ coincided with the field data, and the maximum difference is less than 0.16%. However, δ_{field} and $\delta_{spacing}$ did not fall within the boundaries and beneath the lower boundaries, which was defined in previous chapter. Therefore, the improvement on the boundary lines may be required.

6.2.3 Case C

The calculation of equivalent results had been described in Case A of previous section. δ_{field} and $\delta_{spacing}$ are listed in Table 4.15, and plotted in Figure 6.7 together with the two boundaries. The cross walls spacing in Case C is about 10 m. $\delta_{spacing}$ is in general coincided with δ_{field} and the maximum difference is less than 0.06%. Since the spacing of cross walls is smaller than 15 m, the upper and lower boundaries fail to cover δ_{field} and $\delta_{spacing}$. Therefore, improvement on the boundary lines may be required.

6.2.4 Case Z1

The calculation of equivalent results had been described in Case A of previous section. δ_{field} and $\delta_{spacing}$ are listed in Table 6.6, and plotted in Figure 6.8 together with the two boundaries. The cross wall spacing in Case Z1 is approximately 25 m. $\delta_{spacing}$ is slightly smaller than δ_{field}, but both of them fall near the lower boundary.

6.2.5 Case Z2

The calculation of equivalent results had been described in Case A of previous

doi:10.6342/NTU201900743

section. δ_{field} and $\delta_{spacing}$ are listed in Table 6.12, and plotted in Figure 6.9 together with the two boundaries. Though it can be seen that $\delta_{spacing}$ are similar to the corresponding δ_{field}, the spacing of cross wall is smaller than 15 m, which situates outside the cut-off line. δ_{field} and $\delta_{spacing}$ did not fall within the bounded area so that improvement on the boundary lines may be required.

6.2.6 Case Z3

The calculation of equivalent results had been described in Case A of previous section. δ_{field} and $\delta_{spacing}$ are listed in Table 6.18, and plotted in Figure 6.10 together with the two boundaries. There are obvious differences between δ_{field} and $\delta_{spacing}$. This differences may be attributed to the fact that Case Z3 mainly consists of sandy soil. Therefore, $\delta_{spacing}$ failed to predict the wall displacements with precision in sandy soil.

6.2.7 Case Z4

The calculation of equivalent results had been described in Case A of previous section. δ_{field} and $\delta_{spacing}$ are listed in Table 6.24, and plotted in Figure 6.11 together with the two boundaries. In Case Z4, the spacing is larger than 15 m, and it is found that the largest difference between δ_{field} and $\delta_{spacing}$ is about 0.1%, which is considered a good prediction with the spacing of cross walls in the vicinity of 15 .

doi:10.6342/NTU201900743

6.3 Discussions

6.3.1 Applicability of the regression equation

As revealed in the previous sections, the regression equation appears to provide reasonable estimation of wall displacement. The best benefit of using the proposed equation is not having to use the complex numerical analysis to obtain the possible wall displacement. However, use of a simplified equation always requires good engineering judgement. Furthermore, it is not applicable for project sites with sandy soil likes Case Z3, the estimated results by the regression equation may differ significantly from the field observation. The regression equation is more suitable for estimation of wall displacements in clayey soil. In addition, this regression equation only considers two key factors and is useful only for projects with cross walls.

To extend the usefulness of the regression equation, the effect of both buttress walls and cross walls simultaneously existed should be further investigated. For cases without cross walls in the excavation zone, the applicability of this regression equation has also to be examined. If sandy soils are encountered, the two key parameters used in the regression equation may have to be modified to cope with the presence of such sandy soil layers. Having done all these, the regression equation will be more versatile and will be suitable for application in most excavation cases.

doi:10.6342/NTU201900743

6.3.2 Effect of cross wall spacing

According to the studies in previous sections, it can be found that the upper and lower boundary lines may not be an effective method in covering the range of possible wall displacements. Therefore, the boundary lines need to be improved. More factors such as the excavation depth, the soil conditions, the effective length of cross wall and the role of secondary wall should be studied. Since these potential factors of influence will also affect the wall deflection of diaphragm wall, a large number of three-dimensional numerical analyses may have to be conducted to delineate the effect of these factors.

The suitable spacing of cross wall for excavation project with soft clay deposit is about 15 m, which is considered the optimal spacing of cross walls. For the limited budget and safety for construction, the cross walls will not be constructed close to each other such as 5 m. The spacing of cross wall should be within 5 to 30 m for future analyses.

doi:10.6342/NTU201900743

Table 6.1 Soil parameters of Case Z1

Type	Depth from	Depth to	γ_s	N	c'	ϕ'	s_u
	m	m	kN/m^3	-	kPa	^{o}	kPa
1CL	0.0	-4.4	19.52	-	0	-	16
2SM	-4.4	-14.4	19.62	9	0	31	-
3CL	-14.4	-24.1	18.93	-	0	-	60
4SM	-24.1	-30.8	19.62	19	0	32	-
5CL	-30.8	-35.2	19.03	-	0	-	73
6SM	-35.2	-42.3	19.62	23	0	32	-
7CL	-42.3	-44.5	20.60	-	0	-	104
8SM	-44.5	-52.5	20.99	30	0	33	-
9GM	-52.5	-62.0	22.00	>100	0	-	144

doi:10.6342/NTU201900743

Table 6.2 Basic parameters for each zone of Case Z1

SI	Zone	B	L	D	PSR_{Ou}	PSR_{Finno}	s_{uu}	s_{ub}	d_T	F_b	S
		m	m	m	-	-	kPa	kPa	m	-	-
1	B	24.8	28.7	39	0.60	0.75	16.35	50.88	17.54	1.15	657
7	C	28.5	24.8	39	0.53	0.70	16.35	53.53	20.15	1.21	657

Table 6.3 Revision of the system stiffness of Case Z1

SI	Zone	B	L	S	PSR_{Ou}	$S_{c,Ou}$	PSR_{Finno}	$S_{c,Finno}$
		m	m	-	-	-	-	-
1	B	24.8	28.7	657	0.60	1094	0.75	880
7	C	28.5	24.8	657	0.53	1239	0.70	943

Table 6.4 Revision of the factor of safety against basal heave of Case Z1

SI	Zone	N_{cw}	L_{cw}	κ	B	s_{uu}	s_{ub}	I_{CL}	s_{ub}*	s_{ub_adj}	F_{b_adj}
		m	m	-	m	kPa	kPa	kPa	kPa	kPa	-
1	B	2	24.8	1	28.7	16.35	50.88	2.73	138.81	94.85	2.15
7	C	2	28.5	1	24.8	16.35	53.53	3.30	176.57	115.05	2.59

Table 6.5 Estimation of wall displacements of Case Z1

SI	S	$S_{c,Ou}$	$S_{c,Finno}$	F_b	F_{b_adj}	δ_{clough}	$\delta_{rev,Ou}$	$\delta_{rev,Finno}$	δ_{field}
	-	-	-	-	-	mm	mm	mm	mm
1	657	1094	880	1.15	2.15	120.75	32.96	34.00	28.00
7	657	1239	943	1.21	2.59	112.70	24.24	25.19	32.00

Table 6.6 Comparison of wall displacements of Case Z1

SI	δ_{Clough} / H_e	$\delta_{rev,Ou}$ / H_e	$\delta_{rev,Finno}$ / H_e	δ_{field} / H_e	$\delta_{spacing}$ / H_e
	%	%	%	%	%
1	0.89	0.244	0.252	0.2074	0.1738
7	0.83	0.180	0.187	0.2370	0.1172

doi:10.6342/NTU201900743

Table 6.7 Soil parameters of Case Z2

Type	Depth from	Depth to	γ_s	N	c'	ϕ'	s_u
	m	m	kN/m^3	-	kPa	o	kPa
1CL	0.0	-7.9	18.70	5	0	30	29.40
2SM	-7.9	-17.1	19.40	18	0	32	-
3CL	-17.1	-20.3	18.90	8	0	30	31.90
4SM	-20.3	-29.3	19.20	24	0	33	-
5CL	-29.3	-39.5	18.60	16	0	32	58.85
6SM	-39.5	-41.4	19.70	24	0	33	-
7GW	-41.4	-60.0	21.10	50	0	38	-

Table 6.8 Basic parameters for each zone of Case Z2

SI	Zone	B	L	D	PSR_{Ou}	PSR_{Finno}	s_{uu}	s_{ub}	d_T	F_b	S
		m	m	m	-	-	kPa	kPa	m	-	-
1	B	31	9	21.8	0.13	0.14	16.82	50.40	21.80	0.80	1819
2	A	23	14	21.8	0.29	0.22	16.82	46.26	16.26	0.75	1819
3	B	31	9	21.8	0.13	0.14	16.82	50.40	21.80	0.80	1819
4	D	10	16	21.8	0.30	0.29	16.82	39.26	7.07	0.68	1819
5	D	16	10	21.8	0.25	0.15	16.82	42.65	11.31	0.71	1819
6	D	10	16	21.8	0.30	0.29	16.82	39.26	7.07	0.68	1819
7	C	13	22	21.8	0.53	0.37	16.82	40.96	9.19	0.69	1819

Table 6.9 Revision of the system stiffness of Case Z2

SI	Zone	B	L	S	PSR_{Ou}	$S_{c,Ou}$	PSR_{Finno}	$S_{c,Finno}$
		m	m	-	-	-	-	-
1	B	31	9	1819	0.13	13992	0.14	13372
2	A	23	14	1819	0.29	6272	0.22	8191
3	B	31	9	1819	0.13	13992	0.14	13372
4	D	10	16	1819	0.30	6063	0.29	6365
5	D	16	10	1819	0.25	7276	0.15	11847
6	D	10	16	1819	0.30	6063	0.29	6365
7	C	13	22	1819	0.53	3432	0.37	4909

doi:10.6342/NTU201900743

Table 6.10 Revision of the factor of safety against basal heave of Case Z2

SI	Zone	N_{cw}	L_{cw}	κ	B	s_{uu}	s_{ub}	I_{CL}	s_{ub}*	s_{ub_adj}	F_{b_adj}
		-	m	-	m	kPa	kPa	kPa	kPa	kPa	-
1	B	2	31	1	9	16.82	50.40	7.89	397.61	224.00	3.56
2	A	**2**	23	2	14	16.82	46.26	7.57	350.29	198.28	3.20
3	B	2	31	1	9	16.82	50.40	7.89	397.61	224.00	3.56
4	D	2	10	2	16	16.82	39.26	3.50	137.42	88.34	1.54
5	D	2	16	2	10	16.82	42.65	7.40	315.60	179.12	2.97
6	D	2	10	2	16	16.82	39.26	3.50	137.42	88.34	1.54
7	C	**3**	13	2	22	16.82	40.96	4.55	186.16	113.56	1.92

Table 6.11 Estimation of wall displacements of Case Z2

SI	S	$S_{c,Ou}$	$S_{c,Finno}$	F_b	F_{b_adj}	δ_{clough}	$\delta_{rev,Ou}$	$\delta_{rev,Finno}$	δ_{field}
	-	-	-	-	-	mm	mm	mm	mm
1	1819	13992	13372	0.80	3.56	201.25	15.15	15.25	6.00
2	1819	6272	8191	0.75	3.20	225.40	20.08	19.33	13.00
3	1819	13992	13372	0.80	3.56	201.25	15.15	15.25	6.00
4	1819	6063	6365	0.68	1.54	228.62	62.64	62.21	5.80
5	1819	7276	11847	0.71	2.97	222.18	22.12	20.63	6.30
6	1819	6063	6365	0.68	1.54	228.62	62.64	62.21	3.20
7	1819	3432	4909	0.69	1.92	225.40	48.41	46.00	9.02

Table 6.12 Comparison of wall displacements of Case Z2

SI	δ_{Clough} / H_e	$\delta_{rev,Ou} / H_e$	$\delta_{rev,Finno} / H_e$	δ_{field} / H_e	$\delta_{spacing} / H_e$
	%	%	%	%	%
1	1.03	0.077	0.078	0.0306	0.0208
2	1.15	0.102	0.099	0.0663	0.0505
3	1.03	0.077	0.078	0.0306	0.0208
4	1.17	0.320	0.317	0.0296	0.1850
5	1.13	0.113	0.105	0.0321	0.0568
6	1.17	0.320	0.317	0.0163	0.1850
7	1.15	0.247	0.235	0.0460	0.2161

doi:10.6342/NTU201900743

Table 6.13 Soil parameters of Case Z3

Type	Depth from	Depth to	γ_s	N	c'	ϕ'	s_u
	m	m	kN/m^3	-	kPa	^{o}	kPa
1CL	0.0	-2.0	19.30	7	-	-	28
2SM	-2.0	-6.5	20.90	8	0	32	-
3CL	-6.5	-8.0	19.70	4	-	-	21
4SM	-8.0	-17.0	20.60	11	0	32	-
5SM	-17.0	-23.5	18.60	11	0	32	-
6SM	-23.5	-28.5	19.60	11	0	33	-
7CL	-28.5	-30.5	18.60	13	-	-	84
8SM	-30.5	-42.0	19.60	22	0	34	-
9SM	-42.0	-60.0	19.60	35	0	34	-

doi:10.6342/NTU201900743

Table 6.14 Basic parameters for each zone of Case Z3

SI	Zone	B	L	D	PSR_{Ou}	PSR_{Finno}	s_{uu}	s_{ub}	d_T	F_b	S
		m	m	m	-	-	kPa	kPa	m	-	-
1	-	20	70	25.2	0.93	1.07	26.77	71.11	14.14	1.30	496
2	-	70	20	25.2	0.26	0.58	26.77	85.72	25.20	1.50	496
3	-	20	70	25.2	0.93	1.07	26.77	71.11	14.14	1.30	496
4	-	70	20	25.2	0.26	0.58	26.77	85.72	25.20	1.50	496

Table 6.15 Revision of the system stiffness of Case Z3

SI	Zone	B	L	S	PSR_{Ou}	$S_{c,Ou}$	PSR_{Finno}	$S_{c,Finno}$
		m	m	-	-	-	-	-
1	-	20	70	496	0.93	534	1.07	462
2	-	70	20	496	0.26	1908	0.58	852
3	-	20	70	496	0.93	534	1.07	462
4	-	70	20	496	0.26	1908	0.58	852

Table 6.16 Revision of the factor of safety against basal heave of Case Z3

SI	Zone	N_{cw}	L_{cw}	κ	B	s_{uu}	s_{ub}	I_{CL}	s_{ub}*	s_{ub_adj}	F_{b_adj}
		m	m	-	m	kPa	kPa	kPa	kPa	kPa	-
1	-	2	20	1	70	26.77	71.11	1.57	111.74	91.43	1.67
2	-	2	**35**	1	20	26.77	85.72	4.50	385.76	235.74	4.13
3	-	2	20	1	70	26.77	71.11	1.57	111.74	91.43	1.67
4	-	2	**35**	1	20	26.77	85.72	4.50	385.76	235.74	4.13

Table 6.17 Estimation of wall displacements of Case Z3

SI	S	$S_{c,Ou}$	$S_{c,Finno}$	F_b	F_{b_adj}	δ_{clough}	$\delta_{rev,Ou}$	$\delta_{rev,Finno}$	δ_{field}
	-	-	-	-	-	mm	mm	mm	mm
1	496	534	462.09	1.30	1.67	144.90	66.95	68.34	67.00
2	496	1908	852.28	1.50	4.13	88.55	13.76	15.44	15.00
3	496	534	462.09	1.30	1.67	144.90	66.95	68.34	65.00
4	496	1908	852.28	1.50	4.13	88.55	13.76	15.44	17.00

Table 6.18 Comparison of wall displacements of Case Z3

SI	δ_{Clough} / H_e	$\delta_{rev,Ou}$ / H_e	$\delta_{rev,Finno}$ / H_e	δ_{field} / H_e	$\delta_{spacing}$ / H_e
	%	%	%	%	%
1	0.86	0.399	0.407	0.3988	0.5740
2	0.53	0.082	0.092	0.0893	0.0446
3	0.86	0.399	0.407	0.3869	0.5740
4	0.53	0.082	0.092	0.1012	0.0446

doi:10.6342/NTU201900743

Table 6.19 Soil parameters of Case Z4

Type	Depth from	Depth to	γ_s	N	c'	ϕ'	s_u
	m	m	kN/m^3	-	kPa	^{o}	kPa
1CL	-1.0	-3.3	19.33	5	0	30	29.4
2SM	-3.3	-8.6	20.21	8	-	30	-
3CL	-8.6	-13.7	19.23	4	0	30	39.2
4CL	-13.7	-23.6	18.34	3	0	29	63.8
5CL	-23.6	-32.2	19.03	6	0	30	88.3
6SM	-32.2	-33.3	19.03	10	-	30	-
7CL	-33.3	-44.2	18.54	9	0	31	108
8CL	-44.2	-54.2	18.54	19	0	33	147
9SM	-54.2	-57.9	19.52	>50	0	35	-
10GW	-57.9	-62.0	21.58	>50	0	40	-

doi:10.6342/NTU201900743

Table 6.20 Basic parameters for each zone of Case Z4

SI	Zone	B	L	D	PSR_{Ou}	PSR_{Finno}	q	s_{uu}	s_{ub}	d_T	F_b	S
		m	m	m	-	-	kN/m^2	kPa	kPa	m	-	-
2	B	36	17	36.3	0.29	0.36	39.24	31.69	94.15	25.46	1.26	1474
3	A	16	16	36.3	0.35	0.37	0	31.69	77.46	11.31	1.26	1474
5	B	36	17	36.3	0.29	0.39	0	31.69	94.15	25.46	1.39	1474
8	C	14	16	36.3	0.37	0.34	49.05	31.69	75.70	9.90	1.10	1474

Table 6.21 Revision of the system stiffness of Case Z4

SI	Zone	B	L	S	PSR_{Ou}	$S_{c,Ou}$	PSR_{Finno}	$S_{c,Finno}$
		m	m	-	-	-	-	-
2	B	36	17	1474	0.29	5082	0.36	4074
3	A	16	16	1474	0.35	4210	0.37	4000
5	B	36	17	1474	0.29	5082	0.39	3803
8	C	14	16	1474	0.37	3983	0.34	4285

Table 6.22 Revision of the factor of safety against basal heave of Case Z4

SI	Zone	N_{cw}	L_{cw}	κ	B	s_{uu}	s_{ub}	I_{CL}	s_{ub}*	s_{ub_adj}	F_{b_adj}
		m	m	-	m	kPa	kPa	kPa	kPa	kPa	-
2	B	2	10	1	17	31.69	94.15	2.18	204.91	149.53	2.01
3	A	2	16	1	16	31.69	77.46	3.00	232.37	154.91	2.51
5	B	2	10	1	17	31.69	94.15	2.18	204.91	149.53	2.21
8	C	2	14	1	16	31.69	75.70	2.75	208.16	141.93	2.06

Table 6.23 Estimation of wall displacements of Case Z4

SI	S	$S_{c,Ou}$	$S_{c,Finno}$	F_b	F_{b_adj}	δ_{clough}	$\delta_{rev,Ou}$	$\delta_{rev,Finno}$	δ_{field}
	-	-	-	-	-	mm	mm	mm	mm
2	1474	5082	4074	1.26	2.01	58.32	46.98	48.49	33.08
3	1474	4210	4000	1.26	2.51	77.76	34.13	34.38	15.37
5	1474	5082	3803	1.39	2.21	58.32	40.43	42.14	31.71
8	1474	3983	4285	1.10	2.06	82.08	46.63	46.15	32.42

Table 6.24 Comparison of wall displacements of Case Z4

SI	δ_{Clough} / H_e	$\delta_{rev,Ou} / H_e$	$\delta_{rev,Finno} / H_e$	δ_{field} / H_e	$\delta_{spacing} / H_e$
	%	%	%	%	%
2	0.27	0.218	0.224	0.1531	0.0921
3	0.36	0.158	0.159	0.0712	0.0692
5	0.27	0.187	0.195	0.1468	0.0929
8	0.38	0.216	0.214	0.1501	0.0758

doi:10.6342/NTU201900743

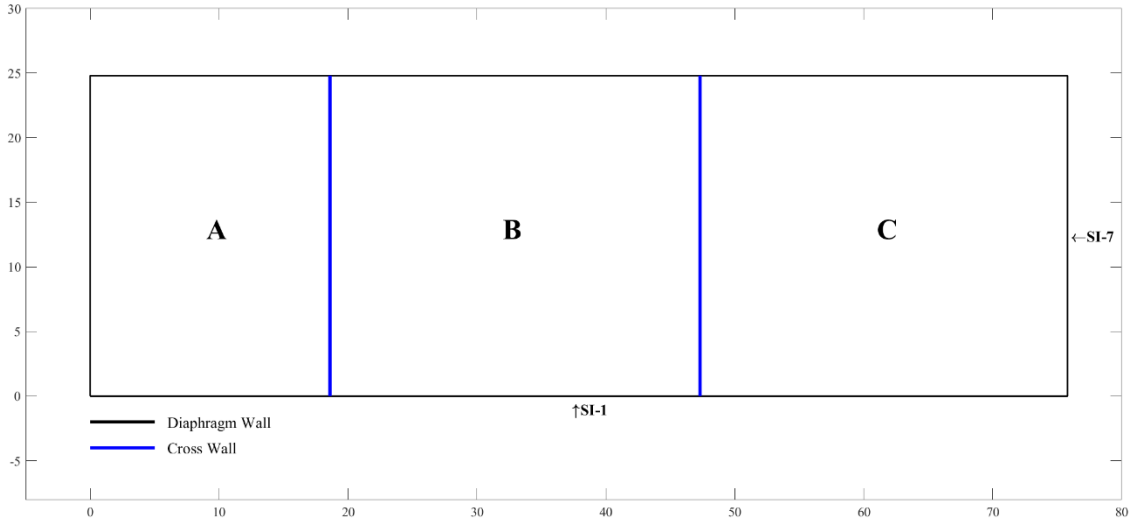

Figure 6.1 Site plan of Case Z1

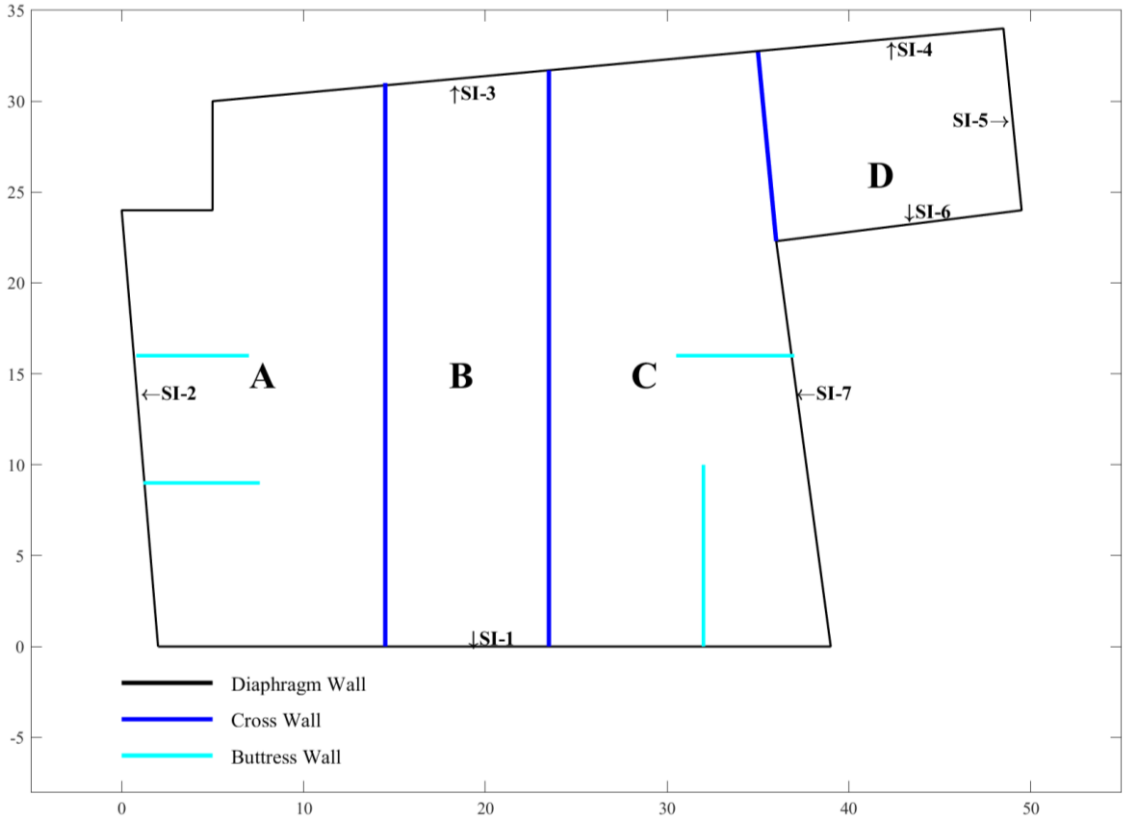

Figure 6.2 Site plan of Case Z2

doi:10.6342/NTU201900743

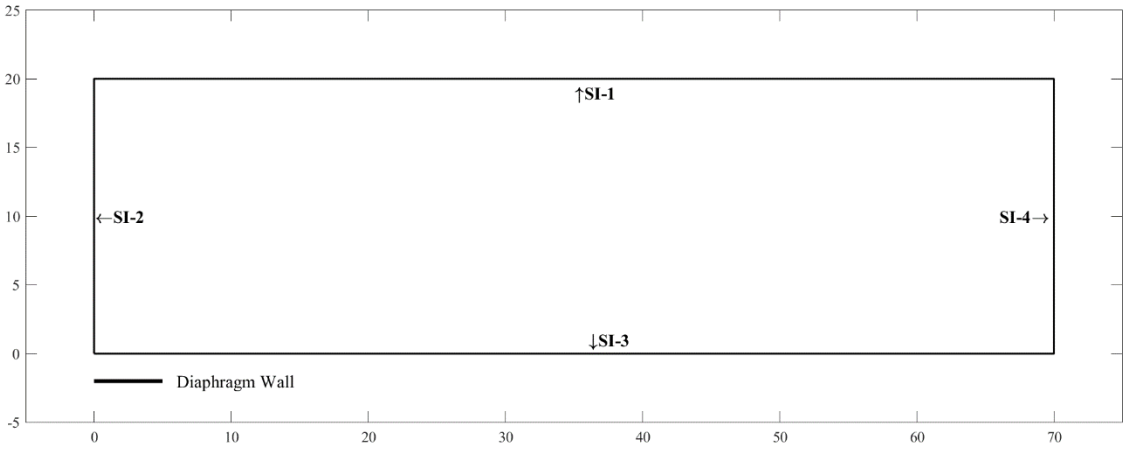

Figure 6.3 Site plan of Case Z3

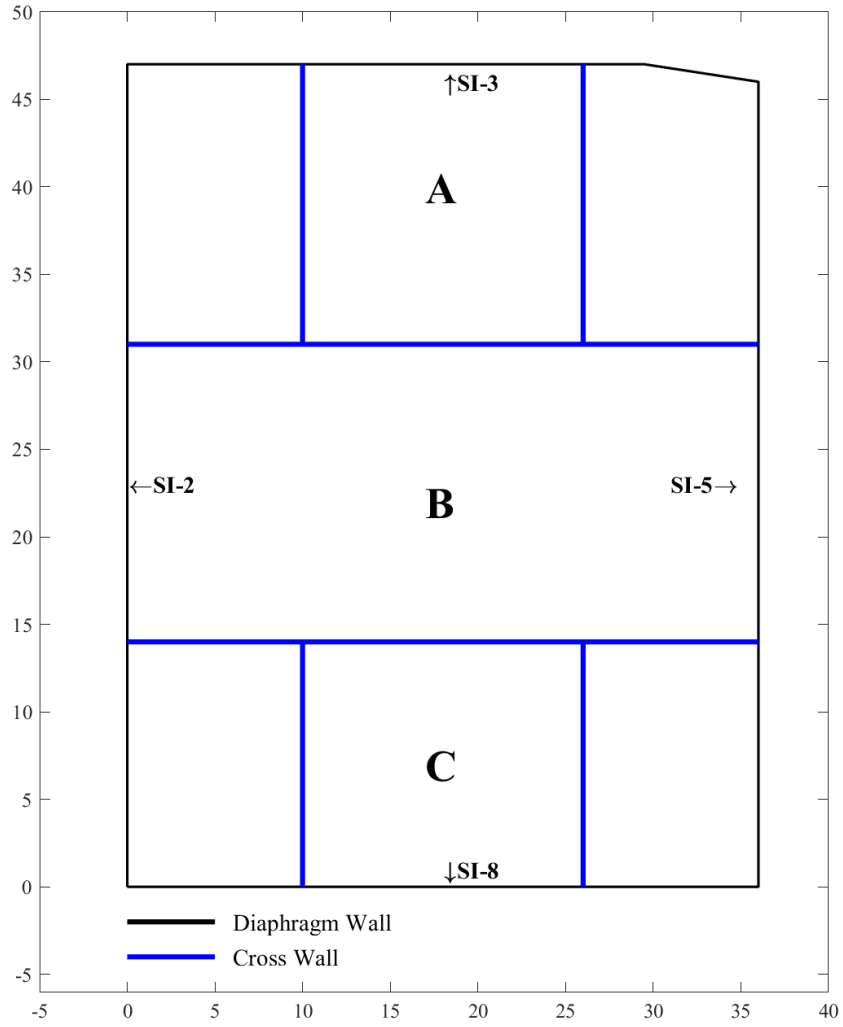

Figure 6.4 Site plan of Case Z4

doi:10.6342/NTU201900743

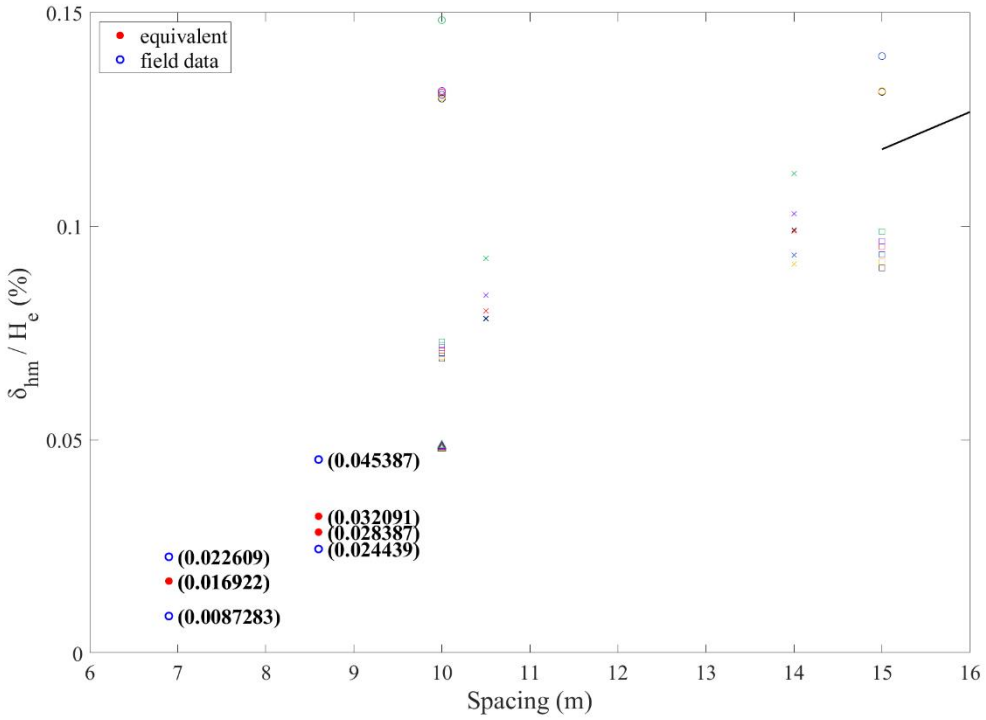

Figure 6.5 Effect of cross wall spacing in Case A

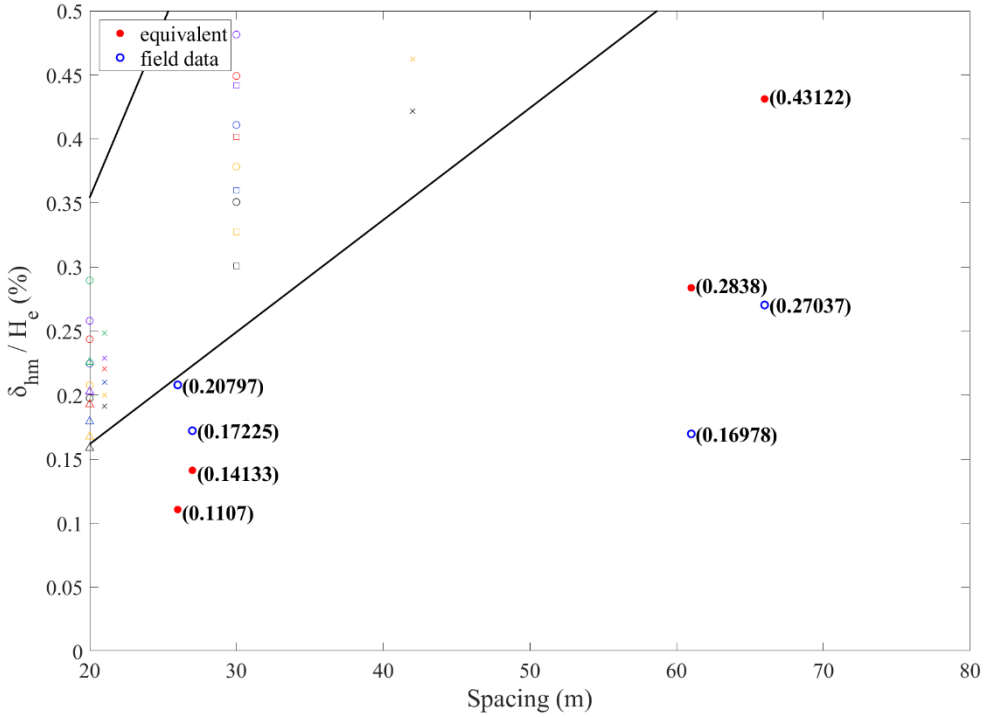

Figure 6.6 Effect of cross wall spacing in Case B

doi:10.6342/NTU201900743

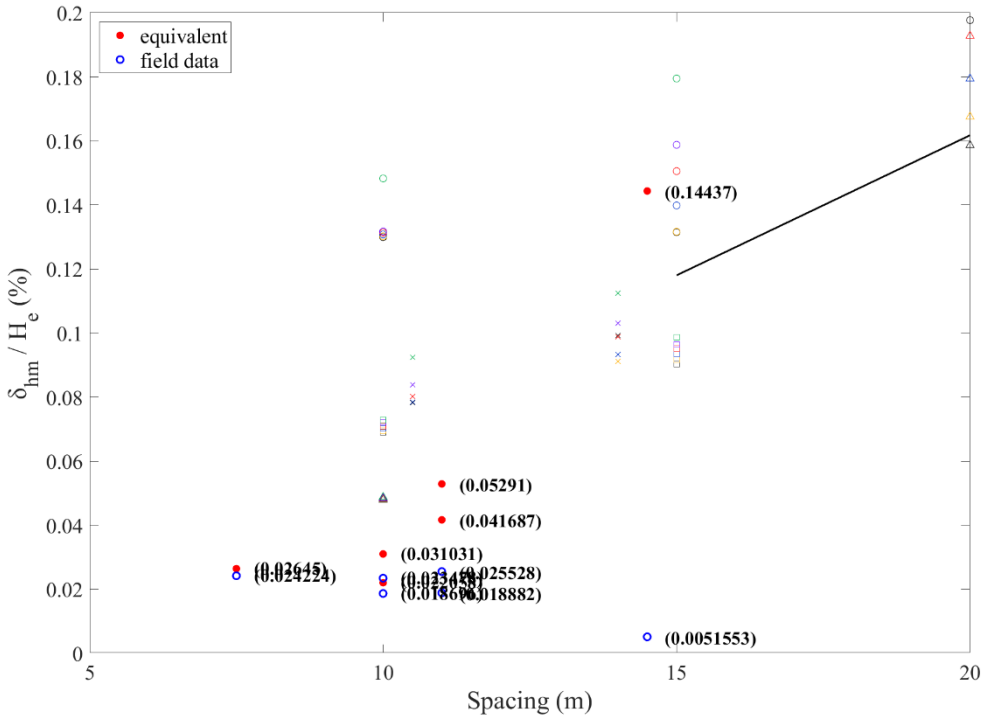

Figure 6.7 Effect of cross wall spacing in Case C

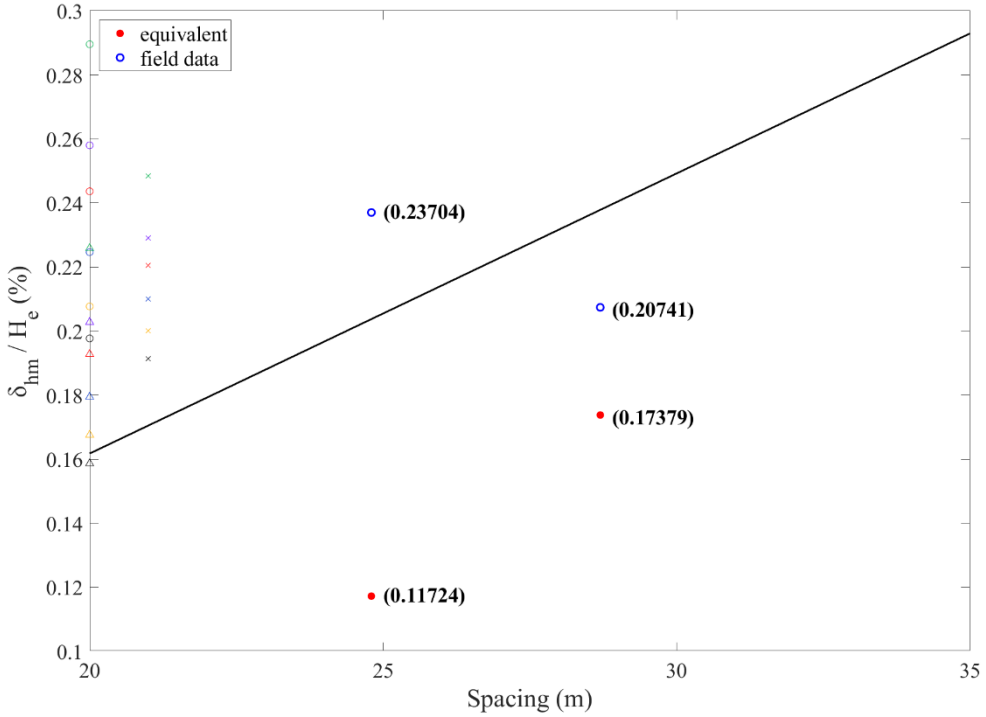

Figure 6.8 Effect of cross wall spacing in Case Z1

doi:10.6342/NTU201900743

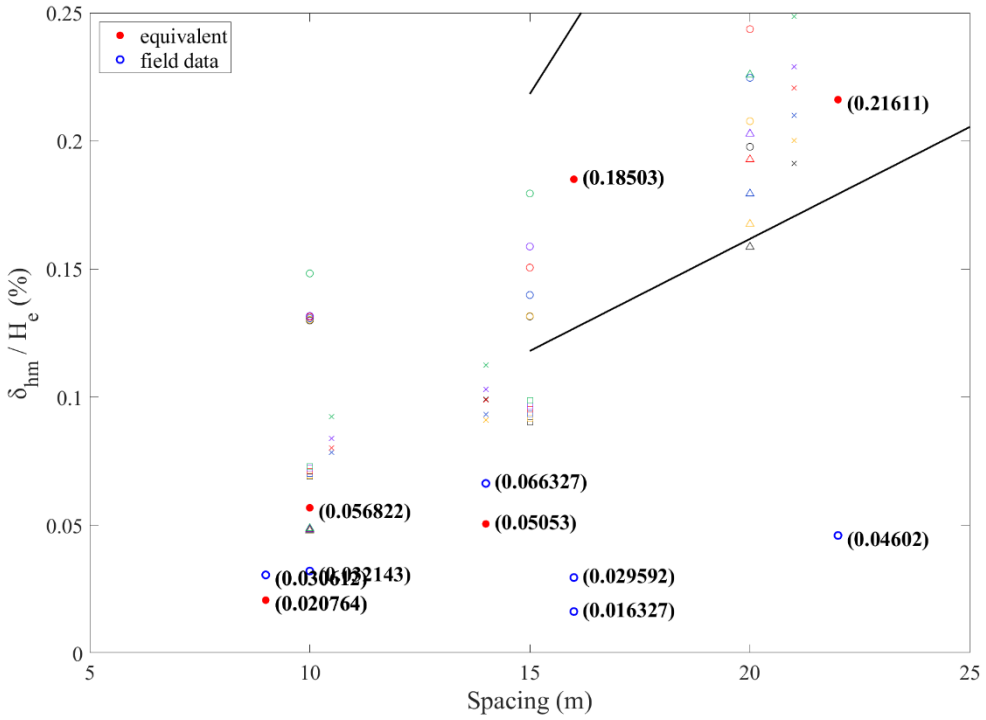

Figure 6.9 Effect of cross wall spacing in Case Z2

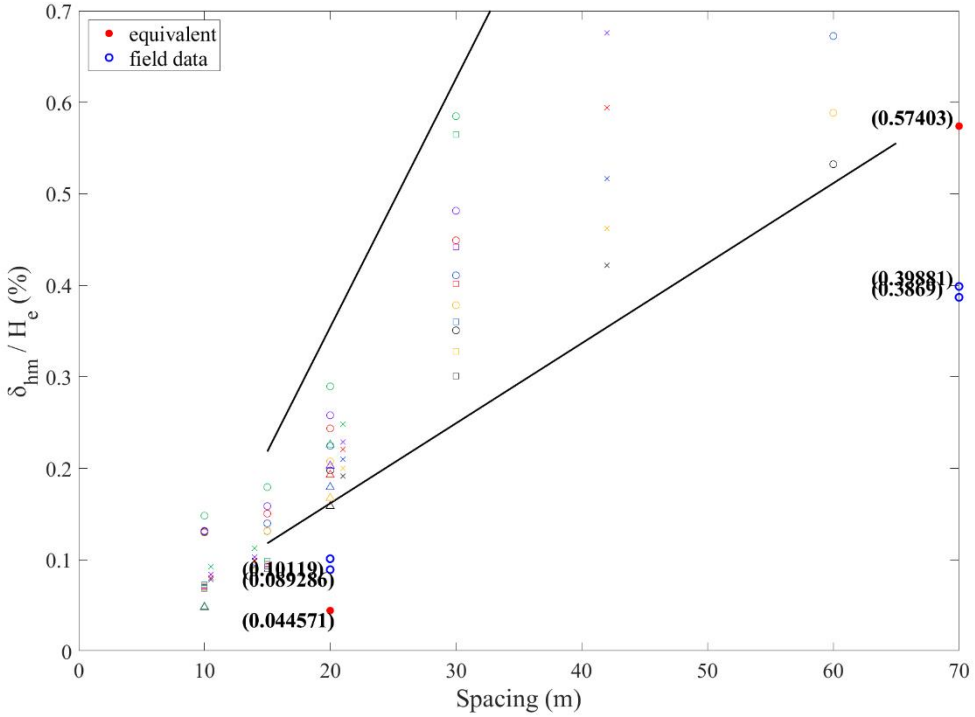

Figure 6.10 Effect of cross wall spacing in Case Z3

doi:10.6342/NTU201900743

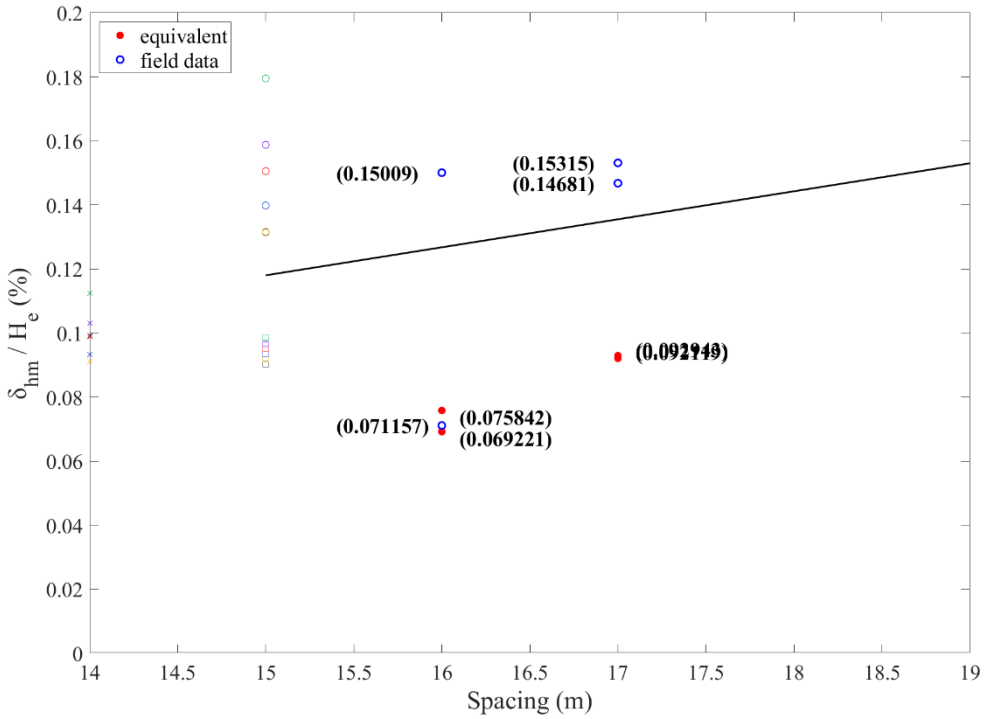

Figure 6.11 Effect of cross wall spacing in Case Z4

doi:10.6342/NTU201900743

Chapter 7 Conclusions and Recommendations

7.1 Conclusions

The effect of cross walls is modeled as increases in system stiffness and factor of safety against basal heave, resulting in a combined system stiffness (S_c) and an adjusted factor of safety against basal heave (F_{b_adj}) that can be further used to estimate the wall displacements together with Clough's design curves. Clough's design curves were also extended by extrapolation techniques to cover area of low displacements where the values of system stiffness and factor of safety against basal heave are high due to the effect of cross walls. A series of case histories were used to verify the correctness of the revised scheme, and parametric studies using finite element program, PLAXIS 3D were also conducted to quantify the effect of cross walls spacing on wall displacement. Based on the outcome of case histories and parametric studies by three-dimensional analysis, the following conclusions can be drawn.

1. The case histories show that the effect of cross walls is significant in restraining the wall deflection to a quite low level. The estimated results from the original Clough's chart is conservative for design. Using the revised Clough's scheme, which accounts for the effect of cross walls, the prediction on wall displacement is more suitable for modern excavations with cross walls.

2. δ_{rev} by the revised scheme can be one order higher than the field observation.

doi:10.6342/NTU201900743

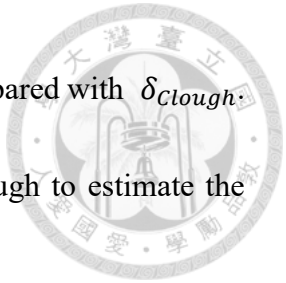

However, δ_{rev} is in much better agreement with field data compared with δ_{Clough}. The revised scheme is considered suitable and reasonable enough to estimate the wall displacement for modern excavations.

3. A spacing of 15 m between cross walls appears to be an optimal number. With cross walls 15 m apart, the wall displacement can be reduced to a very low value that satisfies the design requirement.

4. Not adopting the whole length but the equivalent length of cross walls seems to be more reasonable to quantify the magnification factor (I_{CL}) in increasing the undrained shear strength. Otherwise, the magnification factor would be overestimated that results in an unreasonable factor of safety against basal heave.

7.2 Recommendations for Future Work

The following topics are suggested for future research.

1. The regression equation should be calibrated against more cases with various layout of cross walls and buttress walls to ensure its applicability and versatility.

2. An equivalent factor of safety similar with the factor of safety against basal heave is required for sandy soil to calculate the possible displacement of diaphragm wall for excavations in sandy soil. The Clough's chart may need revision for this purpose.

3. In this study, the spacing of cross walls is the only factor considered. Other factors such as the depth, the thickness and the stiffness of cross walls should be

doi:10.6342/NTU201900743

incorporated in the parametric studies. In particular, the equivalent length of cross walls should be investigated in depth.

doi:10.6342/NTU201900743

References

[1] Bowles, J.E. (1996). Foundation analysis and design, 5th Edition, McGraw-Hill Book Company, New York, USA.

[2] Bryson, L.S., and Zapata-Medina, D.G. (2012). Method of estimation system stiffness for excavation support walls. *Journal of Geotechnical and Geoenvironmental Engineering*, Vol. 138, pp. 1104-1115.

[3] Clough, G.W., Smith, E.M., and Sweeney, B.P. (1989). Movement control of excavation support systems by iterative design. *Current Principles and Practices, Foundation Engineering Congress*, Vol. 2, pp. 869-884.

[4] Finno, R.J., Blackburn, J.T., and Roboski, J.F. (2007). Three dimensional effects for supported excavations in clay. *Journal of Geotechnical and Geoenvironmental Engineering*, ASCE, Vol. 133, No. 1, pp. 30-36.

[5] Hsieh, H.S. and Lu, F.C. (1999). A note on the analysis and design of diaphragm wall with buttresses. *Sino-Geotechnics*, Vol. 76, pp. 39-50 (in Chinese).

[6] Hsieh, H.S., Hsu, W.T., and Chou, C.J. (2015). Incorporating three-dimensional effect in the design of a small excavation in soft clay. *International Conference on Soft Ground Engineering*, Singapore, pp. 669-677.

[7] Hsieh, H.S. and Huang Y.H., Hsu, W.T. and Ge, L. (2017). On the system stiffness of deep excavation in soft clay. *Journal of GeoEngineering*, Vol. 12, No. 1, pp. 21-34.

[8] Hsiung, B.B. (2009). A case study on the behavior of a deep excavation in sand. *Computers and Geotechnics*, Vol. 36, pp. 665-675.

[9] Hsieh, P.G., Ou, C.Y., Liu, H.T. (2008). Basal heave analysis of excavations with consideration of anisotropic undrained strength of clay. *Canadian Geotechnical Journal*, Vol. 45, pp. 788-799.

[10] Khoiri, M. and Ou, C.Y. (2013). Evaluation of deformation parameter for deep excavation in sand through case histories. *Computers and Geotechnics*, Vol. 47, pp.57-67.

[11] Likitlersuang, S., Surarak, C., Wanatowski, D., Oh, E., and Balasubramaniam, A. (2013). Finite element analysis of a deep excavation: a case study from the Bangkok MRT. *Soil and Foundations*, Vol. 53, No. 5, pp. 756-773.

[12] Lim, A., Ou, C.Y., and Hsieh, P.G. (2010). Evaluation of clay constitutive models for analysis of deep excavation under undrained conditions. *Journal of GeoEngineering*, TGS, Vol. 5, No. 1, pp. 9-20.

[13] Long, M. (2001). Database for retaining wall and ground movements due to deep excavations. *Journal of Geotechnical and Geoenvironmental Engineering*, Vol. 127, No. 3, pp. 203-224.

[14] Moormann, C. (2004). Analysis of wall and ground movements due to deep

doi:10.6342/NTU201900743

excavations in soft soil based on a new worldwide database. *Journal of the Japanese Geotechnical Society*, Vol. 44, No. 1, pp. 97-98.

[15] Ou, C.Y., Chiou, D.C., and Wu, T.S. (1996). Three-dimensional finite element analysis of deep excavations. *Journal of Geotechnical Engineering*, ASCE, Vol. 122, No. 5, pp. 337-345.

[16] Ou, C.Y. (2006). Deep Excavation; Theory and Practice, Taylor and Francis, Netherland.

[17] PLAXIS 3D (2017) Computer software. PLAXIS, Delft.

[18] Terzaghi, K. (1943). Theoretical Soil Mechanics, John Wiley & Sons, New York.

[19] Ukritchon, B., Whittle, A.J. and Sloan, S.W. (2003). Undrained stability of braced excavations in clay. *Journal of Geotechnical and Geoenvironmental Engineering*, ASCE, Vol. 129, No. 8, pp. 738-755.

[20] Wu, S.H., Ching, J.Y., and Ou, C.Y. (2013). Predicting wall displacements for excavations with cross walls in soft clay. *Journal of Geotechnical and Geoenvironmental Engineering*, Vol. 139, No. 6, pp. 914-927.

[21] 內政部營建署 (2011)，「混凝土結構設計規範」，民國一百年，台北。

[22] 內政部營建署 (2003)，「大眾捷運系統兩側禁建限建辦法」，民國九十二年，台北。

[23] 張智博 (2016)。深開挖基地三維幾何配置於連續壁壁體變位之影響。國立臺灣大學土木工程學研究所碩士論文，台北市。

[24] 吳軒蘋 (2017)。考慮扶壁效應於開挖行為之簡化分析。國立臺灣大學土木工程學研究所碩士論文，台北市。

doi:10.6342/NTU201900743

APPENDIX A

The parameters and predicted results by using the full length of cross walls

doi:10.6342/NTU201900743

Type	Spacing y (L, B')	Spacing x (B, L')	PSR_x	PSR_y	S	F_{bx}	F_{by}	S_{cx}	S_{cy}	$F_{bx\ adj}$	$F_{by\ adj}$	δ_x / H_e (%)	δ_y / H_e (%)	δ_{revx} / H_e (%)	δ_{revy} / H_e (%)	check x	check y
S60, m033, 0h0v	60	60	0.85	0.85	542	2.47	2.47	637	637	3.65	3.65	0.53	0.53	0.12	0.12	x	x
S60, m033, 1h0v	30	60	0.45	0.91	542	1.85	2.47	1204	595	4.69	3.46	0.35	0.53	0.07	0.13	x	x
S60, m033, 1h1v	30	30	0.61	0.61	542	1.85	1.85	888	888	3.90	3.90	0.36	0.36	0.10	0.10	x	x
S60, m033, 1h2v	30	20	0.66	0.38	542	1.85	1.68	821	1426	3.64	5.26	0.36	0.21	0.11	0.06	x	x
S60, m033, 1h3v	30	15	0.69	0.27	542	1.85	1.61	785	2007	3.51	4.83	0.35	0.14	0.12	0.06	x	x
S60, m033, 2h0v	20	60	0.28	0.92	542	1.68	2.47	1935	589	7.09	3.40	0.20	0.52	0.04	0.13	x	x
S60, m033, 2h1v	20	30	0.38	0.65	542	1.68	1.85	1426	833	5.26	3.64	0.21	0.36	0.06	0.11	x	x
S60, m033, 2h2v	20	20	0.42	0.42	542	1.68	1.68	1290	1290	4.65	4.65	0.21	0.21	0.07	0.07	x	x
S60, m033, 2h3v	20	15	0.45	0.20	542	1.68	1.61	1204	2709	4.35	3.76	0.21	0.14	0.08	0.09	x	x
S60, m033, 3h0v	15	60	0.19	0.94	542	1.61	2.47	2851	576	8.06	3.37	0.13	0.52	0.03	0.13	x	x
S60, m033, 3h1v	15	30	0.27	0.69	542	1.61	1.85	2007	785	4.83	3.51	0.14	0.35	0.06	0.12	x	x
S60, m033, 3h2v	15	20	0.20	0.45	542	1.61	1.68	2709	1204	3.76	4.35	0.14	0.21	0.09	0.08	x	x
S60, m033, 3h3v	15	15	0.35	0.35	542	1.61	1.61	1548	1548	3.22	3.22	0.14	0.14	0.12	0.12		
S60, m033, 5h0v	10	60	0.12	0.96	542	1.60	2.47	4515	564	**11.21**	3.34	0.13	0.48	0.02	0.14	x	x
S60, m030, 0h0v	60	60	0.85	0.85	542	2.24	2.24	637	637	3.31	3.31	0.59	0.59	0.13	0.13	x	x
S60, m030, 1h0v	30	60	0.45	0.91	542	1.67	2.24	1204	595	4.24	3.14	0.38	0.59	0.08	0.15	x	x
S60, m030, 1h1v	30	30	0.61	0.61	542	1.67	1.67	888	888	3.53	3.53	0.39	0.39	0.12	0.12	x	x
S60, m030, 1h2v	30	20	0.66	0.38	542	1.67	1.51	821	1426	3.29	4.74	0.38	0.21	0.13	0.07	x	x
S60, m030, 1h3v	30	15	0.69	0.27	542	1.67	1.45	785	2007	3.17	4.34	0.38	0.14	0.14	0.08	x	x
S60, m030, 2h0v	20	60	0.28	0.92	542	1.51	2.24	1935	589	6.39	3.08	0.21	0.57	0.04	0.15	x	x
S60, m030, 2h1v	20	30	0.38	0.65	542	1.51	1.67	1426	833	4.74	3.29	0.21	0.38	0.07	0.13	x	x
S60, m030, 2h2v	20	20	0.42	0.42	542	1.51	1.51	1290	1290	4.19	4.19	0.22	0.22	0.08	0.08	x	x
S60, m030, 2h3v	20	15	0.45	0.20	542	1.51	1.45	1204	2709	3.91	3.37	0.22	0.14	0.09	0.11	x	
S60, m030, 3h0v	15	60	0.19	0.94	542	1.45	2.24	2851	576	7.23	3.05	0.13	0.57	0.03	0.15	x	x
S60, m030, 3h1v	15	30	0.27	0.69	542	1.45	1.67	2007	785	4.34	3.17	0.14	0.38	0.08	0.14	x	x
S60, m030, 3h2v	15	20	0.20	0.45	542	1.45	1.51	2709	1204	3.37	3.91	0.14	0.22	0.11	0.09		x
S60, m030, 3h3v	15	15	0.35	0.35	542	1.45	1.45	1548	1548	2.89	2.89	0.14	0.14	0.15	0.15		
S60, m030, 5h0v	10	60	0.12	0.96	542	1.43	2.24	4515	564	**9.98**	3.02	0.13	0.53	0.02	0.16	x	x
S60, m027, 0h0v	60	60	0.85	0.85	542	2.01	2.01	637	637	2.97	2.97	0.67	0.67	0.16	0.16	x	x
S60, m027, 1h0v	30	60	0.45	0.91	542	1.50	2.01	1204	595	3.79	2.82	0.41	0.66	0.10	0.17	x	x
S60, m027, 1h1v	30	30	0.61	0.61	542	1.50	1.50	888	888	3.16	3.16	0.42	0.42	0.14	0.14	x	x
S60, m027, 1h2v	30	20	0.66	0.38	542	1.50	1.35	821	1426	2.94	4.23	0.42	0.23	0.16	0.08	x	x
S60, m027, 1h3v	30	15	0.69	0.27	542	1.50	1.29	785	2007	2.84	3.86	0.41	0.14	0.17	0.09	x	x
S60, m027, 2h0v	20	60	0.28	0.92	542	1.35	2.01	1935	589	5.70	2.77	0.22	0.65	0.05	0.18	x	x
S60, m027, 2h1v	20	30	0.38	0.65	542	1.35	1.50	1426	833	4.23	2.94	0.23	0.42	0.08	0.16	x	x
S60, m027, 2h2v	20	20	0.42	0.42	542	1.35	1.35	1290	1290	3.74	3.74	0.23	0.23	0.10	0.10	x	x
S60, m027, 2h3v	20	15	0.45	0.20	542	1.35	1.29	1204	2709	3.49	3.00	0.23	0.14	0.11	0.13	x	
S60, m027, 3h0v	15	60	0.19	0.94	542	1.29	2.01	2851	576	6.43	2.74	0.14	0.64	0.04	0.18	x	x
S60, m027, 3h1v	15	30	0.27	0.69	542	1.29	1.50	2007	785	3.86	2.84	0.14	0.41	0.09	0.17	x	x
S60, m027, 3h2v	15	20	0.20	0.45	542	1.29	1.35	2709	1204	3.00	3.49	0.14	0.23	0.13	0.11		x
S60, m027, 3h3v	15	15	0.35	0.35	542	1.29	1.29	1548	1548	2.57	2.57	0.14	0.14	0.18	0.18		
S60, m027, 5h0v	10	60	0.12	0.96	542	1.26	2.01	4515	564	**8.80**	2.71	0.13	0.60	0.02	0.19	x	x
S60, m024, 0h0v	60	60	0.85	0.85	542	1.78	1.78	637	637	2.63	2.63	0.81	0.80	0.19	0.19	x	x

doi:10.6342/NTU201900743

Type	Spacing y (L, B')	Spacing x (B, L')	PSR_x	PSR_y	S	F_{bx}	F_{by}	S_{cx}	S_{cy}	F_{bx_adj}	F_{by_adj}	δ_x / H_e (%)	δ_y / H_e (%)	δ_{revx} / H_e (%)	δ_{revy} / H_e (%)	check x	check y
S60, m024, 1h0v	30	60	0.45	0.91	542	1.32	1.78	1204	595	3.35	2.50	0.45	0.78	0.12	0.21	x	x
S60, m024, 1h1v	30	30	0.61	0.61	542	1.32	1.32	888	888	2.79	2.79	0.46	0.45	0.17	0.17	x	x
S60, m024, 1h2v	30	20	0.66	0.38	542	1.32	1.19	821	1426	2.60	3.72	0.45	0.25	0.19	0.10	x	x
S60, m024, 1h3v	30	15	0.69	0.27	542	1.32	1.13	785	2007	2.51	3.38	0.45	0.14	0.20	0.11	x	
S60, m024, 2h0v	20	60	0.28	0.92	542	1.19	1.78	1935	589	5.02	2.45	0.24	0.75	0.06	0.22	x	x
S60, m024, 2h1v	20	30	0.38	0.65	542	1.19	1.32	1426	833	3.72	2.60	0.25	0.45	0.10	0.19	x	x
S60, m024, 2h2v	20	20	0.42	0.42	542	1.19	1.19	1290	1290	3.29	3.29	0.25	0.25	0.12	0.12	x	x
S60, m024, 2h3v	20	15	0.45	0.20	542	1.19	1.13	1204	2709	3.07	2.63	0.25	0.14	0.14	0.16	x	
S60, m024, 3h0v	15	60	0.19	0.94	542	1.13	1.78	2851	576	5.64	2.43	0.15	0.75	0.05	0.22	x	x
S60, m024, 3h1v	15	30	0.27	0.69	542	1.13	1.32	2007	785	3.38	2.51	0.14	0.45	0.11	0.20		x
S60, m024, 3h2v	15	20	0.20	0.45	542	1.13	1.19	2709	1204	2.63	3.07	0.14	0.25	0.16	0.14		x
S60, m024, 3h3v	15	15	0.35	0.35	542	1.13	1.13	1548	1548	2.26	2.26	0.15	0.14	0.22	0.22		
S60, m024, 5h0v	10	60	0.12	0.96	542	1.10	1.78	4515	564	**7.67**	2.41	0.13	0.69	0.03	0.22	x	x
S60, m022, 0h0v	60	60	0.85	0.85	542	1.63	1.63	637	637	2.41	2.41	0.95	0.94	0.22	0.22	x	x
S60, m022, 1h0v	30	60	0.45	0.91	542	1.21	1.63	1204	595	3.06	2.28	0.48	0.90	0.14	0.24	x	x
S60, m022, 1h1v	30	30	0.61	0.61	542	1.21	1.21	888	888	2.55	2.55	0.49	0.48	0.19	0.19	x	x
S60, m022, 1h2v	30	20	0.66	0.38	542	1.21	1.08	821	1426	2.37	3.39	0.49	0.26	0.22	0.12	x	x
S60, m022, 1h3v	30	15	0.69	0.27	542	1.21	1.03	785	2007	2.29	3.08	0.48	0.14	0.23	0.13	x	
S60, m022, 2h0v	20	60	0.28	0.92	542	1.08	1.63	1935	589	4.57	2.24	0.26	0.86	0.07	0.25	x	x
S60, m022, 2h1v	20	30	0.38	0.65	542	1.08	1.21	1426	833	3.39	2.37	0.26	0.49	0.12	0.22	x	x
S60, m022, 2h2v	20	20	0.42	0.42	542	1.08	1.08	1290	1290	3.00	3.00	0.27	0.26	0.14	0.14	x	x
S60, m022, 2h3v	20	15	0.45	0.20	542	1.08	1.03	1204	2709	2.80	2.39	0.27	0.14	0.16	0.18	x	
S60, m022, 3h0v	15	60	0.19	0.94	542	1.03	1.63	2851	576	5.13	2.22	0.16	0.87	0.06	0.25	x	x
S60, m022, 3h1v	15	30	0.27	0.69	542	1.03	1.21	2007	785	3.08	2.29	0.14	0.48	0.13	0.23		x
S60, m022, 3h2v	15	20	0.20	0.45	542	1.03	1.08	2709	1204	2.39	2.80	0.14	0.27	0.18	0.16		x
S60, m022, 3h3v	15	15	0.35	0.35	542	1.03	1.03	1548	1548	2.05	2.05	0.15	0.14	0.25	0.25		
S60, m022, 5h0v	10	60	0.12	0.96	542	0.99	1.63	4515	564	**6.94**	2.20	0.13	0.79	0.03	0.26	x	x
S60, m018, 0h0v	60	60	0.85	0.85	542	1.33	1.33	637	637	1.96	1.96	1.43	1.35	0.30	0.30	x	x
S60, m018, 1h0v	30	60	0.45	0.91	542	0.98	1.33	1204	595	2.48	1.86	0.58	1.26	0.19	0.33	x	x
S60, m018, 1h1v	30	30	0.61	0.61	542	0.98	0.98	888	888	2.07	2.07	0.58	0.58	0.27	0.27	x	x
S60, m018, 1h2v	30	20	0.66	0.38	542	0.98	0.87	821	1426	1.93	2.74	0.58	0.29	0.30	0.16	x	x
S60, m018, 1h3v	30	15	0.69	0.27	542	0.98	0.83	785	2007	1.86	2.48	0.56	0.16	0.32	0.18	x	
S60, m018, 2h0v	20	60	0.28	0.92	542	0.87	1.33	1935	589	3.69	1.83	0.29	1.21	0.10	0.34	x	x
S60, m018, 2h1v	20	30	0.38	0.65	542	0.87	0.98	1426	833	2.74	1.93	0.29	0.58	0.16	0.30	x	x
S60, m018, 2h2v	20	20	0.42	0.42	542	0.87	0.87	1290	1290	2.42	2.42	0.30	0.30	0.20	0.20	x	
S60, m018, 2h3v	20	15	0.45	0.20	542	0.87	0.83	1204	2709	2.26	1.93	0.30	0.15	0.22	0.25		
S60, m018, 3h0v	15	60	0.19	0.94	542	0.83	1.33	2851	576	4.13	1.81	0.18	1.22	0.08	0.35	x	x
S60, m018, 3h1v	15	30	0.27	0.69	542	0.83	0.98	2007	785	2.48	1.86	0.16	0.56	0.18	0.32		x
S60, m018, 3h2v	15	20	0.20	0.45	542	0.83	0.87	2709	1204	1.93	2.26	0.15	0.30	0.25	0.22		
S60, m018, 3h3v	15	15	0.35	0.35	542	0.83	0.83	1548	1548	1.65	1.65	0.15	0.15	0.35	0.35		
S60, m018, 5h0v	10	60	0.12	0.96	542	0.79	1.33	4515	564	**5.53**	1.79	0.15	1.08	0.05	0.35	x	x
S42, m033, 0h0v	42	42	0.72	0.72	542	2.09	2.09	752	752	3.64	3.64	0.42	0.42	0.11	0.11	x	x
S42, m033, 1h0v	21	42	0.34	0.82	542	1.69	2.09	1593	661	5.69	3.37	0.19	0.42	0.05	0.13	x	x

doi:10.6342/NTU201900743

Type	Spacing y (L, B')	Spacing x (B, L')	PSR_x	PSR_y	S	F_{bx}	F_{by}	S_{cx}	S_{cy}	F_{bx_adj}	F_{by_adj}	δ_x / H_e (%)	δ_y / H_e (%)	δ_{revx} / H_e (%)	δ_{revy} / H_e (%)	check x	check y
S42, m033, 1h1v	21	21	0.47	0.47	542	1.69	1.69	1153	1153	4.53	4.53	0.20	0.20	0.08	0.08	x	x
S42, m033, 1h2v	21	14	0.53	0.28	542	1.69	1.60	1022	1935	4.15	4.01	0.20	0.10	0.09	0.09	x	
S42, m033, 1h3v	21	10.5	0.51	0.20	542	1.69	1.60	1062	2709	3.95	4.79	0.20	0.08	0.10	0.06	x	
S42, m033, 2h0v	14	42	0.20	0.86	542	1.60	2.09	2709	630	6.41	3.27	0.10	0.41	0.04	0.14	x	x
S42, m033, 2h1v	14	21	0.26	0.53	542	1.60	1.69	2084	1022	4.01	4.15	0.10	0.20	0.08	0.09		x
S42, m033, 2h2v	14	14	0.30	0.30	542	1.60	1.60	1806	1806	3.21	3.21	0.11	0.10	0.12	0.12		
S42, m033, 2h3v	14	10.5	0.32	0.23	542	1.60	1.60	1693	2355	2.81	3.73	0.11	0.09	0.15	0.09		
S42, m033, 3h0v	10.5	42	0.15	0.89	542	1.60	2.09	3612	609	7.99	3.23	0.08	0.40	0.03	0.14	x	x
S42, m033, 3h1v	10.5	21	0.20	0.51	542	1.60	1.69	2709	1062	4.79	3.95	0.08	0.20	0.06	0.10		x
S42, m033, 3h2v	10.5	14	0.23	0.32	542	1.60	1.60	2355	1693	3.73	2.81	0.09	0.11	0.09	0.15		
S42, m033, 3h3v	10.5	10.5	0.25	0.25	542	1.60	1.60	2167	2167	3.19	3.19	0.09	0.09	0.12	0.12		
S42, m030, 0h0v	42	42	0.72	0.72	542	1.89	1.89	752	752	3.30	3.30	0.46	0.46	0.13	0.13	x	x
S42, m030, 1h0v	21	42	0.34	0.82	542	1.52	1.89	1593	661	5.13	3.05	0.20	0.45	0.06	0.15	x	x
S42, m030, 1h1v	21	21	0.47	0.47	542	1.52	1.52	1153	1153	4.08	4.08	0.21	0.21	0.09	0.09	x	x
S42, m030, 1h2v	21	14	0.53	0.28	542	1.52	1.44	1022	1935	3.74	3.59	0.21	0.10	0.10	0.10	x	
S42, m030, 1h3v	21	10.5	0.51	0.20	542	1.52	1.42	1062	2709	3.56	4.27	0.21	0.08	0.11	0.07	x	
S42, m030, 2h0v	14	42	0.20	0.86	542	1.44	1.89	2709	630	5.75	2.96	0.09	0.44	0.05	0.16	x	x
S42, m030, 2h1v	14	21	0.26	0.53	542	1.44	1.52	2084	1022	3.59	3.74	0.10	0.21	0.10	0.10		x
S42, m030, 2h2v	14	14	0.30	0.30	542	1.44	1.44	1806	1806	2.87	2.87	0.11	0.10	0.14	0.14		
S42, m030, 2h3v	14	10.5	0.32	0.23	542	1.44	1.42	1693	2355	2.51	3.32	0.11	0.09	0.18	0.11		
S42, m030, 3h0v	10.5	42	0.15	0.89	542	1.42	1.89	3612	609	7.12	2.92	0.08	0.44	0.03	0.16	x	x
S42, m030, 3h1v	10.5	21	0.20	0.51	542	1.42	1.52	2709	1062	4.27	3.56	0.08	0.21	0.07	0.11		x
S42, m030, 3h2v	10.5	14	0.23	0.32	542	1.42	1.44	2355	1693	3.32	2.51	0.09	0.11	0.11	0.18		
S42, m030, 3h3v	10.5	10.5	0.25	0.25	542	1.42	1.42	2167	2167	2.85	2.85	0.09	0.09	0.14	0.14		
S42, m027, 0h0v	42	42	0.72	0.72	542	1.70	1.70	752	752	2.95	2.95	0.52	0.52	0.16	0.16	x	x
S42, m027, 1h0v	21	42	0.34	0.82	542	1.36	1.70	1593	661	4.57	2.73	0.21	0.50	0.07	0.18	x	x
S42, m027, 1h1v	21	21	0.47	0.47	542	1.36	1.36	1153	1153	3.64	3.64	0.22	0.22	0.11	0.11	x	x
S42, m027, 1h2v	21	14	0.53	0.28	542	1.36	1.28	1022	1935	3.33	3.19	0.22	0.10	0.12	0.12	x	
S42, m027, 1h3v	21	10.5	0.51	0.20	542	1.36	1.26	1062	2709	3.18	3.77	0.23	0.09	0.13	0.09	x	
S42, m027, 2h0v	14	42	0.20	0.86	542	1.28	1.70	2709	630	5.10	2.66	0.09	0.49	0.06	0.19	x	x
S42, m027, 2h1v	14	21	0.26	0.53	542	1.28	1.36	2084	1022	3.19	3.33	0.10	0.22	0.12	0.12		x
S42, m027, 2h2v	14	14	0.30	0.30	542	1.28	1.28	1806	1806	2.55	2.55	0.11	0.10	0.17	0.17		
S42, m027, 2h3v	14	10.5	0.32	0.23	542	1.28	1.26	1693	2355	2.23	2.93	0.11	0.09	0.22	0.13		
S42, m027, 3h0v	10.5	42	0.15	0.89	542	1.26	1.70	3612	609	6.29	2.62	0.08	0.48	0.04	0.20	x	x
S42, m027, 3h1v	10.5	21	0.20	0.51	542	1.26	1.36	2709	1062	3.77	3.18	0.09	0.23	0.09	0.13		x
S42, m027, 3h2v	10.5	14	0.23	0.32	542	1.26	1.28	2355	1693	2.93	2.23	0.09	0.11	0.13	0.22		
S42, m027, 3h3v	10.5	10.5	0.25	0.25	542	1.26	1.26	2167	2167	2.51	2.51	0.09	0.09	0.17	0.17		
S42, m024, 0h0v	42	42	0.72	0.72	542	1.50	1.50	752	752	2.61	2.61	0.59	0.59	0.19	0.19	x	x
S42, m024, 1h0v	21	42	0.34	0.82	542	1.20	1.50	1593	661	4.03	2.42	0.22	0.57	0.09	0.22	x	x
S42, m024, 1h1v	21	21	0.47	0.47	542	1.20	1.20	1153	1153	3.21	3.21	0.23	0.23	0.13	0.13	x	x
S42, m024, 1h2v	21	14	0.53	0.28	542	1.20	1.12	1022	1935	2.94	2.80	0.24	0.10	0.15	0.15	x	
S42, m024, 1h3v	21	10.5	0.51	0.20	542	1.20	1.10	1062	2709	2.80	3.29	0.24	0.09	0.16	0.11		
S42, m024, 2h0v	14	42	0.20	0.86	542	1.12	1.50	2709	630	4.47	2.35	0.10	0.55	0.07	0.23		x

doi:10.6342/NTU201900743

Type	Spacing y (L, B')	Spacing x (B, L')	PSR_x	PSR_y	S	F_{bx}	F_{by}	S_{cx}	S_{cy}	F_{bx_adj}	F_{by_adj}	δ_x / H_e (%)	δ_y / H_e (%)	δ_{revx} / H_e (%)	δ_{revy} / H_e (%)	check x	check y
S42, m024, 2h1v	14	21	0.26	0.53	542	1.12	1.20	2084	1022	2.80	2.94	0.10	0.24	0.15	0.15		x
S42, m024, 2h2v	14	14	0.30	0.30	542	1.12	1.12	1806	1806	2.24	2.24	0.11	0.11	0.21	0.21		
S42, m024, 2h3v	14	10.5	0.32	0.23	542	1.12	1.10	1693	2355	1.96	2.56	0.11	0.09	0.26	0.17		
S42, m024, 3h0v	10.5	42	0.15	0.89	542	1.10	1.50	3612	609	5.48	2.32	0.08	0.54	0.05	0.24	x	x
S42, m024, 3h1v	10.5	21	0.20	0.51	542	1.10	1.20	2709	1062	3.29	2.80	0.09	0.24	0.11	0.16		
S42, m024, 3h2v	10.5	14	0.23	0.32	542	1.10	1.12	2355	1693	2.56	1.96	0.09	0.11	0.17	0.26		
S42, m024, 3h3v	10.5	10.5	0.25	0.25	542	1.10	1.10	2167	2167	2.19	2.19	0.09	0.09	0.21	0.21		
S42, m022, 0h0v	42	42	0.72	0.72	542	1.37	1.37	752	752	2.39	2.39	0.68	0.67	0.22	0.22	x	x
S42, m022, 1h0v	21	42	0.34	0.82	542	1.09	1.37	1593	661	3.67	2.21	0.23	0.63	0.10	0.25	x	x
S42, m022, 1h1v	21	21	0.47	0.47	542	1.09	1.09	1153	1153	2.93	2.93	0.24	0.24	0.15	0.15	x	x
S42, m022, 1h2v	21	14	0.53	0.28	542	1.09	1.02	1022	1935	2.68	2.54	0.25	0.10	0.18	0.17		
S42, m022, 1h3v	21	10.5	0.51	0.20	542	1.09	0.99	1062	2709	2.55	2.98	0.20	0.08	0.19	0.13		
S42, m022, 2h0v	14	42	0.20	0.86	542	1.02	1.37	2709	630	4.06	2.15	0.10	0.61	0.08	0.26		x
S42, m022, 2h1v	14	21	0.26	0.53	542	1.02	1.09	2084	1022	2.54	2.68	0.10	0.25	0.17	0.18		
S42, m022, 2h2v	14	14	0.30	0.30	542	1.02	1.02	1806	1806	2.03	2.03	0.11	0.11	0.25	0.25		
S42, m022, 2h3v	14	10.5	0.32	0.23	542	1.02	0.99	1693	2355	1.78	2.32	0.11	0.09	0.31	0.19		
S42, m022, 3h0v	10.5	42	0.15	0.89	542	0.99	1.37	3612	609	4.96	2.12	0.08	0.60	0.06	0.27		x
S42, m022, 3h1v	10.5	21	0.20	0.51	542	0.99	1.09	2709	1062	2.98	2.55	0.08	0.20	0.13	0.19		
S42, m022, 3h2v	10.5	14	0.23	0.32	542	0.99	1.02	2355	1693	2.32	1.78	0.09	0.11	0.19	0.31		
S42, m022, 3h3v	10.5	10.5	0.25	0.25	542	0.99	0.99	2167	2167	1.99	1.99	0.09	0.09	0.25	0.25		
S42, m018, 0h0v	42	42	0.72	0.72	542	1.12	1.12	752	752	1.94	1.94	0.94	0.93	0.30	0.30	x	x
S42, m018, 1h0v	21	42	0.34	0.82	542	0.88	1.12	1593	661	2.97	1.80	0.25	0.83	0.14	0.35	x	x
S42, m018, 1h1v	21	21	0.47	0.47	542	0.88	0.88	1153	1153	2.37	2.37	0.26	0.26	0.21	0.21		
S42, m018, 1h2v	21	14	0.53	0.28	542	0.88	0.82	1022	1935	2.16	2.04	0.27	0.11	0.24	0.24		
S42, m018, 1h3v	21	10.5	0.51	0.20	542	0.88	0.79	1062	2709	2.06	2.38	0.27	0.09	0.26	0.18		
S42, m018, 2h0v	14	42	0.20	0.86	542	0.82	1.12	2709	630	3.27	1.75	0.11	0.81	0.11	0.36		x
S42, m018, 2h1v	14	21	0.26	0.53	542	0.82	0.88	2084	1022	2.04	2.16	0.11	0.27	0.24	0.24		
S42, m018, 2h2v	14	14	0.30	0.30	542	0.82	0.82	1806	1806	1.63	1.63	0.11	0.11	0.35	0.35		
S42, m018, 2h3v	14	10.5	0.32	0.23	542	0.82	0.79	1693	2355	1.43	1.85	0.11	0.09	0.43	0.28		
S42, m018, 3h0v	10.5	42	0.15	0.89	542	0.79	1.12	3612	609	3.96	1.72	0.09	0.77	0.08	0.37		x
S42, m018, 3h1v	10.5	21	0.20	0.51	542	0.79	0.88	2709	1062	2.38	2.06	0.09	0.27	0.18	0.26		
S42, m018, 3h2v	10.5	14	0.23	0.32	542	0.79	0.82	2355	1693	1.85	1.43	0.09	0.11	0.28	0.43		
S42, m018, 3h3v	10.5	10.5	0.25	0.25	542	0.79	0.79	2167	2167	1.59	1.59	0.09	0.09	0.35	0.35		
S30, m033, 0h0v	30	30	0.56	0.56	542	1.85	1.85	967	967	3.90	3.90	0.30	0.30	0.10	0.10	x	x
S30, m033, 1h0v	15	30	0.28	0.68	542	1.61	1.85	1935	797	4.83	3.51	0.09	0.30	0.06	0.12		x
S30, m033, 2h0v	10	30	0.15	0.71	542	1.60	1.85	3612	763	6.41	3.38	0.07	0.29	0.04	0.13	x	x
S30, m030, 0h0v	30	30	0.56	0.56	542	1.67	1.67	967	967	3.53	3.53	0.33	0.33	0.12	0.12	x	x
S30, m030, 1h0v	15	30	0.28	0.68	542	1.45	1.67	1935	797	4.34	3.17	0.09	0.33	0.08	0.14		x
S30, m030, 2h0v	10	30	0.15	0.71	542	1.43	1.67	3612	763	5.70	3.05	0.07	0.32	0.05	0.15	x	x
S30, m027, 0h0v	30	30	0.56	0.56	542	1.50	1.50	967	967	3.16	3.16	0.36	0.36	0.14	0.14	x	x
S30, m027, 1h0v	15	30	0.28	0.68	542	1.29	1.50	1935	797	3.86	2.84	0.09	0.36	0.09	0.17		x
S30, m027, 2h0v	10	30	0.15	0.71	542	1.26	1.50	3612	763	5.03	2.73	0.07	0.35	0.05	0.18		x
S30, m024, 0h0v	30	30	0.56	0.56	542	1.32	1.32	967	967	2.79	2.79	0.40	0.40	0.17	0.17	x	x

doi:10.6342/NTU201900743

Type	Spacing y (L, B')	Spacing x (B, L')	PSR_x	PSR_y	S	F_{bx}	F_{by}	S_{cx}	S_{cy}	F_{bx_adj}	F_{by_adj}	δ_x / H_e (%)	δ_y / H_e (%)	δ_{revx} / H_e (%)	δ_{revy} / H_e (%)	check x	check y
S30, m024, 1h0v	15	30	0.28	0.68	542	1.13	1.32	1935	797	3.38	2.51	0.10	0.40	0.11	0.20		x
S30, m024, 2h0v	10	30	0.15	0.71	542	1.10	1.32	3612	763	4.38	2.41	0.07	0.39	0.07	0.21		x
S30, m022, 0h0v	30	30	0.56	0.56	542	1.21	1.21	967	967	2.55	2.55	0.44	0.44	0.19	0.19	x	x
S30, m022, 1h0v	15	30	0.28	0.68	542	1.03	1.21	1935	797	3.08	2.29	0.10	0.43	0.13	0.23		x
S30, m022, 2h0v	10	30	0.15	0.71	542	0.99	1.21	3612	763	3.96	2.20	0.07	0.42	0.08	0.25		x
S30, m018, 0h0v	30	30	0.56	0.56	542	0.98	0.98	967	967	2.07	2.07	0.56	0.56	0.26	0.26	x	x
S30, m018, 1h0v	15	30	0.28	0.68	542	0.83	0.98	1935	797	2.48	1.86	0.10	0.53	0.18	0.32		x
S30, m018, 2h0v	10	30	0.15	0.71	542	0.79	0.98	3612	763	3.16	1.79	0.07	0.51	0.11	0.34		
S20, m033, 0h0v	20	20	0.39	0.39	542	1.68	1.68	1389	1389	4.65	4.65	0.16	0.16	0.07	0.07	x	x
S20, m033, 1h0v	10	20	0.18	0.50	542	1.60	1.68	3010	1084	4.80	4.04	0.05	0.17	0.06	0.09		x
S20, m030, 0h0v	20	20	0.39	0.39	542	1.51	1.51	1389	1389	4.19	4.19	0.17	0.17	0.08	0.08	x	x
S20, m030, 1h0v	10	20	0.18	0.50	542	1.43	1.51	3010	1084	4.28	3.64	0.05	0.18	0.07	0.11		x
S20, m027, 0h0v	20	20	0.39	0.39	542	1.35	1.35	1389	1389	3.74	3.74	0.18	0.18	0.10	0.10	x	x
S20, m027, 1h0v	10	20	0.18	0.50	542	1.26	1.35	3010	1084	3.77	3.25	0.05	0.19	0.09	0.13		
S20, m024, 0h0v	20	20	0.39	0.39	542	1.19	1.19	1389	1389	3.29	3.29	0.19	0.19	0.12	0.12	x	x
S20, m024, 1h0v	10	20	0.18	0.50	542	1.10	1.19	3010	1084	3.29	2.86	0.05	0.21	0.11	0.16		
S20, m022, 0h0v	20	20	0.39	0.39	542	1.08	1.08	1389	1389	3.00	3.00	0.20	0.20	0.14	0.14		
S20, m022, 1h0v	10	20	0.18	0.50	542	0.99	1.08	3010	1084	2.97	2.60	0.05	0.22	0.13	0.18		
S20, m018, 0h0v	20	20	0.39	0.39	542	0.87	0.87	1389	1389	2.42	2.42	0.23	0.23	0.20	0.20		
S20, m018, 1h0v	10	20	0.18	0.50	542	0.79	0.87	3010	1084	2.37	2.11	0.05	0.25	0.18	0.25		

doi:10.6342/NTU201900743

APPENDIX B

The parameters and predicted results by using the equivalent length of cross walls

doi:10.6342/NTU201900743

Type	Spacing y (L, B')	Spacing x (B, L')	PSR_x	PSR_y	S	F_{bx}	F_{by}	S_{cx}	S_{cy}	$L_{e,x}$	F_{bx_adj}	$L_{e,y}$	F_{by_adj}	δ_x / H_e (%)	δ_y / H_e (%)	δ_{revx} / H_e (%)	δ_{revy} / H_e (%)	check x	check y
S60, m033, 0h0v	60	60	0.85	0.85	542	2.47	2.47	637	637	42.4	3.54	42.4	3.54	0.53	0.53	0.12	0.12	x	x
S60, m033, 1h0v	30	60	0.45	0.91	542	1.85	2.47	1204	595	21.2	3.67	42.4	3.54	0.35	0.53	0.10	0.12	x	x
S60, m033, 1h1v	30	30	0.61	0.61	542	1.85	1.85	888	888	21.2	3.67	21.2	3.67	0.36	0.36	0.11	0.11	x	x
S60, m033, 1h2v	30	20	0.66	0.38	542	1.85	1.68	821	1426	21.2	3.67	14.1	4.29	0.36	0.21	0.11	0.08	x	x
S60, m033, 1h3v	30	15	0.69	0.27	542	1.85	1.61	785	2007	21.2	3.67	10.6	2.75	0.35	0.14	0.11	0.15	x	
S60, m033, 2h0v	20	60	0.28	0.92	542	1.68	2.47	1935	589	14.1	4.29	42.4	3.54	0.20	0.52	0.08	0.12	x	x
S60, m033, 2h1v	20	30	0.38	0.65	542	1.68	1.85	1426	833	14.1	4.29	21.2	3.67	0.21	0.36	0.08	0.11	x	x
S60, m033, 2h2v	20	20	0.42	0.42	542	1.68	1.68	1290	1290	14.1	4.29	14.1	4.29	0.21	0.21	0.08	0.08	x	x
S60, m033, 2h3v	20	15	0.45	0.20	542	1.68	1.61	1204	2709	14.1	4.29	10.6	2.75	0.21	0.14	0.08	0.15	x	
S60, m033, 3h0v	15	60	0.19	0.94	542	1.61	2.47	2851	576	10.6	2.75	42.4	3.54	0.13	0.52	0.14	0.12		x
S60, m033, 3h1v	15	30	0.27	0.69	542	1.61	1.85	2007	785	10.6	2.75	21.2	3.67	0.14	0.35	0.15	0.11		x
S60, m033, 3h2v	15	20	0.20	0.45	542	1.61	1.68	2709	1204	10.6	2.75	14.1	4.29	0.14	0.21	0.15	0.08		x
S60, m033, 3h3v	15	15	0.35	0.35	542	1.61	1.61	1548	1548	10.6	2.75	10.6	2.75	0.14	0.14	0.16	0.16		
S60, m033, 5h0v	10	60	0.12	0.96	542	1.60	2.47	4515	564	7.1	2.73	42.4	3.54	0.13	0.48	0.14	0.12		x
S60, m030, 0h0v	60	60	0.85	0.85	542	2.24	2.24	637	637	42.4	3.21	42.4	3.21	0.59	0.59	0.14	0.14	x	x
S60, m030, 1h0v	30	60	0.45	0.91	542	1.67	2.24	1204	595	21.2	3.32	42.4	3.21	0.38	0.59	0.12	0.14	x	x
S60, m030, 1h1v	30	30	0.61	0.61	542	1.67	1.67	888	888	21.2	3.32	21.2	3.32	0.39	0.39	0.13	0.13	x	x
S60, m030, 1h2v	30	20	0.66	0.38	542	1.67	1.51	821	1426	21.2	3.32	14.1	3.87	0.38	0.21	0.13	0.09	x	x
S60, m030, 1h3v	30	15	0.69	0.27	542	1.67	1.45	785	2007	21.2	3.32	10.6	2.47	0.38	0.14	0.13	0.18	x	
S60, m030, 2h0v	20	60	0.28	0.92	542	1.51	2.24	1935	589	14.1	3.87	42.4	3.21	0.21	0.57	0.09	0.14	x	x
S60, m030, 2h1v	20	30	0.38	0.65	542	1.51	1.67	1426	833	14.1	3.87	21.2	3.32	0.21	0.38	0.09	0.13	x	x
S60, m030, 2h2v	20	20	0.42	0.42	542	1.51	1.51	1290	1290	14.1	3.87	14.1	3.87	0.22	0.22	0.10	0.10	x	x
S60, m030, 2h3v	20	15	0.45	0.20	542	1.51	1.45	1204	2709	14.1	3.87	10.6	2.47	0.22	0.14	0.10	0.17	x	
S60, m030, 3h0v	15	60	0.19	0.94	542	1.45	2.24	2851	576	10.6	2.47	42.4	3.21	0.13	0.57	0.17	0.14		x
S60, m030, 3h1v	15	30	0.27	0.69	542	1.45	1.67	2007	785	10.6	2.47	21.2	3.32	0.14	0.38	0.18	0.13		x
S60, m030, 3h2v	15	20	0.20	0.45	542	1.45	1.51	2709	1204	10.6	2.47	14.1	3.87	0.14	0.22	0.17	0.10		x
S60, m030, 3h3v	15	15	0.35	0.35	542	1.45	1.45	1548	1548	10.6	2.47	10.6	2.47	0.14	0.14	0.19	0.19		
S60, m030, 5h0v	10	60	0.12	0.96	542	1.43	2.24	4515	564	7.1	2.43	42.4	3.21	0.13	0.53	0.16	0.14		x
S60, m027, 0h0v	60	60	0.85	0.85	542	2.01	2.01	637	637	42.4	2.88	42.4	2.88	0.67	0.67	0.17	0.17	x	x
S60, m027, 1h0v	30	60	0.45	0.91	542	1.50	2.01	1204	595	21.2	2.97	42.4	2.88	0.41	0.66	0.15	0.17	x	x
S60, m027, 1h1v	30	30	0.61	0.61	542	1.50	1.50	888	888	21.2	2.97	21.2	2.97	0.42	0.42	0.15	0.15	x	x
S60, m027, 1h2v	30	20	0.66	0.38	542	1.50	1.35	821	1426	21.2	2.97	14.1	3.45	0.42	0.23	0.15	0.11	x	x
S60, m027, 1h3v	30	15	0.69	0.27	542	1.50	1.29	785	2007	21.2	2.97	10.6	2.19	0.41	0.14	0.15	0.22	x	
S60, m027, 2h0v	20	60	0.28	0.92	542	1.35	2.01	1935	589	14.1	3.45	42.4	2.88	0.22	0.65	0.11	0.17	x	x
S60, m027, 2h1v	20	30	0.38	0.65	542	1.35	1.50	1426	833	14.1	3.45	21.2	2.97	0.23	0.42	0.11	0.15	x	x
S60, m027, 2h2v	20	20	0.42	0.42	542	1.35	1.35	1290	1290	14.1	3.45	14.1	3.45	0.23	0.23	0.11	0.11	x	x
S60, m027, 2h3v	20	15	0.45	0.20	542	1.35	1.29	1204	2709	14.1	3.45	10.6	2.19	0.23	0.14	0.12	0.21	x	
S60, m027, 3h0v	15	60	0.19	0.94	542	1.29	2.01	2851	576	10.6	2.19	42.4	2.88	0.14	0.64	0.21	0.17		x
S60, m027, 3h1v	15	30	0.27	0.69	542	1.29	1.50	2007	785	10.6	2.19	21.2	2.97	0.14	0.41	0.22	0.15		x
S60, m027, 3h2v	15	20	0.20	0.45	542	1.29	1.35	2709	1204	10.6	2.19	14.1	3.45	0.14	0.23	0.21	0.12		x
S60, m027, 3h3v	15	15	0.35	0.35	542	1.29	1.29	1548	1548	10.6	2.19	10.6	2.19	0.14	0.14	0.22	0.22		
S60, m027, 5h0v	10	60	0.12	0.96	542	1.26	2.01	4515	564	7.1	2.15	42.4	2.88	0.13	0.60	0.20	0.17		x
S60, m024, 0h0v	60	60	0.85	0.85	542	1.78	1.78	637	637	42.4	2.55	42.4	2.55	0.81	0.80	0.20	0.20	x	x
S60, m024, 1h0v	30	60	0.45	0.91	542	1.32	1.78	1204	595	21.2	2.62	42.4	2.55	0.45	0.78	0.18	0.20	x	x
S60, m024, 1h1v	30	30	0.61	0.61	542	1.32	1.32	888	888	21.2	2.62	21.2	2.62	0.46	0.45	0.18	0.18	x	x

doi:10.6342/NTU201900743

Type	Spacing y (L, B')	Spacing x (B, L')	PSR_x	PSR_y	S	F_{bx}	F_{by}	S_{cx}	S_{cy}	$L_{e,x}$	F_{bx_adj}	$L_{e,y}$	F_{by_adj}	δ_x / H_e (%)	δ_y / H_e (%)	δ_{revx} / H_e (%)	δ_{revy} / H_e (%)	check x	check y
S60, m024, 1h2v	30	20	0.66	0.38	542	1.32	1.19	821	1426	21.2	2.62	14.1	3.04	0.45	0.25	0.19	0.14	x	x
S60, m024, 1h3v	30	15	0.69	0.27	542	1.32	1.13	785	2007	21.2	2.62	10.6	1.93	0.45	0.14	0.19	0.26	x	
S60, m024, 2h0v	20	60	0.28	0.92	542	1.19	1.78	1935	589	14.1	3.04	42.4	2.55	0.24	0.75	0.13	0.20	x	x
S60, m024, 2h1v	20	30	0.38	0.65	542	1.19	1.32	1426	833	14.1	3.04	21.2	2.62	0.25	0.45	0.14	0.19	x	x
S60, m024, 2h2v	20	20	0.42	0.42	542	1.19	1.19	1290	1290	14.1	3.04	14.1	3.04	0.25	0.25	0.14	0.14	x	x
S60, m024, 2h3v	20	15	0.45	0.20	542	1.19	1.13	1204	2709	14.1	3.04	10.6	1.93	0.25	0.14	0.14	0.25	x	
S60, m024, 3h0v	15	60	0.19	0.94	542	1.13	1.78	2851	576	10.6	1.93	42.4	2.55	0.15	0.75	0.25	0.20		x
S60, m024, 3h1v	15	30	0.27	0.69	542	1.13	1.32	2007	785	10.6	1.93	21.2	2.62	0.14	0.45	0.26	0.19		x
S60, m024, 3h2v	15	20	0.20	0.45	542	1.13	1.19	2709	1204	10.6	1.93	14.1	3.04	0.14	0.25	0.25	0.14		x
S60, m024, 3h3v	15	15	0.35	0.35	542	1.13	1.13	1548	1548	10.6	1.93	10.6	1.93	0.15	0.14	0.27	0.27		
S60, m024, 5h0v	10	60	0.12	0.96	542	1.10	1.78	4515	564	7.1	1.87	42.4	2.55	0.13	0.69	0.25	0.21		x
S60, m022, 0h0v	60	60	0.85	0.85	542	1.63	1.63	637	637	42.4	2.34	42.4	2.34	0.95	0.94	0.23	0.23	x	x
S60, m022, 1h0v	30	60	0.45	0.91	542	1.21	1.63	1204	595	21.2	2.40	42.4	2.34	0.48	0.90	0.20	0.23	x	x
S60, m022, 1h1v	30	30	0.61	0.61	542	1.21	1.21	888	888	21.2	2.40	21.2	2.40	0.49	0.48	0.21	0.21	x	x
S60, m022, 1h2v	30	20	0.66	0.38	542	1.21	1.08	821	1426	21.2	2.40	14.1	2.77	0.49	0.26	0.21	0.16	x	x
S60, m022, 1h3v	30	15	0.69	0.27	542	1.21	1.03	785	2007	21.2	2.40	10.6	1.75	0.48	0.14	0.22	0.31	x	
S60, m022, 2h0v	20	60	0.28	0.92	542	1.08	1.63	1935	589	14.1	2.77	42.4	2.34	0.26	0.86	0.15	0.23	x	x
S60, m022, 2h1v	20	30	0.38	0.65	542	1.08	1.21	1426	833	14.1	2.77	21.2	2.40	0.26	0.49	0.16	0.21	x	x
S60, m022, 2h2v	20	20	0.42	0.42	542	1.08	1.08	1290	1290	14.1	2.77	14.1	2.77	0.27	0.26	0.16	0.16	x	x
S60, m022, 2h3v	20	15	0.45	0.20	542	1.08	1.03	1204	2709	14.1	2.77	10.6	1.75	0.27	0.14	0.16	0.29	x	
S60, m022, 3h0v	15	60	0.19	0.94	542	1.03	1.63	2851	576	10.6	1.75	42.4	2.34	0.16	0.87	0.29	0.23		x
S60, m022, 3h1v	15	30	0.27	0.69	542	1.03	1.21	2007	785	10.6	1.75	21.2	2.40	0.14	0.48	0.31	0.22		x
S60, m022, 3h2v	15	20	0.20	0.45	542	1.03	1.08	2709	1204	10.6	1.75	14.1	2.77	0.14	0.27	0.29	0.16		x
S60, m022, 3h3v	15	15	0.35	0.35	542	1.03	1.03	1548	1548	10.6	1.75	10.6	1.75	0.15	0.14	0.32	0.32		
S60, m022, 5h0v	10	60	0.12	0.96	542	0.99	1.63	4515	564	7.1	1.69	42.4	2.34	0.13	0.79	0.29	0.24		x
S60, m018, 0h0v	60	60	0.85	0.85	542	1.33	1.33	637	637	42.4	1.90	42.4	1.90	1.43	1.35	0.32	0.32	x	x
S60, m018, 1h0v	30	60	0.45	0.91	542	0.98	1.33	1204	595	21.2	1.94	42.4	1.90	0.58	1.26	0.28	0.32	x	x
S60, m018, 1h1v	30	30	0.61	0.61	542	0.98	0.98	888	888	21.2	1.94	21.2	1.94	0.58	0.58	0.29	0.29	x	x
S60, m018, 1h2v	30	20	0.66	0.38	542	0.98	0.87	821	1426	21.2	1.94	14.1	2.24	0.58	0.29	0.30	0.22	x	
S60, m018, 1h3v	30	15	0.69	0.27	542	0.98	0.83	785	2007	21.2	1.94	10.6	1.41	0.56	0.16	0.30	0.43	x	
S60, m018, 2h0v	20	60	0.28	0.92	542	0.87	1.33	1935	589	14.1	2.24	42.4	1.90	0.29	1.21	0.21	0.32		x
S60, m018, 2h1v	20	30	0.38	0.65	542	0.87	0.98	1426	833	14.1	2.24	21.2	1.94	0.29	0.58	0.22	0.30		x
S60, m018, 2h2v	20	20	0.42	0.42	542	0.87	0.87	1290	1290	14.1	2.24	14.1	2.24	0.30	0.30	0.22	0.22		
S60, m018, 2h3v	20	15	0.45	0.20	542	0.87	0.83	1204	2709	14.1	2.24	10.6	1.41	0.30	0.15	0.23	0.41		
S60, m018, 3h0v	15	60	0.19	0.94	542	0.83	1.33	2851	576	10.6	1.41	42.4	1.90	0.18	1.22	0.41	0.32		x
S60, m018, 3h1v	15	30	0.27	0.69	542	0.83	0.98	2007	785	10.6	1.41	21.2	1.94	0.16	0.56	0.43	0.30		x
S60, m018, 3h2v	15	20	0.20	0.45	542	0.83	0.87	2709	1204	10.6	1.41	14.1	2.24	0.15	0.30	0.41	0.23		
S60, m018, 3h3v	15	15	0.35	0.35	542	0.83	0.83	1548	1548	10.6	1.41	10.6	1.41	0.15	0.15	0.45	0.45		
S60, m018, 5h0v	10	60	0.12	0.96	542	0.79	1.33	4515	564	7.1	1.35	42.4	1.90	0.15	1.08	0.41	0.32		x
S42, m033, 0h0v	42	42	0.72	0.72	542	2.09	2.09	752	752	29.7	3.48	29.7	3.48	0.42	0.42	0.12	0.12	x	x
S42, m033, 1h0v	21	42	0.34	0.82	542	1.69	2.09	1593	661	14.8	4.19	29.7	3.48	0.19	0.42	0.08	0.12	x	x
S42, m033, 1h1v	21	21	0.47	0.47	542	1.69	1.69	1153	1153	14.8	4.19	14.8	4.19	0.20	0.20	0.09	0.09	x	x
S42, m033, 1h2v	21	14	0.53	0.28	542	1.69	1.60	1022	1935	14.8	4.19	9.9	2.74	0.20	0.10	0.09	0.15	x	
S42, m033, 1h3v	21	10.5	0.51	0.20	542	1.69	1.60	1062	2709	14.8	4.19	7.4	2.73	0.20	0.08	0.09	0.15	x	
S42, m033, 2h0v	14	42	0.20	0.86	542	1.60	2.09	2709	630	9.9	2.74	29.7	3.48	0.10	0.41	0.15	0.12		x

doi:10.6342/NTU201900743

Type	Spacing y (L, B')	Spacing x (B, L')	PSR_x	PSR_y	S	F_{bx}	F_{by}	S_{cx}	S_{cy}	$L_{e,x}$	F_{bx_adj}	$L_{e,y}$	F_{by_adj}	δ_x / H_e (%)	δ_y / H_e (%)	δ_{revx} / H_e (%)	δ_{revy} / H_e (%)	check x	check y
S42, m033, 2h1v	14	21	0.26	0.53	542	1.60	1.69	2084	1022	9.9	2.74	14.8	4.19	0.10	0.20	0.15	0.09		x
S42, m033, 2h2v	14	14	0.30	0.30	542	1.60	1.60	1806	1806	9.9	2.74	9.9	2.74	0.11	0.10	0.16	0.16		
S42, m033, 2h3v	14	10.5	0.32	0.23	542	1.60	1.60	1693	2355	9.9	2.74	7.4	2.73	0.11	0.09	0.16	0.15		
S42, m033, 3h0v	10.5	42	0.15	0.89	542	1.60	2.09	3612	609	7.4	2.73	29.7	3.48	0.08	0.40	0.14	0.13		x
S42, m033, 3h1v	10.5	21	0.20	0.51	542	1.60	1.69	2709	1062	7.4	2.73	14.8	4.19	0.08	0.20	0.15	0.09		x
S42, m033, 3h2v	10.5	14	0.23	0.32	542	1.60	1.60	2355	1693	7.4	2.73	9.9	2.74	0.09	0.11	0.15	0.16		
S42, m033, 3h3v	10.5	10.5	0.25	0.25	542	1.60	1.60	2167	2167	7.4	2.73	7.4	2.73	0.09	0.09	0.15	0.15		
S42, m030, 0h0v	42	42	0.72	0.72	542	1.89	1.89	752	752	29.7	3.15	29.7	3.15	0.46	0.46	0.14	0.14	x	x
S42, m030, 1h0v	21	42	0.34	0.82	542	1.52	1.89	1593	661	14.8	3.78	29.7	3.15	0.20	0.45	0.10	0.14	x	x
S42, m030, 1h1v	21	21	0.47	0.47	542	1.52	1.52	1153	1153	14.8	3.78	14.8	3.78	0.21	0.21	0.10	0.10	x	x
S42, m030, 1h2v	21	14	0.53	0.28	542	1.52	1.44	1022	1935	14.8	3.78	9.9	2.45	0.21	0.10	0.10	0.18	x	
S42, m030, 1h3v	21	10.5	0.51	0.20	542	1.52	1.42	1062	2709	14.8	3.78	7.4	2.43	0.21	0.08	0.10	0.18	x	
S42, m030, 2h0v	14	42	0.20	0.86	542	1.44	1.89	2709	630	9.9	2.45	29.7	3.15	0.09	0.44	0.17	0.15		x
S42, m030, 2h1v	14	21	0.26	0.53	542	1.44	1.52	2084	1022	9.9	2.45	14.8	3.78	0.10	0.21	0.18	0.10		x
S42, m030, 2h2v	14	14	0.30	0.30	542	1.44	1.44	1806	1806	9.9	2.45	9.9	2.45	0.11	0.10	0.18	0.18		
S42, m030, 2h3v	14	10.5	0.32	0.23	542	1.44	1.42	1693	2355	9.9	2.45	7.4	2.43	0.11	0.09	0.19	0.18		
S42, m030, 3h0v	10.5	42	0.15	0.89	542	1.42	1.89	3612	609	7.4	2.43	29.7	3.15	0.08	0.44	0.17	0.15		x
S42, m030, 3h1v	10.5	21	0.20	0.51	542	1.42	1.52	2709	1062	7.4	2.43	14.8	3.78	0.08	0.21	0.18	0.10		x
S42, m030, 3h2v	10.5	14	0.23	0.32	542	1.42	1.44	2355	1693	7.4	2.43	9.9	2.45	0.09	0.11	0.18	0.19		
S42, m030, 3h3v	10.5	10.5	0.25	0.25	542	1.42	1.42	2167	2167	7.4	2.43	7.4	2.43	0.09	0.09	0.18	0.18		
S42, m027, 0h0v	42	42	0.72	0.72	542	1.70	1.70	752	752	29.7	2.82	29.7	2.82	0.52	0.52	0.17	0.17	x	x
S42, m027, 1h0v	21	42	0.34	0.82	542	1.36	1.70	1593	661	14.8	3.37	29.7	2.82	0.21	0.50	0.11	0.17	x	x
S42, m027, 1h1v	21	21	0.47	0.47	542	1.36	1.36	1153	1153	14.8	3.37	14.8	3.37	0.22	0.22	0.12	0.12	x	x
S42, m027, 1h2v	21	14	0.53	0.28	542	1.36	1.28	1022	1935	14.8	3.37	9.9	2.18	0.22	0.10	0.12	0.22	x	
S42, m027, 1h3v	21	10.5	0.51	0.20	542	1.36	1.26	1062	2709	14.8	3.37	7.4	2.15	0.23	0.09	0.12	0.21	x	
S42, m027, 2h0v	14	42	0.20	0.86	542	1.28	1.70	2709	630	9.9	2.18	29.7	2.82	0.09	0.49	0.21	0.17		x
S42, m027, 2h1v	14	21	0.26	0.53	542	1.28	1.36	2084	1022	9.9	2.18	14.8	3.37	0.10	0.22	0.22	0.12		x
S42, m027, 2h2v	14	14	0.30	0.30	542	1.28	1.28	1806	1806	9.9	2.18	9.9	2.18	0.11	0.10	0.22	0.22		
S42, m027, 2h3v	14	10.5	0.32	0.23	542	1.28	1.26	1693	2355	9.9	2.18	7.4	2.15	0.11	0.09	0.22	0.22		
S42, m027, 3h0v	10.5	42	0.15	0.89	542	1.26	1.70	3612	609	7.4	2.15	29.7	2.82	0.08	0.48	0.21	0.17		x
S42, m027, 3h1v	10.5	21	0.20	0.51	542	1.26	1.36	2709	1062	7.4	2.15	14.8	3.37	0.09	0.23	0.21	0.12		x
S42, m027, 3h2v	10.5	14	0.23	0.32	542	1.26	1.28	2355	1693	7.4	2.15	9.9	2.18	0.09	0.11	0.22	0.22		
S42, m027, 3h3v	10.5	10.5	0.25	0.25	542	1.26	1.26	2167	2167	7.4	2.15	7.4	2.15	0.09	0.09	0.22	0.22		
S42, m024, 0h0v	42	42	0.72	0.72	542	1.50	1.50	752	752	29.7	2.50	29.7	2.50	0.59	0.59	0.20	0.20	x	x
S42, m024, 1h0v	21	42	0.34	0.82	542	1.20	1.50	1593	661	14.8	2.97	29.7	2.50	0.22	0.57	0.14	0.21	x	x
S42, m024, 1h1v	21	21	0.47	0.47	542	1.20	1.20	1153	1153	14.8	2.97	14.8	2.97	0.23	0.23	0.15	0.15	x	x
S42, m024, 1h2v	21	14	0.53	0.28	542	1.20	1.12	1022	1935	14.8	2.97	9.9	1.91	0.24	0.10	0.15	0.27	x	
S42, m024, 1h3v	21	10.5	0.51	0.20	542	1.20	1.10	1062	2709	14.8	2.97	7.4	1.87	0.24	0.09	0.15	0.27	x	
S42, m024, 2h0v	14	42	0.20	0.86	542	1.12	1.50	2709	630	9.9	1.91	29.7	2.50	0.10	0.55	0.26	0.21		x
S42, m024, 2h1v	14	21	0.26	0.53	542	1.12	1.20	2084	1022	9.9	1.91	14.8	2.97	0.10	0.24	0.27	0.15		x
S42, m024, 2h2v	14	14	0.30	0.30	542	1.12	1.12	1806	1806	9.9	1.91	9.9	1.91	0.11	0.11	0.27	0.27		
S42, m024, 2h3v	14	10.5	0.32	0.23	542	1.12	1.10	1693	2355	9.9	1.91	7.4	1.87	0.11	0.09	0.28	0.27		
S42, m024, 3h0v	10.5	42	0.15	0.89	542	1.10	1.50	3612	609	7.4	1.87	29.7	2.50	0.08	0.54	0.25	0.21		x
S42, m024, 3h1v	10.5	21	0.20	0.51	542	1.10	1.20	2709	1062	7.4	1.87	14.8	2.97	0.09	0.24	0.27	0.15		x
S42, m024, 3h2v	10.5	14	0.23	0.32	542	1.10	1.12	2355	1693	7.4	1.87	9.9	1.91	0.09	0.11	0.27	0.28		

doi:10.6342/NTU201900743

Type	Spacing y (L, B')	Spacing x (B, L')	PSR_x	PSR_y	S	F_{bx}	F_{by}	S_{cx}	S_{cy}	$L_{e,x}$	F_{bx_adj}	$L_{e,y}$	F_{by_adj}	δ_x / H_e (%)	δ_y / H_e (%)	δ_{revx} / H_e (%)	δ_{revy} / H_e (%)	check x	check y
S42, m024, 3h3v	10.5	10.5	0.25	0.25	542	1.10	1.10	2167	2167	7.4	1.87	7.4	1.87	0.09	0.09	0.27	0.27		
S42, m022, 0h0v	42	42	0.72	0.72	542	1.37	1.37	752	752	29.7	2.28	29.7	2.28	0.68	0.67	0.23	0.23	x	x
S42, m022, 1h0v	21	42	0.34	0.82	542	1.09	1.37	1593	661	14.8	2.71	29.7	2.28	0.23	0.63	0.16	0.24		x
S42, m022, 1h1v	21	21	0.47	0.47	542	1.09	1.09	1153	1153	14.8	2.71	14.8	2.71	0.24	0.24	0.17	0.17		
S42, m022, 1h2v	21	14	0.53	0.28	542	1.09	1.02	1022	1935	14.8	2.71	9.9	1.73	0.25	0.10	0.17	0.31		
S42, m022, 1h3v	21	10.5	0.51	0.20	542	1.09	0.99	1062	2709	14.8	2.71	7.4	1.69	0.20	0.08	0.17	0.31		
S42, m022, 2h0v	14	42	0.20	0.86	542	1.02	1.37	2709	630	9.9	1.73	29.7	2.28	0.10	0.61	0.30	0.24		x
S42, m022, 2h1v	14	21	0.26	0.53	542	1.02	1.09	2084	1022	9.9	1.73	14.8	2.71	0.10	0.25	0.31	0.17		
S42, m022, 2h2v	14	14	0.30	0.30	542	1.02	1.02	1806	1806	9.9	1.73	9.9	1.73	0.11	0.11	0.32	0.32		
S42, m022, 2h3v	14	10.5	0.32	0.23	542	1.02	0.99	1693	2355	9.9	1.73	7.4	1.69	0.11	0.09	0.32	0.32		
S42, m022, 3h0v	10.5	42	0.15	0.89	542	0.99	1.37	3612	609	7.4	1.69	29.7	2.28	0.08	0.60	0.30	0.24		x
S42, m022, 3h1v	10.5	21	0.20	0.51	542	0.99	1.09	2709	1062	7.4	1.69	14.8	2.71	0.08	0.20	0.31	0.17		
S42, m022, 3h2v	10.5	14	0.23	0.32	542	0.99	1.02	2355	1693	7.4	1.69	9.9	1.73	0.09	0.11	0.32	0.32		
S42, m022, 3h3v	10.5	10.5	0.25	0.25	542	0.99	0.99	2167	2167	7.4	1.69	7.4	1.69	0.09	0.09	0.32	0.32		
S42, m018, 0h0v	42	42	0.72	0.72	542	1.12	1.12	752	752	29.7	1.86	29.7	1.86	0.94	0.93	0.32	0.32	x	x
S42, m018, 1h0v	21	42	0.34	0.82	542	0.88	1.12	1593	661	14.8	2.19	29.7	1.86	0.25	0.83	0.22	0.33		x
S42, m018, 1h1v	21	21	0.47	0.47	542	0.88	0.88	1153	1153	14.8	2.19	14.8	2.19	0.26	0.26	0.24	0.24		
S42, m018, 1h2v	21	14	0.53	0.28	542	0.88	0.82	1022	1935	14.8	2.19	9.9	1.39	0.27	0.11	0.24	0.44		
S42, m018, 1h3v	21	10.5	0.51	0.20	542	0.88	0.79	1062	2709	14.8	2.19	7.4	1.35	0.27	0.09	0.24	0.44		
S42, m018, 2h0v	14	42	0.20	0.86	542	0.82	1.12	2709	630	9.9	1.39	29.7	1.86	0.11	0.81	0.42	0.33		x
S42, m018, 2h1v	14	21	0.26	0.53	542	0.82	0.88	2084	1022	9.9	1.39	14.8	2.19	0.11	0.27	0.43	0.24		
S42, m018, 2h2v	14	14	0.30	0.30	542	0.82	0.82	1806	1806	9.9	1.39	9.9	1.39	0.11	0.11	0.44	0.44		
S42, m018, 2h3v	14	10.5	0.32	0.23	542	0.82	0.79	1693	2355	9.9	1.39	7.4	1.35	0.11	0.09	0.45	0.45		
S42, m018, 3h0v	10.5	42	0.15	0.89	542	0.79	1.12	3612	609	7.4	1.35	29.7	1.86	0.09	0.77	0.42	0.33		x
S42, m018, 3h1v	10.5	21	0.20	0.51	542	0.79	0.88	2709	1062	7.4	1.35	14.8	2.19	0.09	0.27	0.44	0.24		
S42, m018, 3h2v	10.5	14	0.23	0.32	542	0.79	0.82	2355	1693	7.4	1.35	9.9	1.39	0.09	0.11	0.45	0.45		
S42, m018, 3h3v	10.5	10.5	0.25	0.25	542	0.79	0.79	2167	2167	7.4	1.35	7.4	1.35	0.09	0.09	0.45	0.45		
S30, m033, 0h0v	30	30	0.56	0.56	542	1.85	1.85	967	967	21.2	3.67	21.2	3.67	0.30	0.30	0.11	0.11	x	x
S30, m033, 1h0v	15	30	0.28	0.68	542	1.61	1.85	1935	797	10.6	2.75	21.2	3.67	0.09	0.30	0.15	0.11		x
S30, m033, 2h0v	10	30	0.15	0.71	542	1.60	1.85	3612	763	7.1	2.73	21.2	3.67	0.07	0.29	0.14	0.11		x
S30, m030, 0h0v	30	30	0.56	0.56	542	1.67	1.67	967	967	21.2	3.32	21.2	3.32	0.33	0.33	0.13	0.13	x	x
S30, m030, 1h0v	15	30	0.28	0.68	542	1.45	1.67	1935	797	10.6	2.47	21.2	3.32	0.09	0.33	0.18	0.13		x
S30, m030, 2h0v	10	30	0.15	0.71	542	1.43	1.67	3612	763	7.1	2.43	21.2	3.32	0.07	0.32	0.17	0.13		x
S30, m027, 0h0v	30	30	0.56	0.56	542	1.50	1.50	967	967	21.2	2.97	21.2	2.97	0.36	0.36	0.15	0.15	x	x
S30, m027, 1h0v	15	30	0.28	0.68	542	1.29	1.50	1935	797	10.6	2.19	21.2	2.97	0.09	0.36	0.22	0.15		x
S30, m027, 2h0v	10	30	0.15	0.71	542	1.26	1.50	3612	763	7.1	2.15	21.2	2.97	0.07	0.35	0.21	0.16		x
S30, m024, 0h0v	30	30	0.56	0.56	542	1.32	1.32	967	967	21.2	2.62	21.2	2.62	0.40	0.40	0.18	0.18	x	x
S30, m024, 1h0v	15	30	0.28	0.68	542	1.13	1.32	1935	797	10.6	1.93	21.2	2.62	0.10	0.40	0.27	0.19		x
S30, m024, 2h0v	10	30	0.15	0.71	542	1.10	1.32	3612	763	7.1	1.87	21.2	2.62	0.07	0.39	0.25	0.19		x
S30, m022, 0h0v	30	30	0.56	0.56	542	1.21	1.21	967	967	21.2	2.40	21.2	2.40	0.44	0.44	0.21	0.21	x	x
S30, m022, 1h0v	15	30	0.28	0.68	542	1.03	1.21	1935	797	10.6	1.75	21.2	2.40	0.10	0.43	0.31	0.22		x
S30, m022, 2h0v	10	30	0.15	0.71	542	0.99	1.21	3612	763	7.1	1.69	21.2	2.40	0.07	0.42	0.30	0.22		x
S30, m018, 0h0v	30	30	0.56	0.56	542	0.98	0.98	967	967	21.2	1.94	21.2	1.94	0.56	0.56	0.29	0.29	x	x
S30, m018, 1h0v	15	30	0.28	0.68	542	0.83	0.98	1935	797	10.6	1.41	21.2	1.94	0.10	0.53	0.43	0.30		x
S30, m018, 2h0v	10	30	0.15	0.71	542	0.79	0.98	3612	763	7.1	1.35	21.2	1.94	0.07	0.51	0.42	0.30		x

doi:10.6342/NTU201900743

Type	Spacing y (L, B')	Spacing x (B, L')	PSR_x	PSR_y	S	F_{bx}	F_{by}	S_{cx}	S_{cy}	$L_{e,x}$	F_{bx_adj}	$L_{e,y}$	F_{by_adj}	δ_x / H_e (%)	δ_y / H_e (%)	δ_{revx} / H_e (%)	δ_{revy} / H_e (%)	check x	check y
S20, m033, 0h0v	20	20	0.39	0.39	542	1.68	1.68	1389	1389	14.1	4.29	14.1	4.29	0.16	0.16	0.08	0.08	x	x
S20, m033, 1h0v	10	20	0.18	0.50	542	1.60	1.68	3010	1084	7.1	2.73	14.1	4.29	0.05	0.17	0.15	0.08		x
S20, m030, 0h0v	20	20	0.39	0.39	542	1.51	1.51	1389	1389	14.1	3.87	14.1	3.87	0.17	0.17	0.09	0.09	x	x
S20, m030, 1h0v	10	20	0.18	0.50	542	1.43	1.51	3010	1084	7.1	2.43	14.1	3.87	0.05	0.18	0.17	0.10		x
S20, m027, 0h0v	20	20	0.39	0.39	542	1.35	1.35	1389	1389	14.1	3.45	14.1	3.45	0.18	0.18	0.11	0.11	x	x
S20, m027, 1h0v	10	20	0.18	0.50	542	1.26	1.35	3010	1084	7.1	2.15	14.1	3.45	0.05	0.19	0.21	0.12		x
S20, m024, 0h0v	20	20	0.39	0.39	542	1.19	1.19	1389	1389	14.1	3.04	14.1	3.04	0.19	0.19	0.14	0.14		
S20, m024, 1h0v	10	20	0.18	0.50	542	1.10	1.19	3010	1084	7.1	1.87	14.1	3.04	0.05	0.21	0.26	0.14		
S20, m022, 0h0v	20	20	0.39	0.39	542	1.08	1.08	1389	1389	14.1	2.77	14.1	2.77	0.20	0.20	0.16	0.16		
S20, m022, 1h0v	10	20	0.18	0.50	542	0.99	1.08	3010	1084	7.1	1.69	14.1	2.77	0.05	0.22	0.31	0.16		
S20, m018, 0h0v	20	20	0.39	0.39	542	0.87	0.87	1389	1389	14.1	2.24	14.1	2.24	0.23	0.23	0.22	0.22		
S20, m018, 1h0v	10	20	0.18	0.50	542	0.79	0.87	3010	1084	7.1	1.35	14.1	2.24	0.05	0.25	0.43	0.23		

doi:10.6342/NTU201900743

APPENDIX C

1. For parametric studies, the effect of cross walls on diaphragm wall can not only considered the thickness, the depth, the stiffness of cross walls, but it should be further discussed the geometry ratio of the excavation zone.

2. Clough's design curves are extended to high system stiffness is in comprehension and reasonability. However, the curves are extended to high factor of safety against basal heave is doubt, due to the factor of safety against basal heave equals to 4 or 5 at most.

doi:10.6342/NTU201900743